
秋田県立大学大学院博士学位論文

**Synthesis of Phosphorus-Containing Flame Retardants and
their Applications in Polymeric Materials**

(リン系難燃剤の合成および高分子材料への応用)

顧 立強

2017年3月

Abstract

Flame retardant functional polymers have been widely used for fire- and heat-resistant applications in industrial fields with more safety and excellent performance. Driven by the urgent need of environmental protection, phosphorus-containing flame retardants (PFRs) for polymer have been developed rapidly as alternatives of traditional halogen flame retardants. However, the widely application of PFRs has confronted with a challenge for their cost, migration and mechanical properties of co-polymers. 9,10-dihydro-9-oxa-10-phosphaphenanthrene 10-oxide (DOPO) group has been drawing intense research interest. Based on the active P—H bond, chemically introducing DOPO into various monomers has become a strategy for preparing novel PFRs. In the present study, three novel types of DOPO-containing flame retardants (Series A: single molecules; Series B: chain-like macromolecules; Series C: functionalizing MWCNTs) are designed and synthesized. The resultant flame retardants are introduced into epoxy resin or poly(lactic acid) (PLA), respectively, to improve both flame retardancy and mechanical properties.

In chapter 1, the research backgrounds, research significance, summary of the research and the construction of this thesis are described. The objectives of the research are to synthesis novel DOPO-containing flame retardants for epoxy resin and PLA.

In chapter 2, the properties of experiment materials, as well as experimental methods and characterizations are presented.

In chapter 3, three types of novel DOPO-containing flame retardants (Series A: single molecules; Series B: chain-like macromolecules; Series C: functionalizing MWCNTs) were synthesized based on the Pudovik reactions. Flame retardants series A were characterized by ^1H , ^{13}C and ^{31}P NMR spectroscopy, elemental analysis (EA) and Fourier transform infrared (FT-IR) spectroscopy. For series B, FT-IR and X-ray photoelectron spectroscopy (XPS) were taken to confirm their compositions. The structures and compositions of flame retardants series C were confirmed by FT-IR,

Raman, XPS, transmission electron microscope (TEM) and Thermogravimetric analyses (TGA).

In chapter 4, three types of DOPO-containing flame retardants were well dispersed into epoxy resin matrix with DDM as harder forming flame-retardant epoxy resin composites. Flame retardancy tests indicated that Ax/Bx-modified epoxy resin composites with phosphorus content of 0.75 wt% could reach UL 94 V-0 flammability rating with high *LOI* values. Meanwhile, Cx/AlPi/(P%-Y) epoxy resin nanocomposite with 1.00 wt% Cx and phosphorus content of 1.00 wt% can reach UL 94 V-0 rating. Moreover, TGA results showed that all those flame retardant epoxy resin composites produced high char yields. The mechanical properties of Cx-modified epoxy resin nanocomposites deteriorated slightly with addition of Cx, with notched impact strengths from 2.23 ± 0.15 to 2.90 ± 0.22 kJ·m⁻². Despite this, Cx/AlPi/(P%-Y) epoxy resin nanocomposites showed satisfactory mechanical properties for applications with high storage modulus and *T_g*s.

In chapter 5, three types of DOPO-containing flame retardants were well dispersed into PLA matrix via melt blending forming flame-retardant PLA composites to improve both flame retardancy and mechanical properties. Flame retardancy tests indicated that Ax/Bx-modified PLA composites with filler content of 30 wt% could reach UL 94 V-0 flammability rating, with high *LOI* values. Meanwhile, Cx-modified PLA nanocomposite with synergistic effect of 1 wt% Cx and AHP content of 15 wt% can reach UL 94 V-0 rating. Moreover, TGA results showed that all those flame retardant PLA composites produced high char yields for preventing the anti-dropping. The tensile-enhanced properties of Cx-modified PLA nanocomposites can be attributed to that Cx can form three-dimensional network structure and promote the dispersion of AHP in PLA matrix. The notched impact strengths of Cx-modified PLA nanocomposites were slightly increased with introduction of Cx into flame retardant AHP/PLA systems.

In chapter 6, Core-shell nanostructured flame retardant Cx were introduced into aluminum hypophosphite/poly(lactic acid) (AHP/PLA) flame retardant systems to

improve their flame retardancy. In order to improve the mechanical properties and ductility of such flame retardant PLA nanocomposites, as well as extend their industrial applications, a cold rolling process was performed in this work. Such cold rolling process was conducive for improving the comprehensive mechanical properties of flame retardant PLA nanocomposites with the increasing of both tensile strength and fracture strain. With addition of 1 wt% Cx, when the rolling ratio increased from 0% to 70%, the tensile strength and fracture strain was increased greatly than that of AHP-modified PLA composites. Additionally, the Cx-modified PLA nanocomposites were homogenized at a high rolling ratio, resulting reinforced tensile properties according to the cold rolling process.

In chapter 7, general conclusions of the study are made. These high-efficiency flame retardant epoxy resin/PLA composites with good mechanical properties obtained in this study will become a potential candidate for fire- and heat-resistant applications in automotive engineering and building fields with more safety and excellent performance.

Content

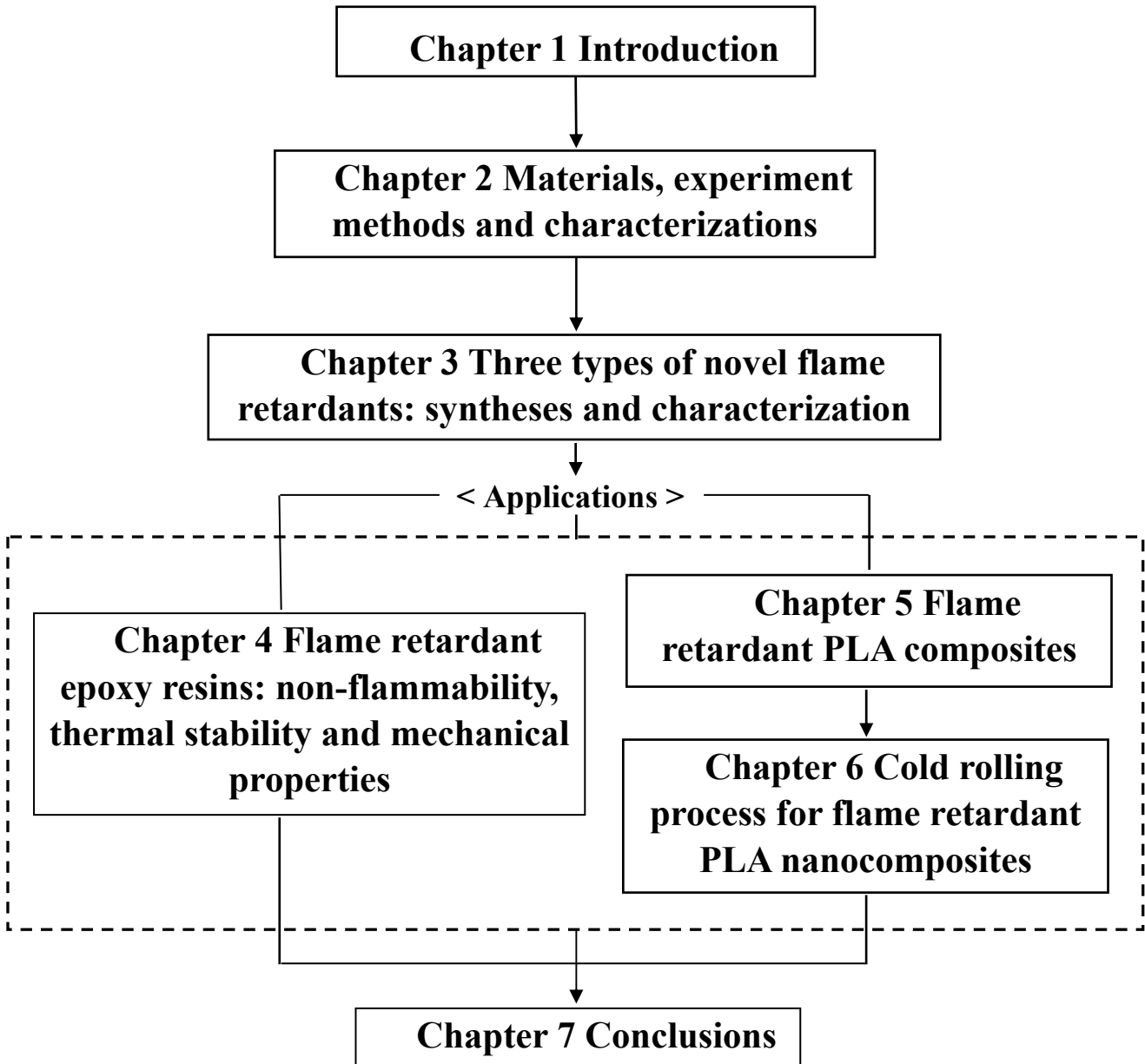
Abstract.....	i
Schematic drawing of structure	viii
Chapter 1 Introduction.....	1
1.1 Background.....	1
1.2 Polymer flame retardants.....	2
1.2.1 Halogen-containing flame retardants	4
1.2.2 Metal hydrate flame retardants	6
1.2.3 Nitrogen- and boron-containing flame retardants	8
1.2.4 Phosphorus-containing flame retardants	9
1.3 Flame retardant mechanisms and guidelines for novel flame retardants.....	12
1.3.1 Flame retardant mechanisms	12
1.3.2 Guidelines for design novel flame retardants.....	15
1.4 Nanotechnology and flame retardancy	16
1.4.1 Polymer nanocomposite technology.....	16
1.4.2 Development of flame retardant nanocomposite.....	17
1.5 Purpose of this research.....	19
References	21
Chapter 2 Materials, Experiment and Characterizations	30
2.1 Materials	30
2.1.1 9, 10-dihydro-9-oxa-10-phosphaphenanthrene 10-oxide (DOPO)....	30
2.1.2 DDM, DDE and DDS.....	31
2.1.3 Multi-walled carbon nanotubes (MWCNTs).....	32
2.1.4 Bisphenol-A diglycidyl ether E51 (DGEBA).....	33
2.1.5 Poly(lactic acid) (PLA).....	34
2.2 Experiment methods	35
2.2.1 Pudovik reaction.....	35

2.2.2 Functionalizing MWCNTs	36
2.2.3 Curing of epoxy resin	37
2.2.4 General methods for testing of polymer materials flammability.....	39
2.3 Instruments and characteristics.....	41
2.3.1 Twin-screw extruder	41
2.3.2 Injection molding machine	42
2.3.3 Rolling machine.....	43
2.3.4 UL-94 vertical burning instrument.....	44
2.3.5 Limiting oxygen index (LOI)	45
2.3.6 Thermogravimetric analyses (TGA).....	45
2.3.7 Tensile test	46
2.3.8 Charpy impact test.....	47
2.3.9 Dynamic mechanical analyzer (DMA).....	48
2.4 Conclusions	48
References	50
Chapter 3 Three Types of Novel Flame Retardants: Syntheses and Characterization	51
3.1 Introduction	51
3.2 Experimental.....	53
3.2.1 Materials	53
3.2.2 Syntheses of flame retardants-series A base on Pudovik reaction	53
3.2.3 Syntheses of flame retardants-series B.....	55
3.2.4 Flame retardants-series C of functionalizing MWCNTs.....	56
2.3.5 Instruments and measurements.....	60
3.3 Results and discussion.....	60
3.3.1 Characterization of flame retardants-series A	60
3.3.2 Characterization of flame retardants-series B	65
3.3.3 Characterization of flame retardants-series C	68
3.4 Conclusions	74

References	76
Chapter 4 Flame Retardant Epoxy Resins: Non-Flammability, Thermal Stability and Mechanical Properties	81
4.1 Introduction	81
4.2 Experimental.....	83
4.2.1 Materials	83
4.2.2 Instruments and measurements.....	83
4.2.3 Preparation of flame retardant epoxy resins.....	83
4.3 Results and discussion.....	86
4.3.1 Non-flammability and residual char analysis.....	86
4.3.2 The thermal stability of epoxy resin composites.....	91
4.3.3 Mechanical properties of Cx-modified epoxy resin nanocomposites	96
4.4 Conclusions	99
References	100
Chapter 5 Flame Retardant PLA Composites: Preparation, Non-Flammability, Thermal Behaviors and Mechanical Properties.....	103
5.1 Introduction	103
5.2 Experimental.....	105
5.2.1 Materials	105
5.2.2 Preparation of PLA-based conductive composites.....	106
5.2.3 Preparation of Ax- or Bx-modified PLA composites.....	107
5.2.4 Preparation of Cx-based PLA nanocomposites	107
5.3 Results and discussion.....	108
5.3.1 Non-flammability and residual char analysis.....	108
5.3.2 The thermal stability of PLA composites.....	113
5.3.3 Mechanical properties of Cx-modified PLA nanocomposites	119
5.4 Conclusions	123
References	124

Chapter 6 Cold Rolling Process for Flame Retardant PLA Nanocomposites	129
6.1 Introduction	129
6.2 Experimental.....	131
6.2.1 Materials	131
6.2.2 Instruments and Measurements	131
6.2.3 Instruments and measurements.....	132
6.3 Results and discussion.....	132
6.3.1 Effect of rolling ratio on tensile properties.....	132
6.3.2 Mechanism of tensile-reinforcing properties with cold rolling process	135
6.3.3 Dynamic mechanical analysis (DMA)	137
6.4 Conclusions	138
References	139
Chapter 7 Conclusions.....	142
Publications	145
Acknowledgements	147

Schematic drawing of structure



Chapter 1 Introduction

1.1 Background

Polymers have played important roles in our daily life and demonstrated endless possibilities for their applications. However, high flammability as one of the main drawbacks for polymeric materials greatly restricts their further developments and applications in many areas [1-5]. The interests in flame retardant polymers can go back to the middle 19th century when highly flammable cellulose nitrate and celluloid were discovered. In more recent years, a large volume of conventional flame retardant polymers were discovered and applied in our daily life, such as phenolics, rigid PVC, melamine resins and so on [6-8]. By the 1970s, the major flame retardant polymers were considered to be thermosets, for instance, unsaturated polyesters or epoxy resins, which utilized reactive halogen compounds or alumina hydrate as additive(s) [9].

Halogen-containing flame retardant polymers in 1970s were much less than that of the other flame retardant polymers mainly Dechlorane Plus, chlorinated acyclic (for polyolefins), tris-(dibromopropyl) phosphate, brominated aromatics, pentabromochloro cyclohexane and hexabromocyclododecane (for polystyrene) [10]. In the next five years, a number of new brominated additives were available on the market. At the same time, a large number of novel Dechlorane-named flame retardants were produced, namely, Dechlorane Plus, a coupled product of two moles of hexachlorocyclopentadiene containing 78% chlorine, a Diels-Alder reaction product of cyclooctadiene and hexachlorocyclopentadiene with 65% chlorine, a Diels-Alder product with furan and a product containing both bromine and chlorine with 77% halogen (for the polystyrene and ABS) [11-15]. In past decades, halogen-containing flame retardant polymers have been developed to meet the considerable secure requirements [16].

However, these halogen-systems cause serious environmental problems, i.e., the release of toxic and corrosive gases associated with the burning during combustion, such

as hydrogen halides, which are greatly potential health hazard [17-19]. In recent years, driven by the urgent need of environmental protection, researches on halogen-free flame retardant (HFFR) of environment friendly, so called “green flame retardant”, have received considerable attention from both the scientific and industrial communities [20-23].

Nowadays, the global flame retardants market is primarily driven by technological advancements in flame retardant safety solutions and regulations. Strong regulations for regarding fire safety of buildings & construction and automobile have resulted into strong growth of flame retardants [24].

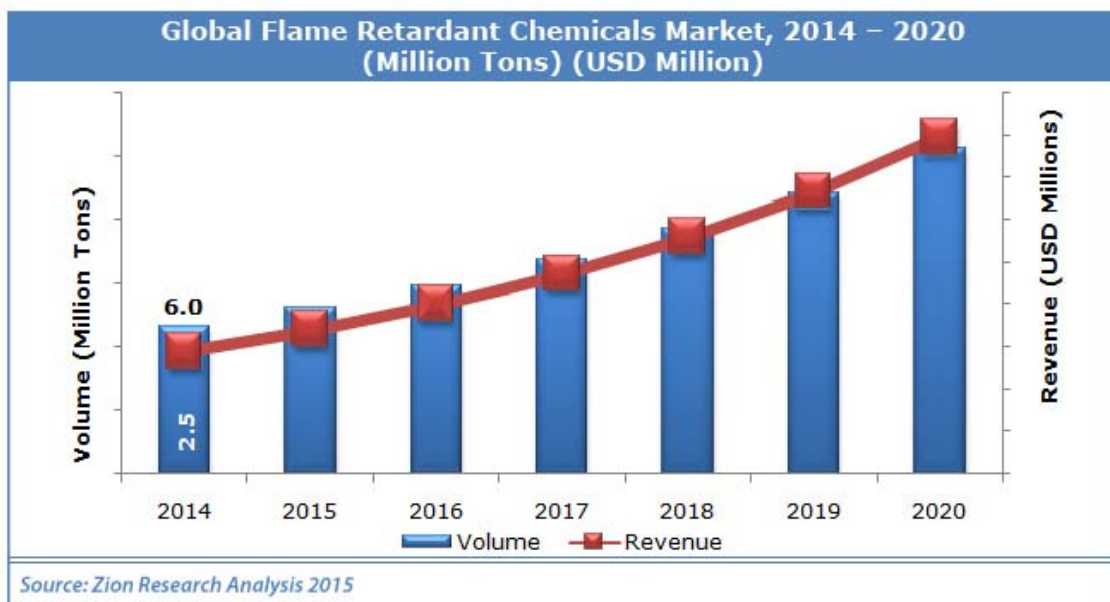


Fig. 1-1 Global flame retardant Chemicals market [25].

Much works are still remained to be solved for complete replacement of harmful flame retardants. But the final issue is obvious. All efforts should give positive results in search of novel environment-friendly flame retardants.

1.2 Polymer flame retardants

Scientists have suggested three basic solutions to improve the flame retardancy of polymers [26]:

1. The addition of some flame retardant(s) that produce radicals of low-molecular mass

and low-activity at high temperatures. For instance, halogen flame retardants contain bromine or chlorine at high temperatures produce Br or Cl atoms with low activity, which can terminate the propagation of the radical chain reactions of combustion.

2. Incorporating some additive(s) that can create cokes or other coating onto polymer surface. These layers prevent the processes of heat and mass transfer. As the atmospheric oxygen and the flame cannot be able to act with any free polymer surface, the combustion process may thus be suppressed.

3. Introduction of chemical compounds that at high temperatures can evaporate, but retaining a high thermal capacity.

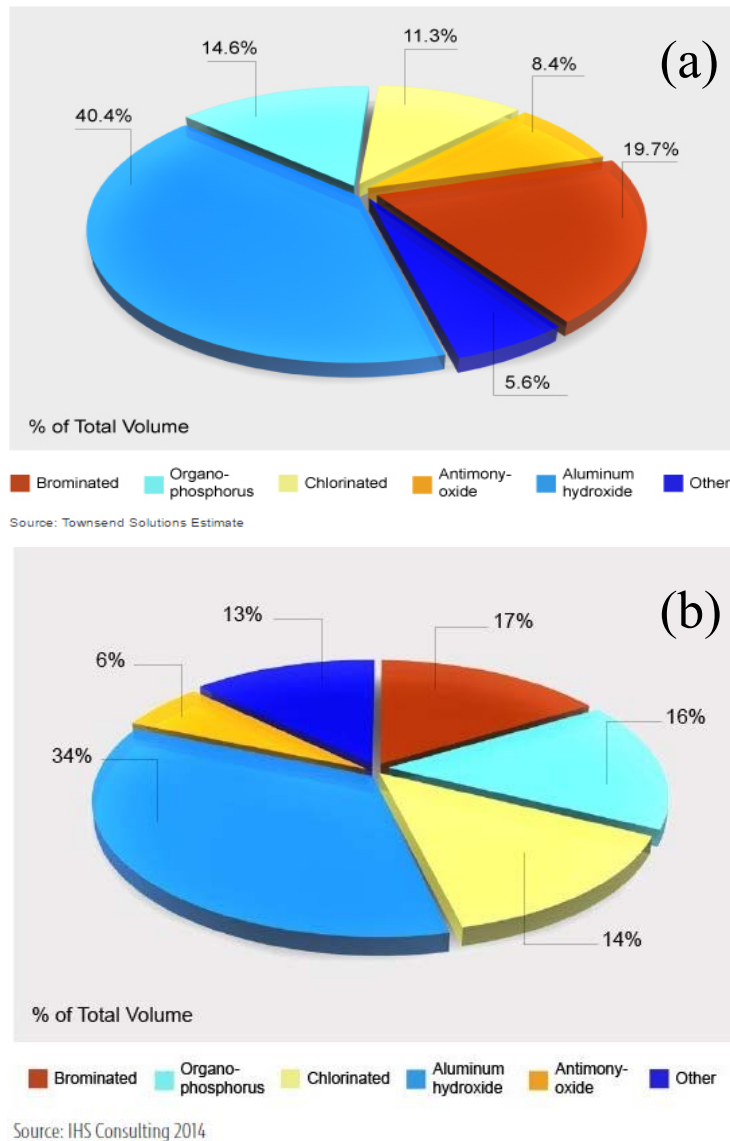


Fig. 1-2 Global Flame Retardants Market by Chemistry, (a) 2011, (b) 2013 [27].

According to a 2014 market study of IHS consulting (Fig. 1-2), the consumption of flame retardants has grown substantially in the past 4 years, notably in electronics, and will continue to grow at a global annualized rate of 3.4% between 2013 and 2018 [27].

Flame retardants are generally classified by their chemical makeup. And the most common classes of flame retardants are halogen and non-halogen ones, exactly as: brominated, chlorinated, metal hydroxide, phosphorus, nitrogen, inorganic and other types (Fig. 1-3) [28-30].

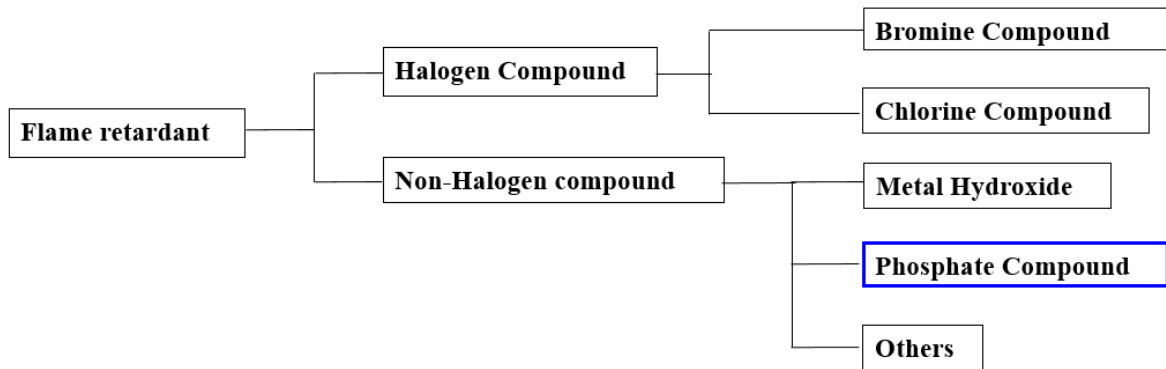
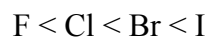


Fig. 1-3 Types of Flame retardants.

1.2.1 Halogen-containing flame retardants

Halogen-containing flame retardants for reducing combustibility of polymer materials can be classified into three types: derivatives of compounds with aliphatic, cycloaliphatic and aromatic structures [31-35]. And in each type of structure, the nature of the halogen atoms is varied. The effectiveness of flame retardation-reactions using halogen-containing compounds with similar structures (differing only in the nature of the halogen) increases in the sequence [36]:



As a function of their structure, the halogen compounds either undergo pyrolysis inside the condensed phase or evaporate and are destroyed in the gaseous phase [37-41].

(1) Commodity halogen-containing flame retardants

The chemical structures of three commodity halogen-containing flame retardants are shown in Fig.1-4. Decabromodiphenyl oxide (DECA) contains about 83% bromine and

melts or decomposes in the 300-310 °C range making it stable for higher temperature processing conditions. DECA is widely used for flame retardant polyolefin, polystyrene and acrylonitrile-butadiene-styrene (ABS) as well as other resin formulations including polyamides, polyesters, polyvinyl chloride (PVC), epoxy and thermoplastic elastomers. DECA [42].

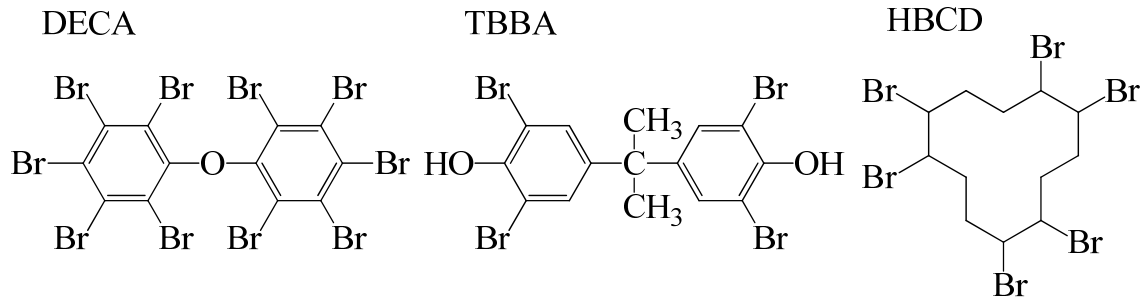


Fig. 1-4 Chemical structures of commodity halogen flame retardants.

Tetrabromobisphenol A (TBBA) contains about 59% bromine and melts in the 178-182 °C range. It is also a brominated aromatic compound used to flame retard ABS, polycarbonate (PC), PC/ABS, HIPS, unsaturated polyesters, epoxy resins and polyurethanes [43].

Hexabromocyclododecane (HBCD), contains about 75% bromine and melts in the 185-195 °C range, which is a brominated compound with no benzene rings. HBCD is used in expandable polystyrene and polystyrene foam applications as well as in adhesives, coatings and textiles [44].

(2) Specialty halogen-containing flame retardants

As shown in Fig.1-5, specialty halogen-containing flame retardants are less frequently used and often priced higher than the commodity products, which are also typically used in specific resin systems and sometimes for specific applications.

Ethylene-bis(tetrabromophthalimide), a 67% brominated aromatic compound, is used for flame retardant polyester resins such as polybutylene terephthalate (PBT), HIPS, ABS and polyethylene (PE) for certain wire and cable applications [45]. TBBP A-bis-(2,3-dibromopropyl ether) is a 68% brominated aromatic compound used for polyolefin resins especially to meet UL94 V-2 applications. it is more suited to lower temperature

resins such as polypropylene for its melting range for this compound is 90-105 °C [46]. The phenoxy terminated carbonate oligomer of TBBA is a 59% brominated aromatic compound used to flame retard PBT and PC resins, whose largest use is in electronic connectors [47]. Brominated polystyrene contains 67% bromine. It is typically used to flame retard polyamide 6 and 6/6 resins along with some usage in PBT applications. The major application is again electrical and electronic connectors [48].

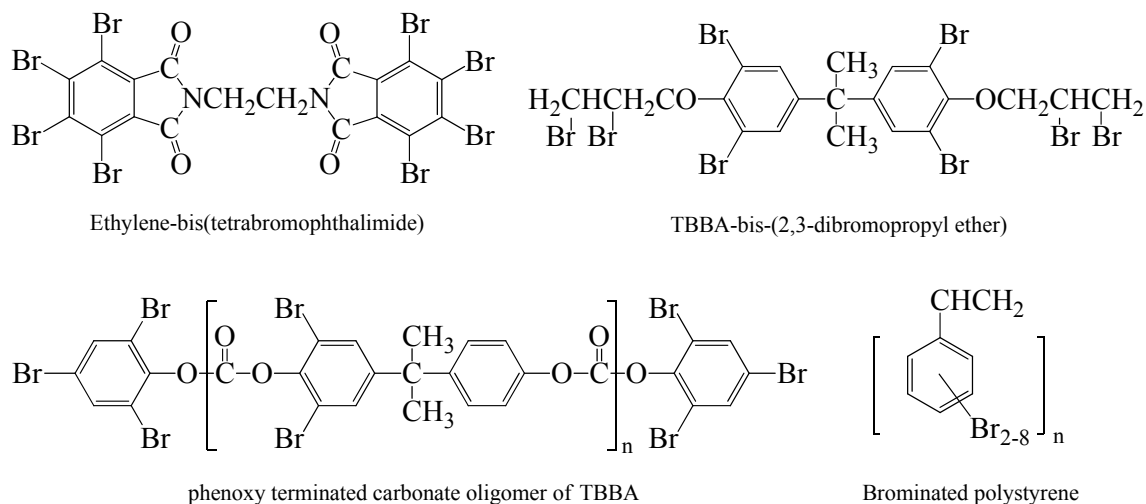


Fig. 1-5 Chemical structures of specialty halogen flame retardants.

(3) Environmental issues

The environmental and human health concerns regarding usage and disposal of flame retardant products are at present mostly focused on the halogen-containing ones. There is legislation in both Europe and USA banning the use of some specific brominated flame retardants. Voluntary withdrawal of some halogen-containing flame retardant products has already occurred in the European market [49-52]. The European Commission of its White Paper, ‘Strategy for a Future Chemicals Policy’ has been adopted since February 2001 [53]. This White Paper creates no legal obligations but does present a strategy for future European Community policy for all chemicals including flame retardants [54].

1.2.2 Metal hydrate flame retardants

Metal hydrate flame retardant (MHFR) products comprise the largest volume flame retardants in the global flame retardant market today [55]. MHFRs include aluminium

trihydroxide (ATH), magnesium hydroxide, and a few other less frequently used products like brucite, mixtures of hydromagnesite and huntite, magnesium aluminium hydroxycarbonates, and certain other mixed metal hydroxides [56]. This type of flame retardants presents almost no risk to environmental and human health, which can therefore be labelled an environmentally friendly FR product type.

(1) Commodity metal hydrate flame retardants

Metal hydrate compounds are widely used as flame retardants for modern polymer materials [57]. ATH, the largest volume metal hydrate flame retardant, is widely used for flame retardant PVC, ethylene-propylene rubber (EPR), ethylene-propylene-diene terpolymer rubber (EPDM), ethylene-vinyl acetate copolymer (EVA), polyethylenes, unsaturated polyesters, acrylics, epoxies and phenolics with loading range from 5 to 70% or more depending on the resin and application. Their applications include conduit, pipe, wire and cable, bathroom ware, wall panels, laminated countertops, electronic components like circuit boards, electrical potting compounds, and profiles [58].

Magnesium hydroxide, $Mg(OH)_2$, is another metal hydrate flame retardant. $Mg(OH)_2$ is used in polyolefins, thermoplastic olefinic elastomers (TPO), EVA, some polyamides, and epoxies [59]. Its applications include wire and cable, various building products such as construction laminates, roofing membranes and plastic lumber [60-61].

(2) Specialty metal hydrate products

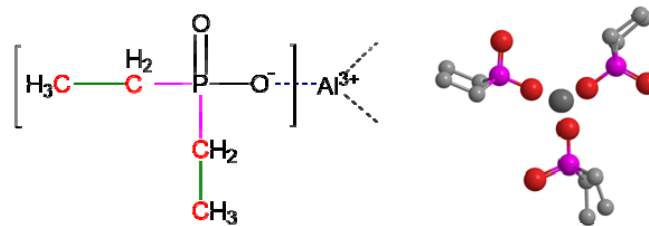


Fig. 1-6 Chemical structures of AlPi.

In 2012, Liu et al. [62] compared the flame retardancy and mechanical properties of aluminum diethylphosphinate (Al(DEP) or AlPi) and aluminum methylethylphosphinate (Al(MEP))-filled epoxy composites, and found that both Al(DEP)- and

Al(MEP)-modified epoxy resins reached UL 94 V-0 flammability rating at the content of 15 wt.%.

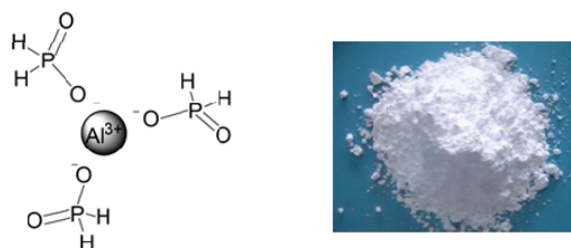


Fig. 1-7 Chemical structures of AHP.

Aluminum hypophosphite (AHP), as an effective inorganic phosphorus-containing flame retardant, has been widely used in many engineering plastics, i.e., polyethylene terephthalate (PET), Polybutylene terephthalate (PBT) and Polyamide (PA) [63]. Tang, G. et al. [64] has reported that flame-retardant PLA with 20 wt% AHP can reach V-0 rating under the UL 94 test. Zhou X. et al. [65] has introduced AHP into a conventional PLA/IFR system (IFR was a combination of APP and PER in a weight ratio 3:1), which showed a synergistic effect for the well flame retardancy.

1.2.3 Nitrogen- and boron-containing flame retardants

(1) Nitrogen-containing flame retardants

Nitrogen-containing compounds are a small but rapidly growing as environmentally friendly flame retardants. Their efficiency lies between that of halogen compounds and that of aluminum trihydrate and magnesium hydroxide. Moreover, their low toxicity, solid state, the absence of dioxin and halogen acids as combustion products as well as their low evolution of smoke in case of fire. The main applications of nitrogen-containing flame retardants are melamine for polyurethane flexible foams, melamine cyanurate in nylons, melamine phosphates in polyolefins, melamine and melamine phosphates or dicyandiamide in intumescent paints, guanidine phosphates for textiles and guanidine sulfamate for wallpapers [66-68].

(2) Boron-containing flame retardants

Boron-containing flame retardants have a synergistic effect with halogenated

compounds, which are particularly attractive because they are lower in cost than antimony oxide. Zinc borate has been used as a partial replacement for antimony oxide in a number of applications, such as unsaturated polyester, polypropylene, and flexible PVC. Boron compounds are also useful in reducing or eliminating after-glow in halogen-containing compositions. Boron compounds act in the condensed phase by redirecting the decomposition process in favor of carbon formation rather than CO or CO₂. The second mechanism may involve formation of a surface layer as protective char, which prevents the oxidation of carbon by limiting the accessible oxygen [69-70].

1.2.4 Phosphorus-containing flame retardants

As ecofriendly flame retardants, phosphorus-containing compounds have been developed greatly by advantage of that: effective at low concentration-organic types; easy incorporation and processing; relatively little detrimental effect on physical properties and so on [71-72]. Phosphorus-containing flame retardants including ammonium polyphosphate (APP), red phosphorus, organic phosphates and phosphonates, choroaliphatic and bromoaromatic phosphates, and a newer product type, organic metal phosphinates, comprise the third major flame retardant group of products (Fig. 1-2) [27]. These flame retardants are typically described as char formers with regard to their flame retardant mechanism.

(1) Commodity phosphorus-containing flame retardants

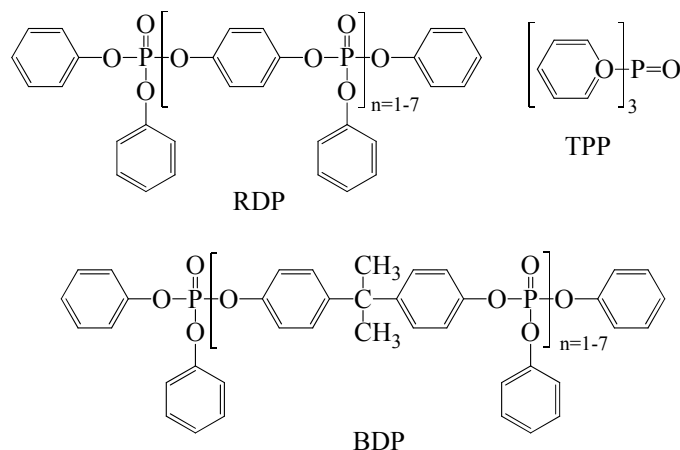
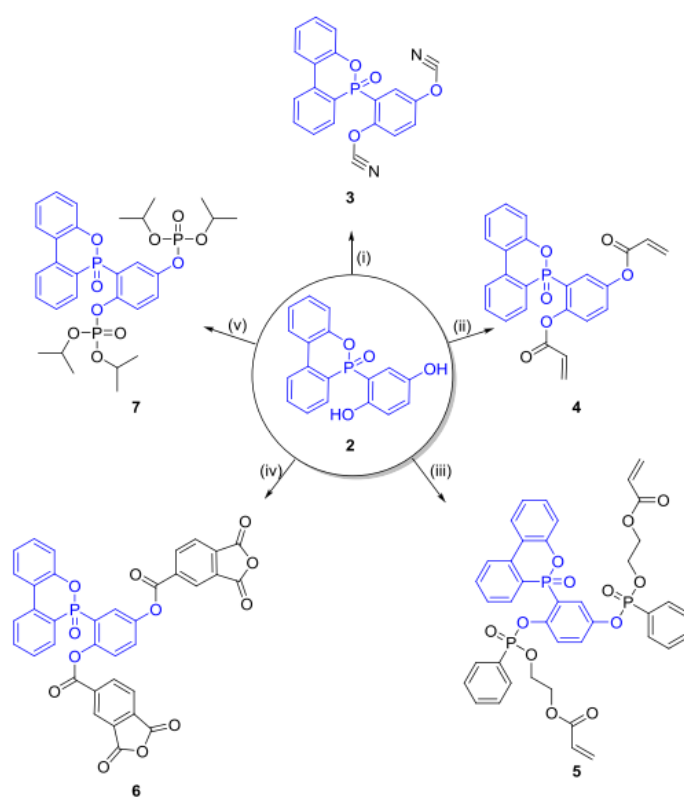


Fig. 1-8 Chemical structures of commodity phosphorus containing flame retardants.

Commodity phosphorus-containing flame retardants include the phosphate esters, APP, and chloroalkyl phosphates. And phosphate esters include RDP, BDP, triphenyl phosphate (TPP), triaryl phosphates, alkyl diaryl phosphates and trialkyl phosphates (Fig. 1-8) [73], whose major use is in PVC as non-flammable plasticisers. RDP and BDP are widely used in ABS/PC and PPO applications. The most important inorganic nitrogen-phosphorus compound used as a flame retardant is ammonium polyphosphate which is applied in intumescent coatings and in rigid polyurethane foams.

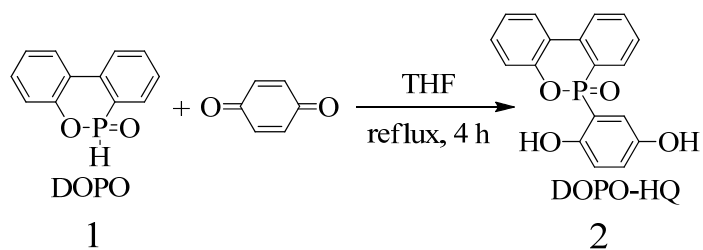
(2) DOPO-containing phosphorus flame retardants



Scheme 1-1. Synthetic routes for some derivatives from DOPO-HQ [75].

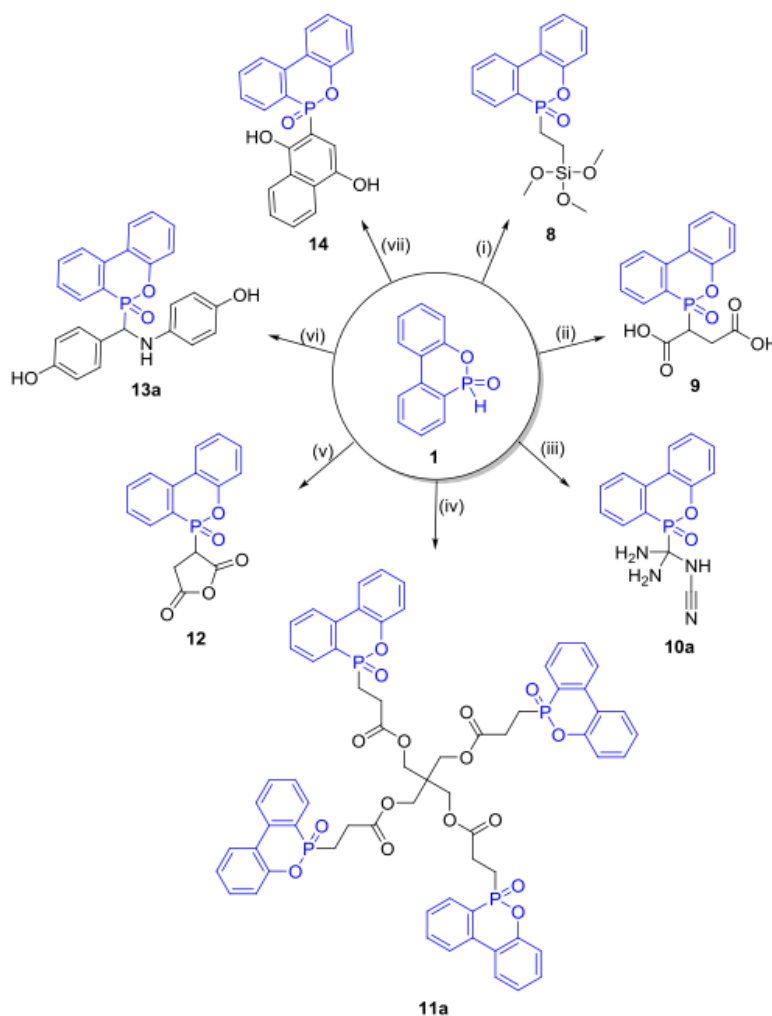
Synthesis of organophosphorus compounds based on 9,10-dihydro-9-oxa-10-phosphaphenanthrene-10-oxide(DOPO) and their application as flame retardant have attracted increasing attention in the flame retardant community [74]. Such DOPO-containing flame retardants are a product of P—H bond substitution with P—C bond (Scheme 1-2 and 1-3). These P—C bond derivatives (DOPO-containing flame retardants) can be prepared by two main approaches, namely nucleophilic addition/substitution and via

molecular rearrangement.



Scheme 1-2. Synthesis of DOPO-HQ (2).

In the past few decades, synthesis of various organophosphorus compounds (Scheme 1-1 and 1-3) for different applications (mainly as flame retardants) has usually started from DOPO and DOP-HQ (Scheme 1-2).



Scheme 1-3. Synthetic routes for some derivatives from DOPO [75].

These DOPO-containing flame retardants are mainly in epoxy resins, for applications

in adhesives, composites, printed wiring boards and others, which are considered as suitable alternative to halogenated flame retardants because of their versatile flame extinguishing behavior in gas phase and condensed phase [75]. New market demand of improved thermal stability, better processability (better flow and recyclability), and miniaturized parts (better mechanical properties) will continue to push the envelope of fire retardant technology. Novel halogen-free technologies such as DOPO are steadily gaining more market share [76].

(3) Environmental Issues

Like specific halogen-containing flame retardants, there are human health and environmental safety questions about certain phosphorus containing flame retardant products. The Phosphate Ester Flame Retardants Consortium (PEFRC) was formed in February 2002 to support phosphate ester flame retardants through advocacy, scientific programs, and education.

A report issued in 2002 includes results from a study carried out for the Swiss Federal Office of Public Health to evaluate indoor air exposures of ten phosphorus based flame retardants. These ten test compounds were selected based on prior indications of emissions to indoor air or of risk to people exposed to those substances. Samples were taken from furniture and electronic appliance showrooms, open-plan offices, car interiors, and in a theatre auditorium. Essentially, this particular study showed risks to be very low and concluded that large-scale measuring campaigns were not required at this time [77].

1.3 Flame retardant mechanisms and guidelines for design flame retardants

1.3.1 Flame retardant mechanisms

(1) General flame retardant mechanisms

Although the chemical structure of flame retardants may differ from each other, certain general mechanisms are applicable to various types of flame retardants. The

separation of flame retardants normally distinguishes gas-phase-active and condensed-phase-active ones. Some gas-phase-active flame retardants show the chemical mechanism of action in the gas phase, which act primarily through scavenging free radicals responsible for the branching of radical chain reactions in the flame. Other flame retardants show physical mechanism of action in the gas phase, which generate large amounts of noncombustible gases, dilute flammable gases, sometimes dissociate endothermically, and decrease the temperature by absorbing heat. [78].

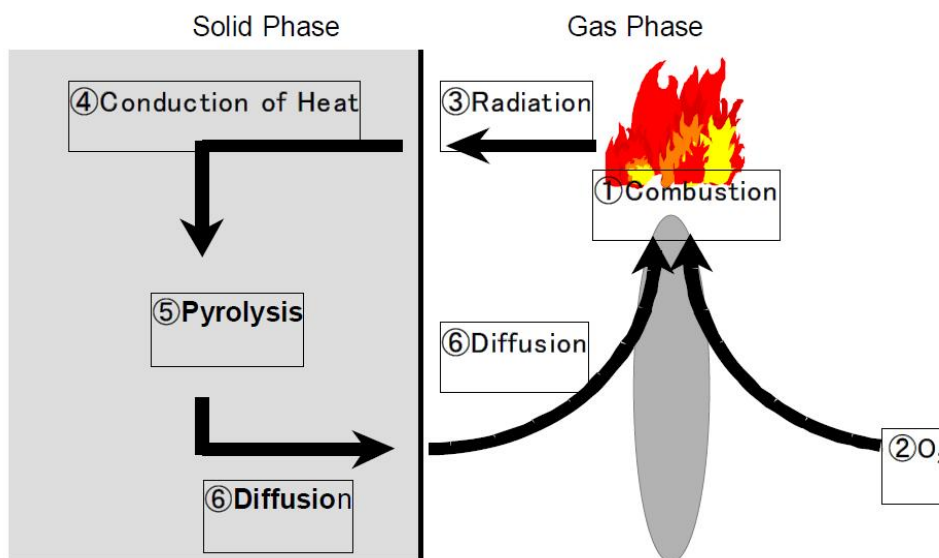


Fig. 1-9 Combustion-Model of polymer [78].

Condensed-phase mechanisms (condensed-phase-active flame retardants) are usually more numerous than gas-phase mechanisms (gas-phase-active flame retardants). The most common condensed-phase mechanism of action is charring. At the same time, charring could also be promoted either by chemical interaction of the flame retardant or by physical retention of the polymer in the condensed phase. In general, catalysis or oxidative dehydrogenation could promote the charring process.

However, some flame retardants, such as aluminum hydroxide and magnesium hydroxide, show almost exclusively a physical mode of action. On the other hand, no single flame retardant will operate exclusively only a chemical mode of action without physical ones, in other words, chemical mechanisms are always accompanied by one or several physical mechanisms [79-80].

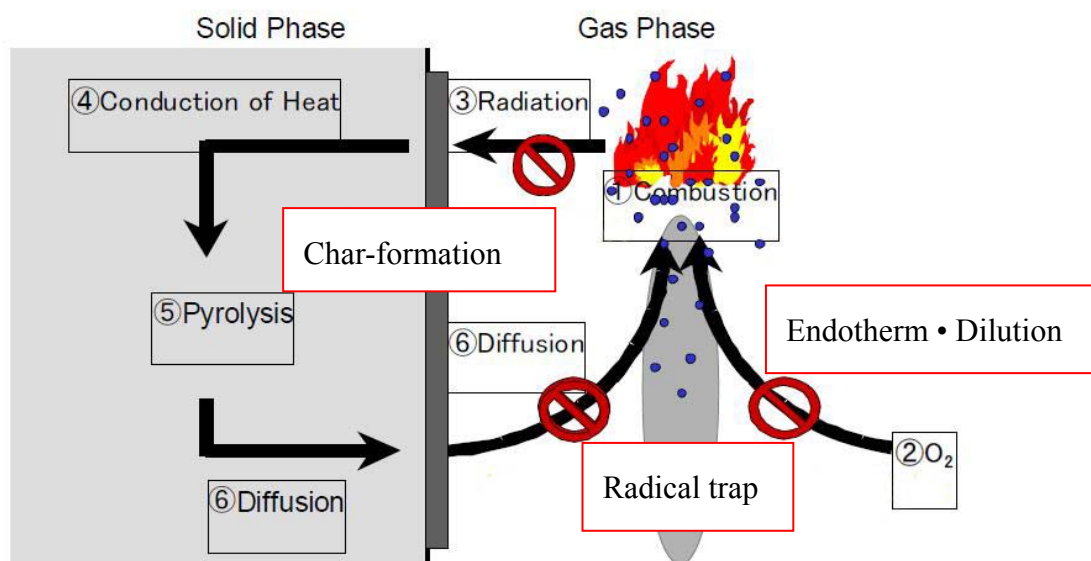
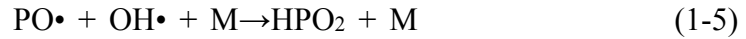
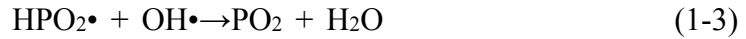


Fig. 1-10 Flame retardant model of polymer [78].

(2) Phosphorus-containing flame retardant mechanisms

Phosphorus-containing flame retardants are significantly more effective in oxygen- or nitrogen-containing polymers. The condensed phase mechanism and vapor phase mechanism are mainly suggested to explain the phosphorylation [80-82]. A lot of studies based on these two mechanisms have been carried out to predict the composite properties of flame retardancy and develop efficient phosphorus-containing fire-retardant composites. The presence of phosphorus promotes forming a carbonaceous char or a barrier layer of polyphosphoric acid on burning of the polymer in the condensed phase. Moreover, phosphorus flame retardants can act as potent scavengers of $H\cdot$ or $OH\cdot$ radicals when volatilize into the gas phase. Volatile phosphorus-containing compounds are one of the most effective inhibitors during combustion. The mechanisms of radical scavenging from phosphorus-containing flame retardants were suggested by Hastie and Bonnell [83]. The most abundant phosphorus-containing radicals during combustion are $HPO_2\cdot$, $PO\cdot$, $PO_2\cdot$ and $HPO\cdot$, in the order of significance that $HPO_2\cdot < PO\cdot < PO_2\cdot < HPO\cdot$. Some examples of phosphorus-containing radical that scavenge with participation of $HPO_2\cdot$ and $PO\cdot$ radicals are shown in the following reactions from (1-1) to (1-5) [83].





In the right conditions, phosphorus-containing flame retardants can volatilize and be oxidized, producing active radicals during combustion (radical-mechanism). On the other hand, phosphorus-containing flame retardants can take reaction with the polymer and oxidize to phosphoric acid in the condensed phase (condensed-phase mechanism). Nowadays, it is still a challenge for phosphorus-containing flame retardants that will volatilize into the flame (gas-phase mechanism and radical-mechanism) at relatively low temperatures while will keep the stability during polymer processing.

1.3.2 Guidelines for design novel flame retardants

Tab. 1-1 Guidelines for designing novel polymer flame retardants [84].

Properties	Comment	e.g.)
High efficiency flame retardant	Low addition and good flame retardancy	(1) <u>Atomization and dispersion technology</u> (2) High synergistic effect (3) Char promoting compound
Environment friendly	Halogen-free, Low hazard, Low heavy metals, Non-phosphorus materials	(1) <u>High flame retardant compound</u> (2) Silicone and higher fatty acid metal (3) <u>Low toxic-gas and smoke</u>
Recyclability	Repeatedly, Excellent thermal stability	(1) Can be used repeatedly (2) Recycling by pyrolysis, gasification and liquidation (3) Solvent extraction separation method (4) <u>Biodegradable flame retardants</u>
Function materials	Other functions with high performance	(1) <u>Conductivity, vibration damping, antibacterial, light functionality and non-ion release flame retardant materials</u>
Moldability	Excellent mold-ability, plume, discoloration, low pressure-sensitive	(1) Low-addition flame retardants (2) Reactive flame retardants

Nowadays, the strategies for development of novel flame retardants are mainly focus on two ways, i.e., synergistic effect of silicone, a hydrated metal compound and boric acid, as well as flame retardant nanocomposite. Especially, flame retardant nanocomposite has attracted the increasing attention for their excellent performance.

Tab. 1-1 shows the guidelines for design novel flame retardants [84]. From this table, flame retardant nanocomposite will be rapidly growing group of flame retardants, which may widely relative to the required properties of novel high-performance flame retardants.

1.4 Nanotechnology and flame retardancy

1.4.1 Polymer nanocomposite technology

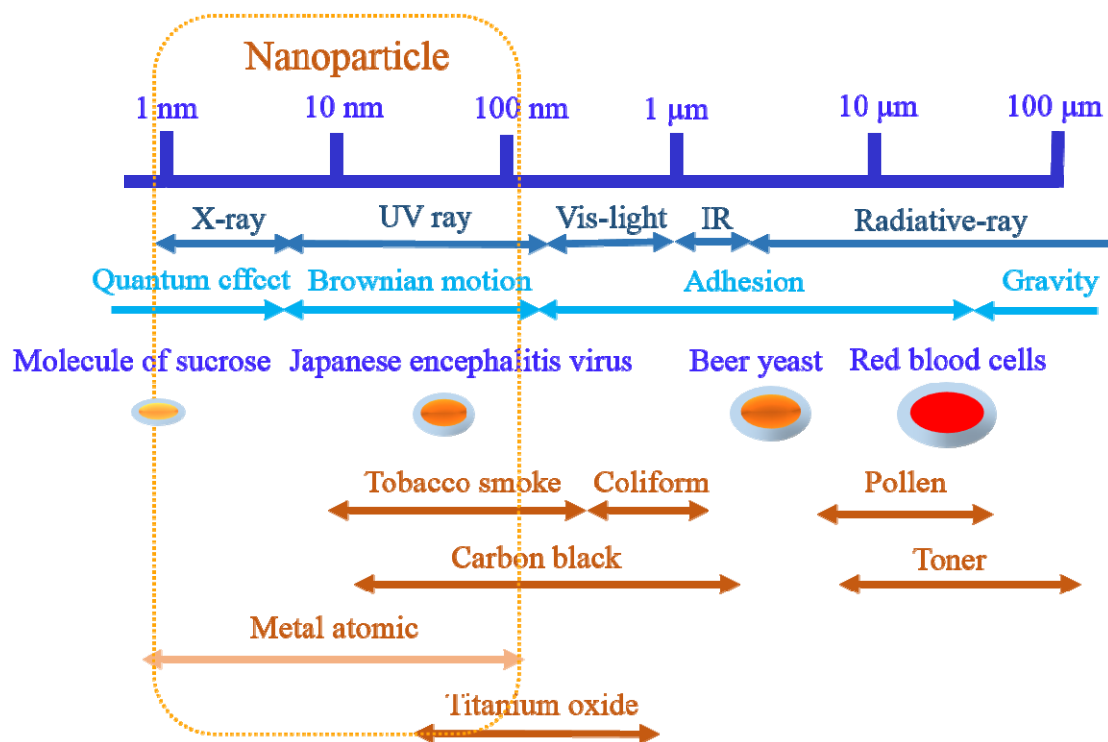


Fig. 1-11 Nanoparticle and spectrum [84].

The subject of polymer nanocomposites has spawned a huge amount of research and attracted considerable interest since the early 1990s. Polymer nanocomposites consist of a polymer or copolymer, which have nanoparticles or nano-fillers (1~100 nm, as shown in Fig. 1-11) dispersed in the polymer matrix. Such polymer nanocomposites have shown

great performance improvements over traditional polymer composites in mechanical, thermal, gas barrier, conductivity, flammability, electromagnetic shielding, and other properties [85]. The advancement of new technology have enabled a number of commercial applications, including highly efficient catalysts, micro-electronics, medical devices, and advanced plastics. For advanced function plastics, the major area of development is focus on the dispersion of fillers (less than 100 nm). In some condition, nano-sized inorganic frameworks have been introduce into some polymer nanocomposites to achieve confinement of polymers, following with unique properties [86]. These nano-sized inorganic frameworks show different morphologies, such as one-dimension (1-D) fiber, needle-like structures, two-dimension (2-D) sheet, platy-like structures, 3-dimension (3-D) frame work structures and other morphologies.

Polymer nanocomposites, in the sense of hybrid materials, show a number of novel properties beyond the field of unfilled polymers or conventional polymer composites, enabling new advance uses and applications of function polymer materials [87].

1.4.2 Development of flame retardant nanocomposite

Nanotechnology is perhaps the newest technology in the FR industry and the chemical industry. In 2007, a book titled ‘Flame retardant polymer nanocomposites has been published by John Wiley & Sons [88]. Clearly this technology has unlimited potential and may lead to next generation technology and products in a variety of industries. This book focus on the improvements in materials flammability. In the FR universe, nanotechnology refers to polymer layered-silicates or clay nanocomposites. Polymer layered-silicate nanocomposites are best described as a hybrid of organic polymer and inorganic silicate materials in alternating nanometre-thick layers. Clays currently used for these layered silicate nanocomposites include montmorillonite, hectorite, saponite and bentonite.

Research on flame retardant nanocomposite technology gained momentum a few years ago and many FR and plastics additives industry conferences now contain technical papers on this subject. A few of these contributions will be reviewed here (Tab. 1-2).

Tab. 1-2 Some publications of flame retardant nanocomposites.

Year	Reference	Materials	Challenge
2004	Kashiwagi Takashi, et al. <i>Polymer</i> 45.3 (2004): 881-891.	polyamide 6–clay nanocomposites	Sufficient amounts of protective floccules to cover the entire sample surface.
2011	Yang, Feng, et al. <i>Polymer Degradation and Stability</i> 96.3 (2011): 270-276.	Polystyrene based nanocomposites (PNCs) with/without flame retardant additives.	Mechanical properties
2014	Gao, Yanshan, et al. <i>Journal of Materials Chemistry A</i> 2.29 (2014): 10996-11016.	Flame retardant polymer–layered double hydroxide (LDH) nanocomposites	The use of LDH dispersions in polymer-based materials
2016	Xing, Weiyi, et al. <i>ACS Applied Materials & Interfaces</i> (2016).	Functionalized Carbon Nanotubes/polystyrene (PS) nanocomposites	UL 94 flame rating

Kashiwagi Takashi, et al. [89] has prepared polyamide 6/clay (2 and 5% by mass fraction) nanocomposites and measured their thermal and flammability properties to determine their high flame retardant performance. Therefore, both PA6/clay nanocomposite samples did not produce sufficient amounts of protective floccules to cover the entire sample surface and vigorous bubbling was observed over the sample surface which was not covered by the protective floccules.

Other current flame retardant nanocomposites focus on polystyrene based nanocomposites (PNCs) with both silica and attapulgite, which show a remarkable reduction in heat release rates. However, there are no enough discussion on the mechanical properties of those PNCs with flame retardant additives [90].

Another type of flame retardant polymer/layered double hydroxide nanocomposites have focused on polymer–layered double hydroxide (LDH) nanocomposites [91]. The

flame retardant mechanism of LDHs, the types of polymers studied, the effect of LDH chemical composition and the synergistic effect with other fire retardants have been reviewed, which also prompt new discussions on the use of LDH dispersions in polymer-based materials.

In the last couple of years functionalized carbon nanotubes and graphene have introduced flame retardant nanocomposites. Xing, Weiyi, et al. [92] have prepared the flame retardant functionalized MWCNT (DPPA-MWCNT) based on the reaction between aminated multiwalled carbon nanotubes (AMWCNT) with diphenylphosphinic chloride (DPP-Cl). As stated, resultant flame retardant polystyrene (PS) nanocomposites have shown good dispersion and interfacial interactions between DPPA-MWCNT and PS matrix, which significantly reduced peak heat release rate, smoke production rate, and carbon monoxide and carbon dioxide release. As most cases, the addition of small quantities of functionalized MWCNTs, usually less than 1 wt%, can dramatically improve the thermal and mechanical properties of polymers, but still fails to pass the traditional flame retardancy such as UL 94 tests.

1.5 Purpose of this research

In recent years, driven by the urgent need of environmental protection, researches on environment friendly halogen-free phosphorus-containing flame retardant (PFR), have received considerable attention. However, the widely application of PFRs has confronted with a challenge for their cost, migration and mechanical properties of co-polymers. So the present study aimed on developing novel high-efficiency PFRs with high performance in polymers. These high-efficiency flame retardant epoxy resin/PLA composites with good mechanical properties obtained in this study will become a potential candidate for fire- and heat-resistant applications in automotive engineering and building fields with more safety and excellent performance.

The overall structure of the present study is presented in Fig. 1-12.

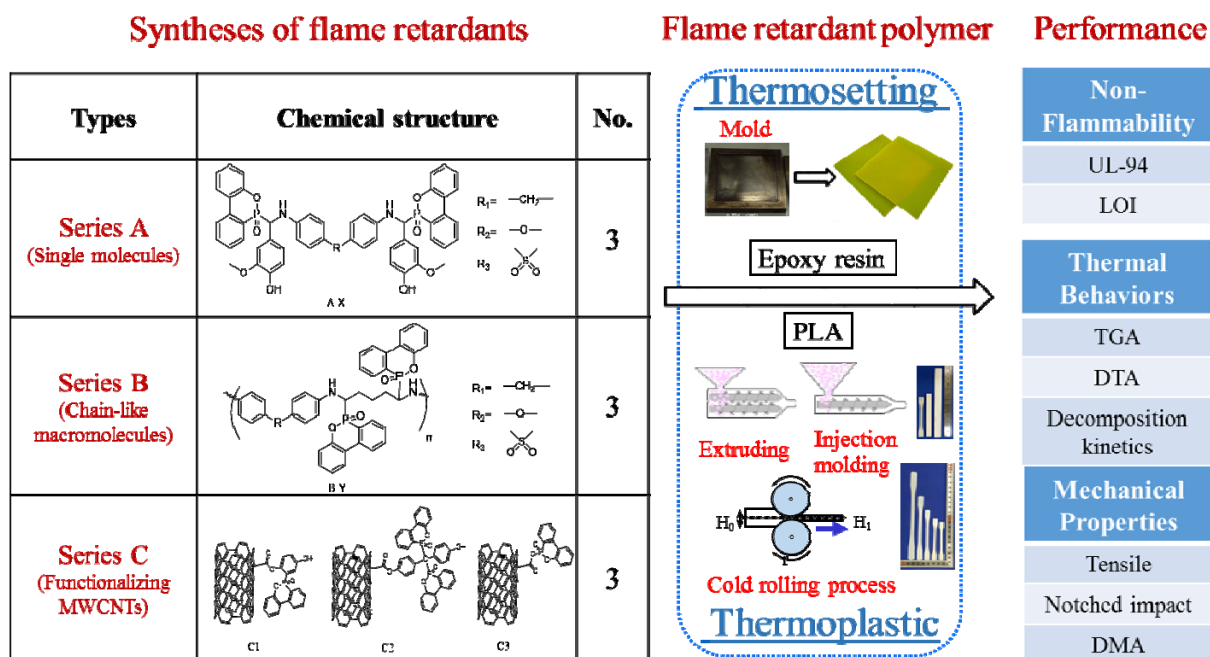


Fig. 1-12 The overall structure of the present study.

References

- [1] Flame Retardant Chemicals Association of Japan (FRCJ), [http://www.frcj.jp/flame-retardants/; accessed in September 2016]
- [2] Bourbigot, S., & Flambard, X. Heat resistance and flammability of high performance fibres: A review. *Fire and materials*, 2002, 26(4-5), 155-168
- [3] Wang, F. Polymer additive analysis by pyrolysis-gas chromatography: II. Flame retardants. *Journal of Chromatography A*, 2000, 886(1), 225-235.
- [4] Snook, G. A., Kao, P., & Best, A. S. Conducting-polymer-based supercapacitor devices and electrodes. *Journal of Power Sources*, 2011, 196(1), 1-12.
- [5] Levchik, S. V. Introduction to flame retardancy and polymer flammability. *Flame retardant polymer nanocomposites*, 2007, 1-29.
- [6] Butt, C. M., & Stapleton, H. M. Inhibition of thyroid hormone sulfotransferase activity by brominated flame retardants and halogenated phenolics. *Chemical research in toxicology*, 2013, 26(11), 1692-1702.
- [7] Ning, Y., & Guo, S. Flame-retardant and smoke-suppressant properties of zinc borate and aluminum trihydrate-filled rigid PVC. *Journal of Applied Polymer Science*, 2000, 77(14), 3119-3127.
- [8] Pearce, E. (Ed.). *Flame-retardant polymeric materials*. Springer Science & Business Media, 2012.
- [9] Levchik, S. V., & Weil, E. D. A review of recent progress in phosphorus-based flame retardants. *Journal of Fire Sciences*, 2006, 24(5), 345-364.
- [10] Shaw, S. Halogenated flame retardants: do the fire safety benefits justify the risks? *Reviews on environmental health*, 2010, 25(4), 261-306.
- [11] Hoh, E., Zhu, L., & Hites, R. A. (2006). Dechlorane Plus, a chlorinated flame retardant, in the Great Lakes. *Environmental science & technology*, 2006, 40(4), 1184-1189.
- [12] Danish, A. A., & Julius, H. U.S. Patent No. 2,658,926. Washington, DC: U.S. Patent

and Trademark Office, 1953.

[13] Mischutin, V. U.S. Patent No. 3,955,032. Washington, DC: U.S. Patent and Trademark Office, 1976.

[14] Corey, E. J., & Loh, T. P. (1993). Catalytic enantioselective Diels-Alder addition to furan provides a direct synthetic route to many chiral natural products. *Tetrahedron letters*, 34(25), 3979-3982.

[15] Grieco, P. A., Nunes, J. J., & Gaul, M. D. Dramatic rate accelerations of Diels-Alder reactions in 5 M lithium perchlorate-diethyl ether: the cantharidin problem reexamined. *Journal of the American Chemical Society*, 1990, 112(11), 4595-4596.

[16] Alae, M., Arias, P., Sjödin, A., & Bergman, Å. An overview of commercially used brominated flame retardants, their applications, their use patterns in different countries/regions and possible modes of release. *Environment international*, 2003, 29(6), 683-689.

[17] Lu, S. Y., & Hamerton, I. Recent developments in the chemistry of halogen-free flame retardant polymers. *Progress in Polymer Science*, 2002, 27(8), 1661-1712.

[18] Horrocks, A. R., & Price, D. (Eds.). *Fire retardant materials*. woodhead Publishing, 2001.

[19] Weil, E. D., & Levchik, S. A review of current flame retardant systems for epoxy resins. *Journal of fire sciences*, 2004, 22(1), 25-40.

[20] Schirp, A., & Su, S. (2016). Effectiveness of pre-treated wood particles and halogen-free flame retardants used in wood-plastic composites. *Polymer Degradation and Stability*, 2016, 126, 81-92.

[21] Li, Z., & Qu, B. Flammability characterization and synergistic effects of expandable graphite with magnesium hydroxide in halogen-free flame-retardant EVA blends. *Polymer Degradation and Stability*, 2003, 81(3), 401-408.

[22] Mauerer, O. New reactive, halogen-free flame retardant system for epoxy resins. *Polymer Degradation and Stability*, 2005, 88(1), 70-73.

[23] Wu, Q., Lü, J., & Qu, B. Preparation and characterization of microcapsulated red

phosphorus and its flame-retardant mechanism in halogen-free flame retardant polyolefins. *Polymer international*, 2003, 52(8), 1326-1331.

[24] May, P. J. Performance-based regulation and regulatory regimes: The saga of leaky buildings. *Law & Policy*, 2003, 25(4), 381-401.

[25] Joel John, Deerfield Beach. Flame Retardant Chemicals (Aluminum Trihydrate (ATH), Antimony Oxides, Bromine, Chlorine, Organophosphorus and Others) Market for Building & Construction, Electronics, Automotive & Transportation, Wires & Cables, Textiles, and Other End-users: Global Industry Perspective, Comprehensive Analysis, and Forecast, 2014-2020. Zion Research Analysis, 2015.

[26] Lomakin, S. M., & Zaikov, G. E. Ecological aspects of polymer flame retardancy (Vol. 10). Vsp. 1999.

[27] FLAMERETARDANTS-ONLINE[<https://www.flameretardants-online.com/flameretardants/market>; accessed in November 2016]

[28] Hoh, E., Zhu, L., & Hites, R. A. Dechlorane Plus, a chlorinated flame retardant, in the Great Lakes. *Environmental science & technology*, 2006, 40(4), 1184-1189.

[29] Covaci, A., Harrad, S., Abdallah, M. A. E., Ali, N., Law, R. J., Herzke, D., & de Wit, C. A. Novel brominated flame retardants: a review of their analysis, environmental fate and behaviour. *Environment international*, 2011, 37(2), 532-556.

[30] Hakk, H., & Letcher, R. J. Metabolism in the toxicokinetics and fate of brominated flame retardants-a review. *Environment international*, 2003, 29(6), 801-828.

[31] Miller, J. A., & Melius, C. F. Kinetic and thermodynamic issues in the formation of aromatic compounds in flames of aliphatic fuels. *Combustion and Flame*, 1992, 91(1), 21-39.

[32] Namieśnik, J., Jastrzebska, A., & Zygmunt, B. Determination of volatile aliphatic amines in air by solid-phase microextraction coupled with gas chromatography with flame ionization detection. *Journal of Chromatography A*, 2003, 1016(1), 1-9.

[33] Tomy, G. T., Pleskach, K., Arsenault, G., Potter, D., McCrindle, R., Marvin, C. H., ... & Tittlemier, S. Identification of the novel cycloaliphatic brominated flame retardant 1,

-
- 2-dibromo-4-(1, 2-dibromoethyl) cyclohexane in Canadian Arctic beluga (Delphinapterus leucas). *Environmental science & technology*, 2007, 42(2), 543-549.
- [34] Troitzsch, J. H. Overview of flame retardants. *Chemistry Today*, 16, 1998.
- [35] Marinov, N. M., Pitz, W. J., Westbrook, C. K., Castaldi, M. J., & Senkan, S. M. Modeling of aromatic and polycyclic aromatic hydrocarbon formation in premixed methane and ethane flames. *Combustion Science and Technology*, 1996, 116(1-6), 211-287.
- [36] Laoutid, F., Bonnaud, L., Alexandre, M., Lopez-Cuesta, J. M., & Dubois, P. New prospects in flame retardant polymer materials: from fundamentals to nanocomposites. *Materials Science and Engineering: R: Reports*, 2009, 63(3), 100-125.
- [37] La Guardia, M. J., & Hale, R. C. Halogenated flame-retardant concentrations in settled dust, respirable and inhalable particulates and polyurethane foam at gymnastic training facilities and residences. *Environment international*, 2015, 79, 106-114.
- [38] Zhang, S., & Horrocks, A. R. A review of flame retardant polypropylene fibres. *Progress in Polymer Science*, 2003, 28(11), 1517-1538.
- [39] Georlette, P., Simons, J., & Costa, L. Halogen-containing fire-retardant compounds. *Fire retardancy of polymeric materials*, 2000, 245-284.
- [40] Georlette, P. Applications of halogen flame retardants. *Fire retardant materials*, 2001, 264-292.
- [41] Zhang, S., & Horrocks, A. R. A review of flame retardant polypropylene fibres. *Progress in Polymer Science*, 2003, 28(11), 1517-1538.
- [42] Stapleton, H. M., Alaei, M., Letcher, R. J., & Baker, J. E. (2004). Debromination of the flame retardant decabromodiphenyl ether by juvenile carp (*Cyprinus carpio*) following dietary exposure. *Environmental Science & Technology*, 2004, 38(1), 112-119.
- [43] Covaci, A., Voorspoels, S., Abdallah, M. A. E., Geens, T., Harrad, S., & Law, R. J. Analytical and environmental aspects of the flame retardant tetrabromobisphenol-A and its derivatives. *Journal of Chromatography A*, 2009, 1216(3), 346-363.
- [44] Letcher, R. Hexabromocyclododecane (HBCD) flame retardant in the environment,

-
- biota and humans: Stereoisomeric paradox. *Toxicology Letters*, 2010, 196, S33.
- [45] Levchik, S. V., & Weil, E. D. Flame retardancy of thermoplastic polyesters-a review of the recent literature. *Polymer International*, 2005, 54(1), 11-35.
- [46] Pullen, S., Boecker, R., & Tiegs, G. The flame retardants tetrabromobisphenol A and tetrabromobisphenol A-bisallylether suppress the induction of interleukin-2 receptor α chain (CD25) in murine splenocytes. *Toxicology*, 2003, 184(1), 11-22.
- [47] Brehme, S., Schartel, B., Goebbels, J., Fischer, O., Pospiech, D., Bykov, Y., & Döring, M. Phosphorus polyester versus aluminium phosphinate in poly (butylene terephthalate)(PBT): flame retardancy performance and mechanisms. *Polymer Degradation and Stability*, 2011, 96(5), 875-884.
- [48] Farrall, M. J., & Frechet, J. M. Bromination and lithiation: Two important steps in the functionalization of polystyrene resins. *The Journal of Organic Chemistry*, 1976, 41(24), 3877-3882.
- [49] Meerts, I. A., Van Zanden, J. J., Luijckx, E. A., van Leeuwen-Bol, I., Marsh, G., Jakobsson, E., ... & Brouwer, A. Potent competitive interactions of some brominated flame retardants and related compounds with human transthyretin in vitro. *Toxicological Sciences*, 2000, 56(1), 95-104.
- [50] Birnbaum, L. S., & Staskal, D. F. Brominated flame retardants: cause for concern? *Environmental health perspectives*, 2004, 112(1), 9.
- [51] Darnerud, P. O. Toxic effects of brominated flame retardants in man and in wildlife. *Environment international*, 2003, 29(6), 841-853.
- [52] La Guardia, M. J., Hale, R. C., & Harvey, E. Detailed polybrominated diphenyl ether (PBDE) congener composition of the widely used penta-, octa-, and deca-PBDE technical flame-retardant mixtures. *Environmental science & technology*, 2006, 40(20), 6247-6254.
- [53] Rogers, M. D. The European Commission's White Paper "strategy for a future chemicals policy": a review. *Risk Analysis*, 2003, 23(2), 381-388.
- [54] Nordbeck, R., & Faust, M. European chemicals regulation and its effect on

innovation: an assessment of the Eu's White Paper on the strategy for a future chemicals policy. *European Environment*, 2003, 13(2), 79-99.

[55] Sain, M., Park, S. H., Suhara, F., & Law, S. Flame retardant and mechanical properties of natural fibre-PP composites containing magnesium hydroxide. *Polymer Degradation and Stability*, 2004, 83(2), 363-367.

[56] Schartel, B., Knoll, U., Hartwig, A., & Pütz, D. Phosphonium - modified layered silicate epoxy resins nanocomposites and their combinations with ATH and organo - phosphorus fire retardants. *Polymers for advanced technologies*, 2006, 17(4), 281-293.

[57] Lewin, M., & Endo, M. Catalysis of intumescent flame retardancy of polypropylene by metallic compounds. *Polymers for Advanced Technologies*, 2003, 14(1), 3-11.

[58] Cárdenas, M. A., García-López, D., Gobernado-Mitre, I., Merino, J. C., Pastor, J. M., Martínez, J. D. D., ... & Calveras, D. Mechanical and fire retardant properties of EVA/clay/ATH nanocomposites—Effect of particle size and surface treatment of ATH filler. *Polymer Degradation and Stability*, 2008, 93(11), 2032-2037.

[59] Rother, R. N., & Hornsby, P. R. (1996). Flame retardant effects of magnesium hydroxide. *Polymer Degradation and Stability*, 1996, 54(2), 383-385.

[60] Paduani, C., & Rappe, A. M. Design of New Complexes of Inorganic Salts Based on Lithium and Magnesium Hydroxides and Carbonates for Usage as Propellants and Flame Retardants. *The Journal of Physical Chemistry A*, 2016, 120(39), 7764-7770.

[61] Innes, J., & Innes, A. Compounding metal hydrate flame retardants. *Plastics, Additives and Compounding*, 2002, 4(4), 22-26.

[62] Liu, X. Q., Liu, J. Y., & Cai, S. J. Comparative study of aluminum diethylphosphinate and aluminum methylethylphosphinate-filled epoxy flame-retardant composites. *Polymer Composites*, 2012, 33(6), 918-926.

[63] Yang, W., Song, L., Hu, Y., Lu, H., & Yuen, R. K. Enhancement of fire retardancy performance of glass-fibre reinforced poly (ethylene terephthalate) composites with the incorporation of aluminum hypophosphite and melamine cyanurate. *Composites Part B:*

Engineering, 2011, 42(5), 1057-1065.

[64] Tang, G., Wang, X., Xing, W., Zhang, P., Wang, B., Hong, N., ... & Song, L. Thermal degradation and flame retardance of biobased polylactide composites based on aluminum hypophosphite. *Industrial & Engineering Chemistry Research*, 2012, 51(37), 12009-12016.

[65] Zhou, X., Li, J., & Wu, Y. Synergistic effect of aluminum hypophosphite and intumescent flame retardants in polylactide. *Polymers for Advanced Technologies*, 2015, 26(3), 255-265.

[66] Horacek, H., & Grabner, R. Advantages of flame retardants based on nitrogen compounds. *Polymer Degradation and Stability*, 1996, 54(2), 205-215.

[67] Gaan, S., Sun, G., Hutches, K., & Engelhard, M. H. Effect of nitrogen additives on flame retardant action of tributyl phosphate: phosphorus–nitrogen synergism. *Polymer Degradation and Stability*, 2008, 93(1), 99-108.

[68] Yang, S., Wang, J., Huo, S., Wang, J., & Tang, Y. Synthesis of a phosphorus/nitrogen-containing compound based on maleimide and cyclotriphosphazene and its flame-retardant mechanism on epoxy resin. *Polymer Degradation and Stability*, 2016, 126, 9-16.

[69] Martin, C., Ronda, J. C., & Cadiz, V. Boron-containing novolac resins as flame retardant materials. *Polymer Degradation and Stability*, 2006, 91(4), 747-754.

[70] Doğan, M., Yılmaz, A., & Bayramlı, E. Synergistic effect of boron containing substances on flame retardancy and thermal stability of intumescent polypropylene composites. *Polymer Degradation and Stability*, 2010, 95(12), 2584-2588.

[71] Timberlake, L. D., Hanson, M. V., Subramaniam, N., & Fielding, W. R. U.S. Patent No. 8,895,648. Washington, DC: U.S. Patent and Trademark Office. 2014.

[72] Sun, D., & Yao, Y. Synthesis of three novel phosphorus-containing flame retardants and their application in epoxy resins. *Polymer degradation and stability*, 2011, 96(10), 1720-1724.

[73] Green, J. Phosphorus-containing flame retardants. *Fire retardancy of polymeric*

materials, 2000, 147-170.

[74] Levchik, S. V., & Weil, E. D. A review of recent progress in phosphorus-based flame retardants. *Journal of Fire Sciences*, 2006, 24(5), 345-364.

[75] Salmeia, K. A., & Gaan, S. An overview of some recent advances in DOPO-derivatives: chemistry and flame retardant applications. *Polymer Degradation and Stability*, 2015, 113, 119-134.

[76] Kim, W., Hoang, D., Vothi, H., Nguyen, C., Giang, T., An, H., & Kim, J. Synthesis, flame retardancy, and thermal degradation behaviors of novel organo-phosphorus compounds derived from 9, 10-dihydro-9-oxa-10-phosphaphenanthrene-10-oxide (DOPO). *Macromolecular Research*, 2016, 24(1), 66-73.

[77] Chen, M., & Graedel, T. E. A half-century of global phosphorus flows, stocks, production, consumption, recycling, and environmental impacts. *Global Environmental Change*, 2016, 36, 139-152.

[78] Lai, X., Tang, S., Li, H., & Zeng, X. Flame-retardant mechanism of a novel polymeric intumescent flame retardant containing caged bicyclic phosphate for polypropylene. *Polymer Degradation and Stability*, 2015, 113, 22-31.

[79] Fu, M., & Qu, B. Synergistic flame retardant mechanism of fumed silica in ethylene-vinyl acetate/magnesium hydroxide blends. *Polymer Degradation and Stability*, 2004, 85(1), 633-639.

[80] Zhao, C. X., Liu, Y., Wang, D. Y., Wang, D. L., & Wang, Y. Z. Synergistic effect of ammonium polyphosphate and layered double hydroxide on flame retardant properties of poly (vinyl alcohol). *Polymer Degradation and Stability*, 2008, 93(7), 1323-1331.

[81] Wang, H. Formation of nascent soot and other condensed-phase materials in flames. *Proceedings of the Combustion Institute*, 2011, 33(1), 41-67.

[82] Scharrel, B., Perret, B., Dittrich, B., Ciesielski, M., Krämer, J., Müller, P., Altstädt, V., Zang, L., & Döring, M. Flame retardancy of polymers: the role of specific reactions in the condensed phase. *Macromolecular Materials and Engineering*, 2016, 301(1), 9-35.

[83] Morgan, A. B., & Wilkie, C. A. (Eds.). Flame retardant polymer nanocomposites.

John Wiley & Sons, 2007.

[84] S. Todaka, O. Masayuki. Optimum prescription of flame retardant and burning test. Technical Information Institute, 2011.

[85] Ajayan, P. M., Schadler, L. S., & Braun, P. V. Nanocomposite science and technology. John Wiley & Sons, 2006.

[86] Tanaka, T., Montanari, G. C., & Mulhaupt, R. Polymer nanocomposites as dielectrics and electrical insulation-perspectives for processing technologies, material characterization and future applications. *IEEE Transactions on Dielectrics and Electrical Insulation*, 2004, 11(5), 763-784.

[87] Winey, K. I., & Vaia, R. A. Polymer nanocomposites. *MRS bulletin*, 2007, 32(04), 314-322.

[88] Morgan, A. B., & Wilkie, C. A. (Eds.). Flame retardant polymer nanocomposites. John Wiley & Sons, 2007.

[89] Kashiwagi, T., Harris, R. H., Zhang, X., Briber, R. M., Cipriano, B. H., Raghavan, S. R., ... & Shields, J. R. Flame retardant mechanism of polyamide 6–clay nanocomposites. *Polymer*, 2004, 45(3), 881-891.

[90] Yang, F., & Nelson, G. L. Combination effect of nanoparticles with flame retardants on the flammability of nanocomposites. *Polymer Degradation and Stability*, 2011, 96(3), 270-276.

[91] Gao, Y., Wu, J., Wang, Q., Wilkie, C. A., & O'Hare, D. Flame retardant polymer/layered double hydroxide nanocomposites. *Journal of Materials Chemistry A*, 2014, 2(29), 10996-11016.

[92] Xing, W., Yang, W., Yang, W., Hu, Q., Si, J., Lu, H., ... & Yuen, R. K. Functionalized Carbon Nanotubes with Phosphorus-and Nitrogen-Containing Agents: Effective Reinforcer for Thermal, Mechanical, and Flame-Retardant Properties of Polystyrene Nanocomposites. *ACS Applied Materials & Interfaces*, 2016, 8(39), 26266-26274.

Chapter 2 Materials, Experiment and Characterizations

2.1 Materials

2.1.1 9, 10-dihydro-9-oxa-10-phosphaphenanthrene 10-oxide (DOPO)

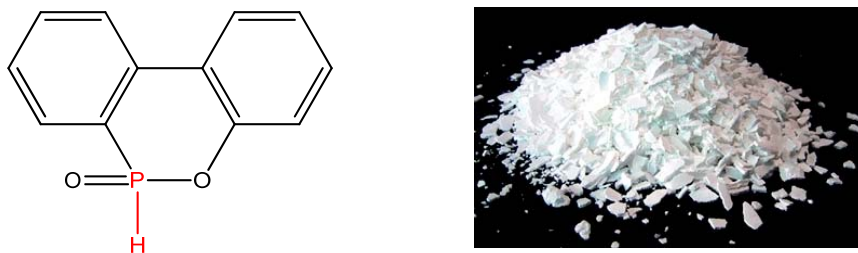
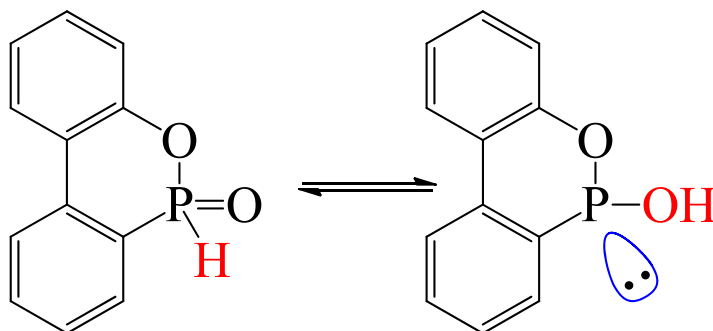


Fig. 2-1 SEM (left) and photo (right) of DOPO.

DOPO was purchased from Eutec trading (Shanghai) Co., Ltd., China. It was purified by recrystallization from absolute ethanol. And its structure and statement are shown in Fig. 2-1.



Scheme 2-1. The tautomeric equilibrium of DOPO.

DOPO is an H-Phosphonate compound that can tautomerize to its P—OH form in a solution (Scheme 2-1). Owing to tautomeric equilibrium between the species 1a and 1b, the phosphorus atom in DOPO can be reactive toward nucleophiles and electrophiles [1]. H-Phosphonates compared to phosphines are stable toward oxygen owing to the presence of the phosphoryl group (P=O). Accordingly, the form 1a in a solution is considered to be the dominant species and it is predicted that 1a species determines the overall reactivity. This equilibrium is also affected by the electronic properties of the substituents

around the phosphorus atom, which may shift the equilibrium to the right [2]. Due this property, DOPO-derivatives and its analogs can be prepared via different synthetic approaches. Fig. 3 shows the FTIR spectrum of DOPO. The P—H stretching vibration can be clearly observed at 2437 cm^{-1} . And the other absorption peaks corresponding to the structure of DOPO are list as follows.

FTIR (KBr) : 925 cm^{-1} , 1234 cm^{-1} (P—O—Ph); 1033 cm^{-1} (Ph—O—C); 1206 cm^{-1} (P=O); 1514 cm^{-1} , 3367 cm^{-1} (N—H); 1594 cm^{-1} (P—Ph); 3510 cm^{-1} (O—H) [3].

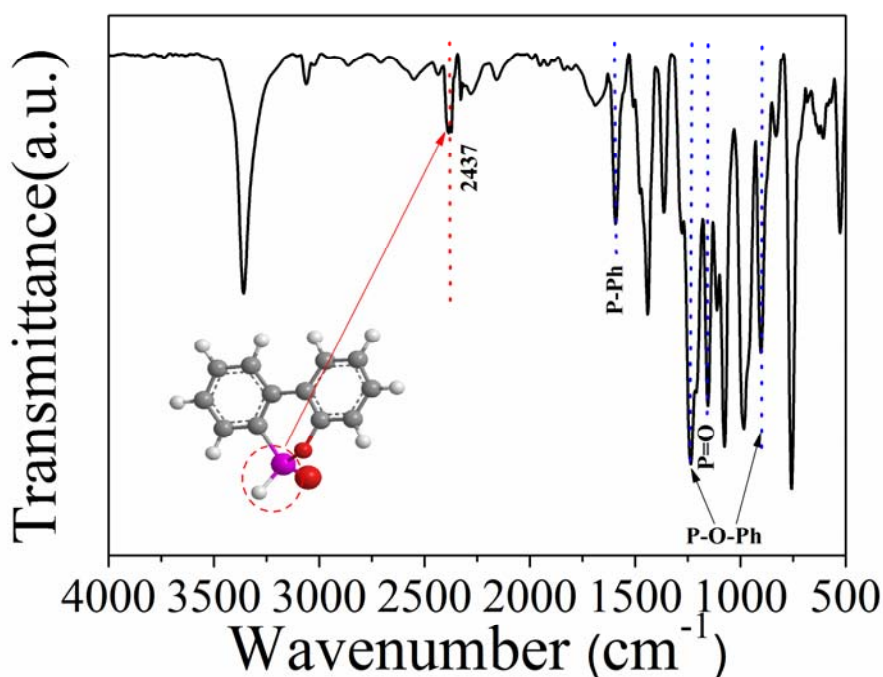
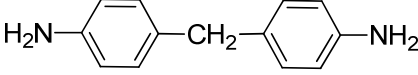
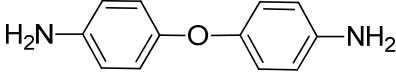
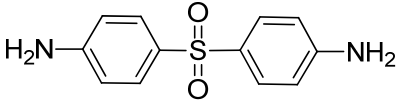


Fig. 2-2 FT-IR spectrum of DOPO.

2.1.2 DDM, DDE and DDS

4,4'-Methylenedianiline (DDM), 4,4'-oxydianiline (DDE), 4,4'-diaminodiphenylsulfone (DDS) are usually used as hardeners in epoxy resins and adhesives, as well as in the production of high-performance polymers. Curing agents play an important role in the curing process of epoxy resin because they relate to the curing kinetics, reaction rate, gel time, degree of cure, viscosity, curing cycle, and the final properties of the cured products.

Tab.2-1 Chemical structure of DDM, DDE and DDS.

Compounds	Chemical structure
DDM	
DDE	
DDS	

In this work, 4,4'-methylenedianiline (DDM), 4,4'-oxydianiline (DDE), 4,4'-diaminodiphenylsulfone (DDS) from Tokyo Chemical Industry Co., Ltd., were used as received.

2.1.3 Multi-walled carbon nanotubes (MWCNTs)

MWCNTs were obtained from Showa Denko Company, Tokyo, Japan, and they are special carbon nanotubes for resin composites. MWCNTs, the Vapor Grown Carbon Fiber (VGCF[®]-X), are synthesized by catalytic chemical vapor deposition method. The average diameter of MWCNTs is approximately 10-12 nm. The parameters of MWCNTs are shown in Table 2-2, and the structure is shown in Fig. 2-3. MWCNTs can give electrical conductivity to insulating resin and rubber when quite a small amount, less than 3 wt% of MWCNTs is added to them. MWCNTs are used for electrical-conductive, electrostatic-dissipative, or antistatic polymer composites as raw material of molded packages and parts, which should be electrically conductive, in electric, electronic and automotive application fields [4].

Tab. 2-2 Parameters of MWCNTs.

parameters	Unit	Value
Average diameter	nm	10-12
Average length	μm	3
Bulk density	g/cm ³	0.08

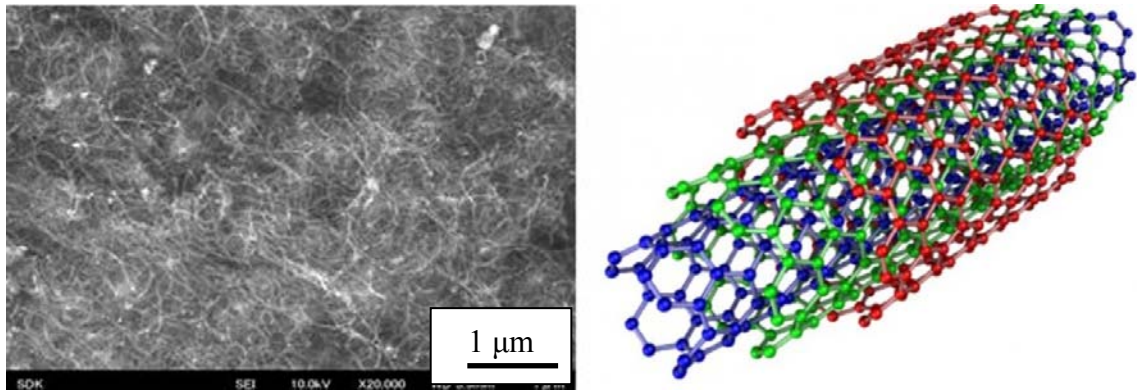


Fig. 2-3 SEM (left) images and Chemical structure (right) of MWCNTs.

Because of unique structure, mechanical and electrical properties of MWCNTs, they have attracted more and more interest for wide applications, such as in the field of electrical conductivity, mechanical strength and thermal conductivity as shown in Fig. 2-4 [5].

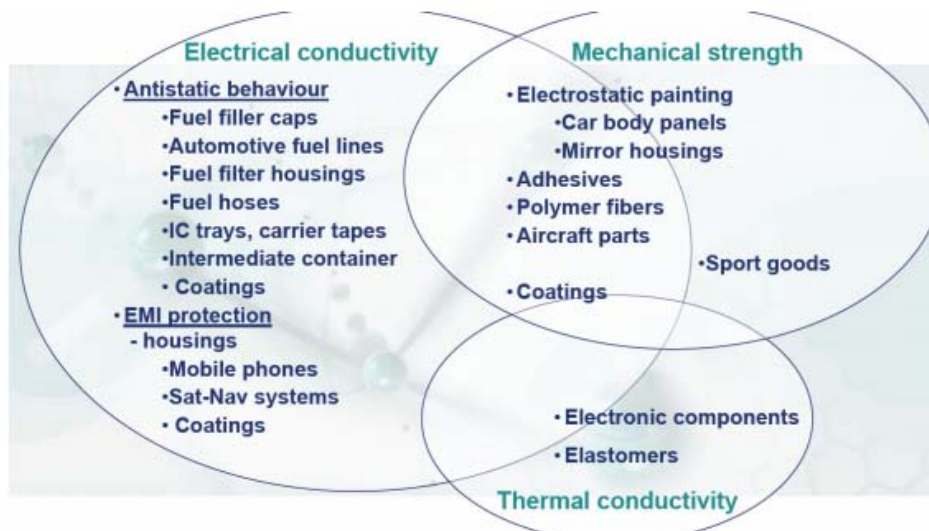


Fig. 2-4 Key properties and potential applications of MWCNTs.

2.1.4 Bisphenol-A diglycidyl ether E51 (DGEBA)

Diglycidyl ether of bisphenol-A (DGEBA) is commonly used epoxy resin, which is characterized by two epoxy groups. Chemical structure of DGEBA is given in Figure 2-5. The chemical nature and the amount used of curing agents or hardeners plays an important role in determining thermomechanical properties of the epoxy resin composites.

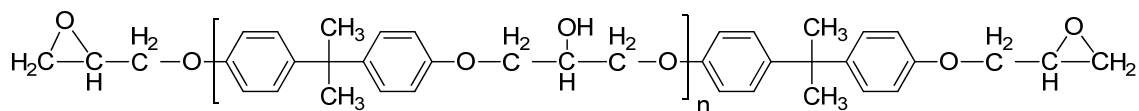


Fig. 2-5 Chemical structure of DGEBA.

2.1.5 Poly(lactic acid) (PLA)

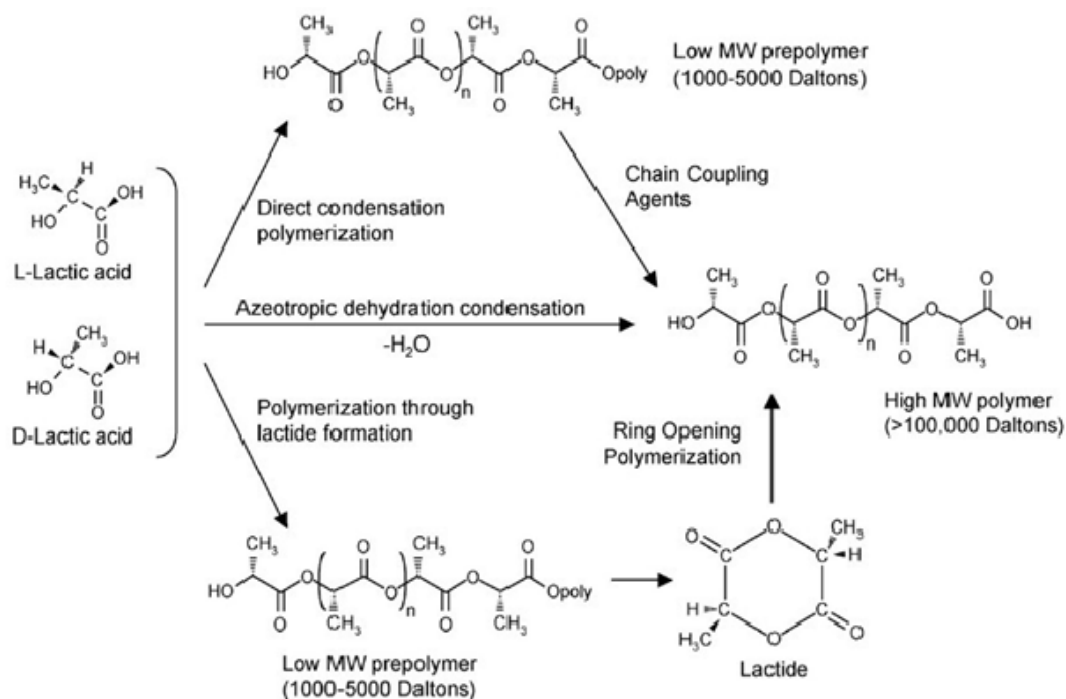


Fig. 2-6 Synthesis methods for obtaining PLA.

Poly(lactic acid) or polylactide (PLA) is aliphatic biodegradable polyester made up of lactic acid (2-hydroxy propionic acid). PLA is a thermoplastic aliphatic polyester derived from renewable resources, such as corn starch (in the United States), tapioca roots, chips or starch (mostly in Asia), or sugarcane (in the rest of the world). Owing to PLA can biodegrade under certain conditions, such as the presence of oxygen, it has been considered as one of the solutions to alleviate white waste disposal problems and to lessen the dependence on petroleum-based plastics for packaging materials.

PLA can be produced using several techniques, including azeotropic dehydrative condensation, direct condensation polymerization and polymerization through lactic acid formation which is pressed in Fig. 2-6.

Poly(lactic acid) (Ingeo 3001D) in pellet form was supplied by NatureWorks LLC, the

biopolymer, is designed for injection molding applications. It is designed for clear applications with heat deflection temperatures lower than 120 °F (49 °C). The properties of PLA are given in Tab. 2-3.

Tab. 2-3 Properties of PLA.

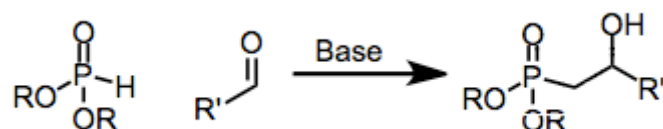
Properties	Unit	Value
Specific gravity	g/cm ³	1.24
MFR	g/10 min (210 °C, 2.16 kg)	22
Tensile yield strength	MPa	62
Tensile elongation	%	3.5
Notched izod impact	J/m	16
Flexural strength	MPa	108
Flexural modulus	MPa	3600
Heat distortion temperature	°C	55

2.2 Experiment methods

2.2.1 Pudovik reaction

The Pudovik reaction is the related conversions of trialkyl and dialkyl phosphites (respectively) to α -hydroxy phosphonates in the presence of carbonyl compounds.

The Pudovik reaction employs dialkyl phosphites under basic conditions, which add to carbonyl compounds upon deprotonation to yield α -hydroxy phosphonates (Scheme 2-2). Group transfer is not necessary in this case, as neutralization of the tetrahedral intermediate occurs via proton transfer. A catalytic, enantioselective variant of the Pudovik reaction has recently been developed.



Scheme 2-2 The Pudovik reaction.

Phosphites add reversibly to the carbonyl carbon of simple carbonyl compounds. Under mild conditions, reversion to the starting materials is faster than both inter- and intramolecular alkyl group transfer—the four-center transition state for intramolecular transfer exhibits poor orbital overlap [6]. Transfer can be facilitated under conditions of high temperature or pressure. If two equivalents of aldehyde are used, addition of the tetrahedral intermediate to a second molecule of aldehyde leads either to cyclic phosphoranes 1 or linear alkyl transfer products 2. More practical is the use of silylated phosphorus sources, which undergo intramolecular silyl group transfer in a frontside fashion, providing α -siloxy phosphorus compounds 3.

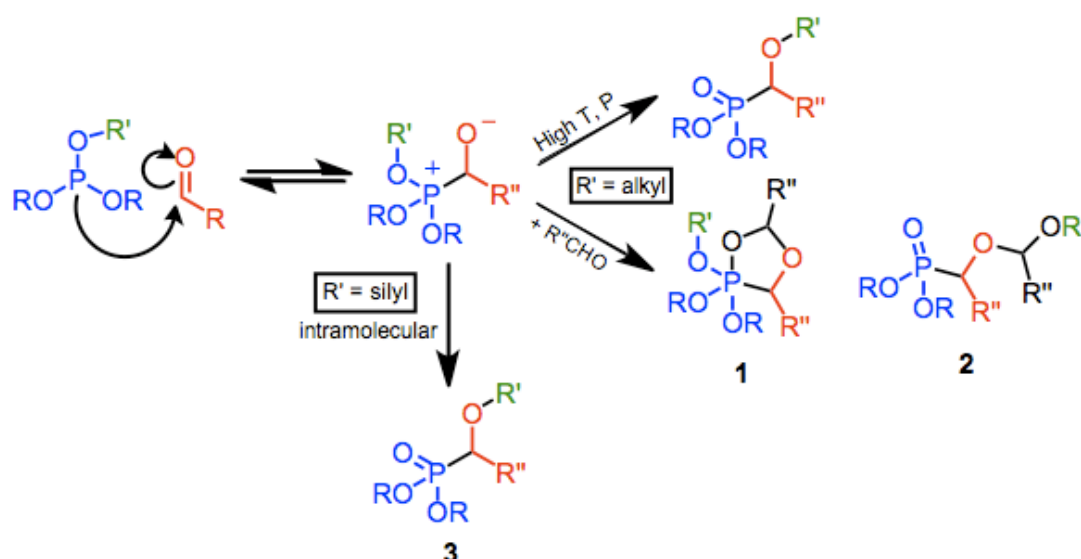


Fig. 2-7 Prevailing Mechanism for Pudovik reaction.

2.2.2 Functionalizing MWCNTs

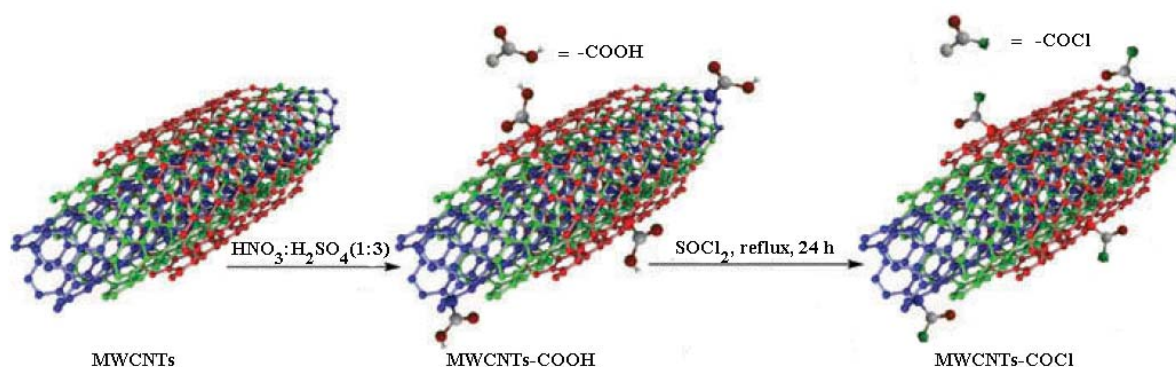


Fig. 2-8 Schematic illustration for the synthesis of MWNT-Cl.

This study aims to graft DOPO-containing flame retardant onto multiwalled carbon nanotubes (MWNTs) and prepare according nanocomposites. It is anticipated that the covalent attachment of DOPO-containing flame retardant onto MWNTs can improve both solubility and flame retardancy of MWNTs, thus promote the development of a new kind of flame retardant polymer/MWNTs nanocomposites.

The obtained MWNTs was purified and shortened with a mixture of nitric acid and sulfuric acid (1 : 3 by volume) in ultrasonic bath at 50 °C for 4 h. The excess acid was washed thoroughly with deionized water until the pH value of water was about 7. The acid-treated MWNTs (MWNTs-COOH) were dried at 80 °C in a vacuum oven overnight and then grinded into powder with a carnelian mortar. The mixture of MWNTs-COOH, thionyl chloride (SOCl₂) and N,N-dimethylformamide (DMF) (a typical ratio of a-MWNTs:SOCl₂:DMF is 100 mg : 20 ml : 1 ml) was dispersed in ultrasonic bath for about 2 h and refluxed at 80 °C for 24 h. Then unreacted SOCl₂ was removed by distillation and the remained black solid (MWNTs-COCl) was dried at room temperature under vacuum [7]. The synthesis routes of the MWNTs-COCl samples are shown in Figure 2-8.

2.2.3 Curing of epoxy resin

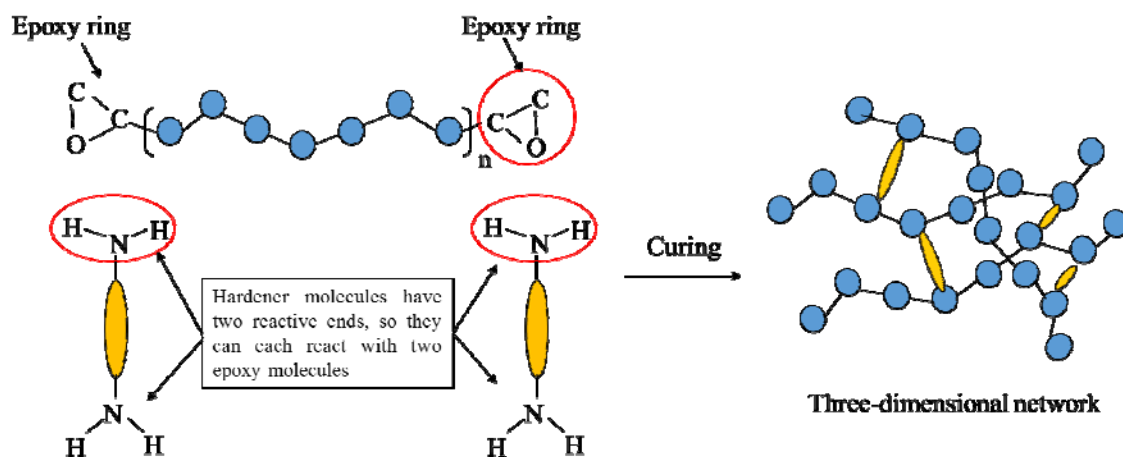


Fig. 2-9 Curing reaction of epoxy resin.

The curing process of epoxy resin is a chemical reaction in which the epoxide groups in

epoxy resin reacts with a curing agent (hardener) to form a highly crosslinked, three-dimensional network. In order to convert epoxy resins into a hard, infusible, and rigid material, it is necessary to cure the resin with hardener. Epoxy resins cure quickly and easily at practically any temperature from 5-150 oC depending on the choice of curing agent (Fig. 2-9).

Mixing epoxy resin and hardener begins a chemical reaction that transforms the combined liquid ingredients to a solid. The time it takes for this transformation is the cure time. As it cures, the epoxy passes from the liquid state, through a gel state, before it reaches a solid state (Figure 2-10) [8].

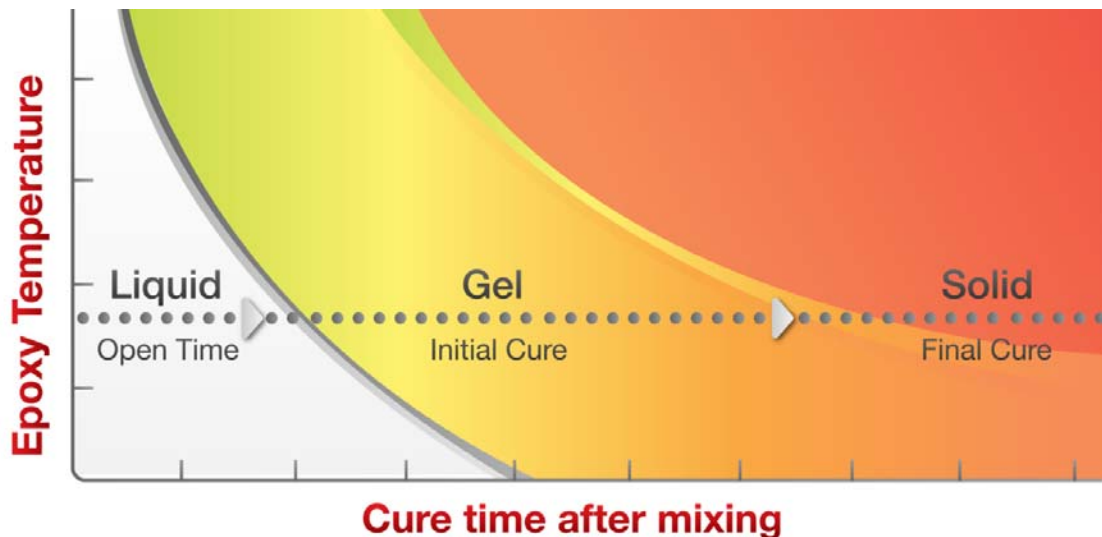


Fig. 2-10 Curing process of epoxy resin [8].

Liquid-Open time

Open time (also working time or wet lay-up time) is the portion of the cure time, after mixing, that the resin/hardener mixture remains a liquid and is workable and suitable for application. All assembly and clamping should take place during the open time to assure a dependable bond

Gel-Initial cure

The mixture passes into an initial cure phase (also called the green stage) when it begins to gel or "kick-off." The epoxy is no longer workable and will progress from a tacky, gel consistency to the firmness of hard rubber, which you will be dent with your

thumbnail.

Because the mixture is only partially cured, a new application of epoxy will still chemically link with it, so the surface may still be bonded to or recoated without special preparation. However, this ability diminishes as the mixture approaches final cure.

Solid-Final cure

The epoxy mixture has cured to a solid state and can be dry sanded and shaped. You should not be able to dent it with your thumbnail. At this point the epoxy has reached about 90% of its ultimate strength, so clamps can be removed. It will continue to cure over the next several days at room temperature.

As it cures, mixed epoxy pass from a liquid state, through a gel state, to a solid state (Fig. 2-10).

2.2.4 General methods for testing of polymer materials flammability

(1) UL 94 vertical burning test

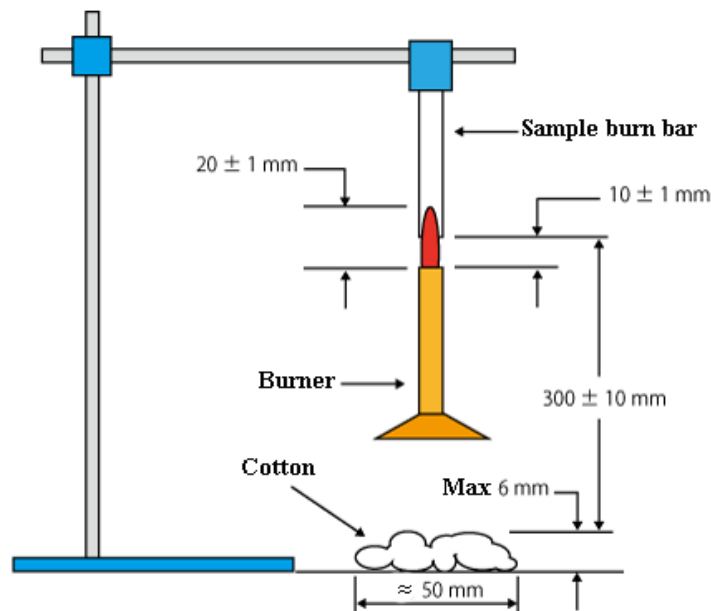


Fig. 2-11 Basic UL 94 vertical test apparatus [9].

The UL 94 test is perhaps the most frequently used small flame burner test. It provides an assessment of flammability for a variety of thermoplastic materials intended for use in

multiple applications in many market segments. The UL 94 standard actually contains several test methods. The most common method used is the vertical burn method where a test specimen (a bar of 13 mm by 125 mm by varying thickness) is ignited while suspended 10 mm above a calibrated methane (Bunsen) burner.

The flame is applied to a total of five test specimens twice for 10 seconds. The amount of burn time is recorded after each flame application for each test bar. Performance is described through one of three ratings, V0, V1 or V2 dependent on the number of seconds of after-flame burn time for each specimen, the total after-flame burn time for all specimens, the afterglow time, and the existence of flaming particles which may ignite a piece of cotton placed beneath the test specimens [9]. Figure 2-11 illustrates the basic UL 94 vertical test apparatus.

Tab. 2-5 UL 94 flammability rating [9].

Flammability rating UL 94			
Criteria Conditions	V-0	V-1	V-2
After flame time for each specimen t1 or t2	≤10	≤30	≤30
Total after flame time for any condition set (t1 + t2 for the 5 specimens)	≤50	≤250	≤250
After flame plus afterglow time for each individual specimen after the second flame application (t2 + t3)	≤30	≤60	≤60
After flame plus afterglow of any specimen up to the holding clamp	no	no	no
Cotton Indicator ignited by flame particles or drops	no	no	yes

It evaluates both the burning and afterglow times after repeated flame application and dripping of the burning test specimen.

(2) Limiting Oxygen Index (LOI) test

Another flammability test, one of the oldest still in use today, is the Limiting Oxygen Index (LOI) test (ASTMD 2863) [10]. Also widely used for multiple plastic materials, this test essentially measures the minimum amount of oxygen in a mixture of oxygen and

nitrogen that will just support combustion. Three test specimens (6.5 mm wide or half the width of the UL 94 test specimen) are evaluated using an apparatus designed specifically to imitate candle-like burning conditions.

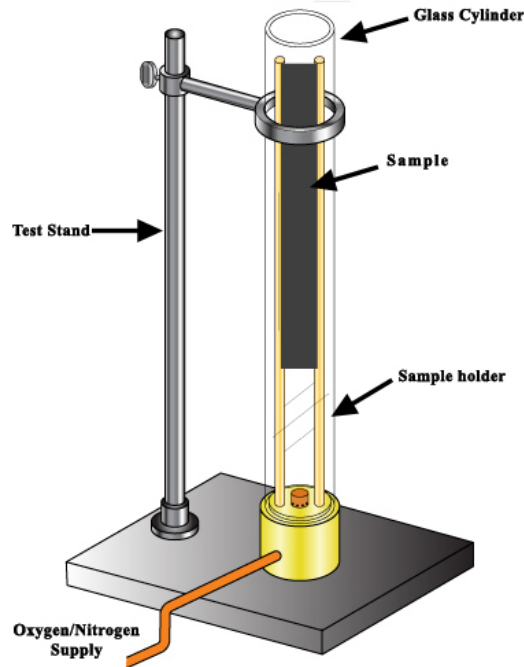


Fig. 2-12 Basic oxygen index test apparatus [10].

The result is actually a percentage. For example, an Oxygen Index test result of 30 indicates that 30% of the oxygen/nitrogen mixture was required to be oxygen in order to support continued combustion of the sample. This indicates a good degree of flame retardancy in the sample when one considers that our atmosphere on planet Earth contains approximately 21% oxygen. Theoretically then our test specimen would resist burning in a real fire scenario as atmospheric oxygen content does not change from that 21%. Figure 2-12 presents the basic Oxygen Index test apparatus.

2.3 Instruments and characteristics

2.3.1 Twin-screw extruder

The flame retardants and polymer matrix with the desired filler weight content are mixed. The mixtures are dried at 80 °C for 24h before extruding. The mixtures are

extruded using a twin-screw extruder (KZW15TW-30MG-NH (-700)-AKTP, Technovel Corporation, Japan) as shown in Fig. 2-13.



Fig. 2-13 The image of twin-screw extruder.

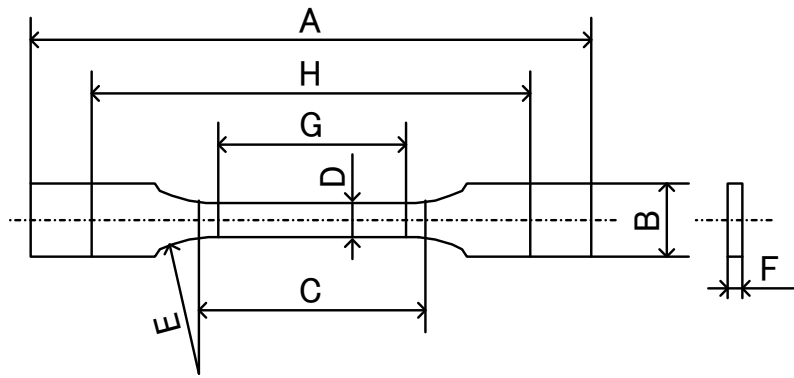
2.3.2 Injection molding machine

The extruding plates are formed into specimens using an injection molding machine (NP7-1F, Nissei Plastic Industrial Co., Ltd., Nagano, Japan) as shown in Fig.2-14.

The shape and measurement of tensile and Charpy impact test specimens are presented in Fig. 2-15 and Fig. 2-22, respectively.



Fig. 2-14 Injection molding machine.



unit: [mm]

A : whole length	75	E : radius	30
B : width	10	F : thickness	2
C : length of parallel	30	G : Fulcrum distance	25
D : width of parallel	5	H : grips distance	58±2

Fig. 2-15 Shape and measurement of tensile test specimens (JIS K 7113).

2.3.3 Rolling machine

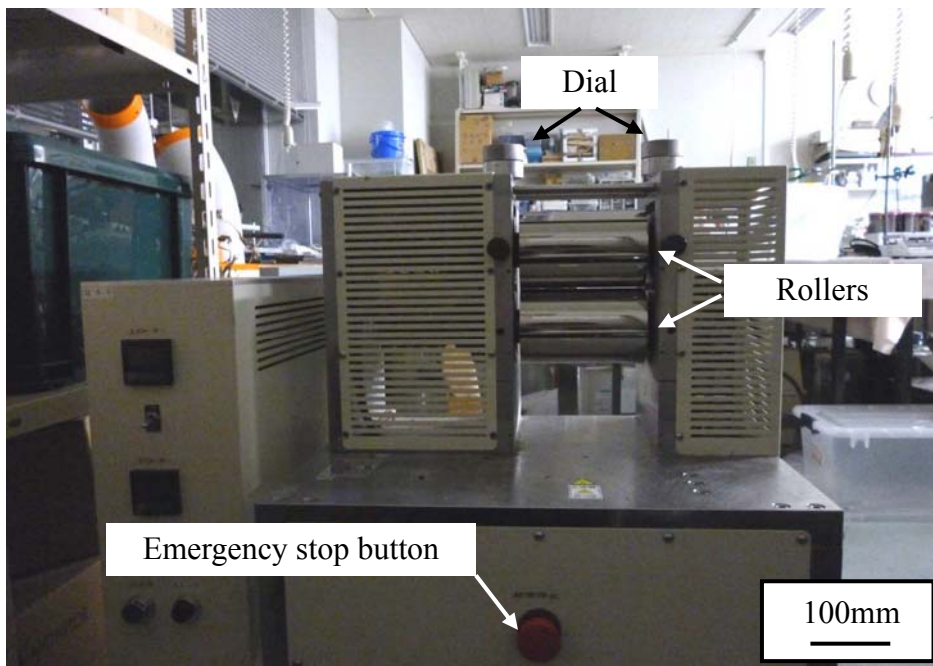


Fig. 2-16 Rolling machine.

The extruded flame retardant PLA nanocomposites were used for rolling process. The rolling process was performed with different rolling ratios ($\xi = 0\%$, 10%, 30%, 50, 70%)

to evaluate the effect of rolling ratio on the properties and morphology of flame retardant PLA nanocomposites. The rolling processing was carried out by a rolling machine (TKE-0; Imoto Machinery Co., Ltd., Japan) at room temperature (23 ± 2 °C) with the rotation speed of 3 m/min (shown in Fig. 2-17).

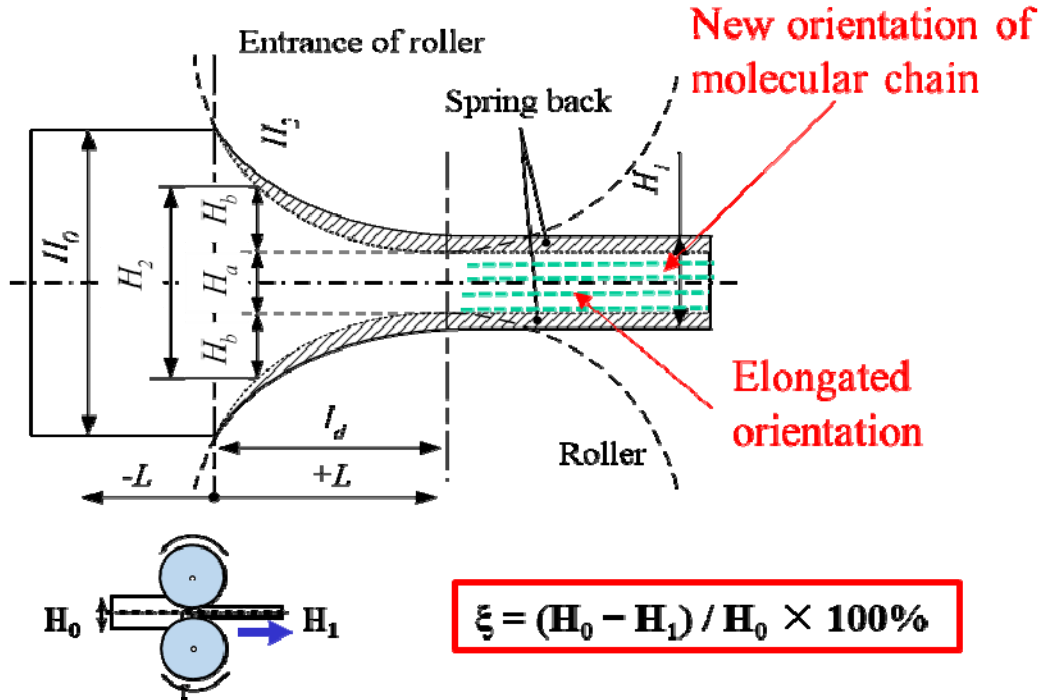


Fig. 2-17 Schematic drawing showing spring back and the definitions.

The rolling direction was matched to the extrusion direction and the effective width and diameter of each roller were 150 and 100 mm, respectively. The rolling ratio ξ was calculated by using the following equation

$$\xi = [(H_0 - H_1) / H_0] \times 100\% \quad (2-1)$$

Where, H_0 is the initial thickness of specimen (mm); H_1 is the thickness of rolled specimen (mm), which was measured by a micrometer after rolling process.

2.3.4 UL-94 vertical burning instrument

The Underwriter Laboratories 94 vertical tests (UL-94) were performed according to JIS C60695-11-10: 2006 (or IEC 60695-11-10:1999) using a horizontal and vertical burning instrument (FZ-5401, Dongguan Hanyang electronic instrument Co., Ltd, China) (Fig. 2-18).



Fig. 2-18 UL-94 vertical burning instrument.

2.3.5 Limiting oxygen index (LOI)

The *LOI* test was performed according to the testing procedure of JIS K7201-2:2007 (or ISO 4589-2:1996) using a horizontal and vertical burning instrument (HC-A2, Nanjing Jiangning Analytical instrument Co., Ltd, China) (Fig. 2-19). Test specimen bar is 7~15 cm in length, 6.5 ± 0.5 mm in width and 3.0 ± 0.5 mm in thickness



Fig. 2-19 Limiting oxygen index (LOI) test instrument.

2.3.6 Thermogravimetric analyses (TGA)

Thermogravimetric analyses (TGA) and differential thermal analyses (DTA) were carried out with Shimadzu DTG-60/60H from 30 °C to 600 °C at heating rates of 10 °C·min⁻¹, whereas the flow of nitrogen was maintained at 50 mL·min⁻¹.



Fig. 2-20 Thermal gravimetric analyses instrument.

2.3.7 Tensile test

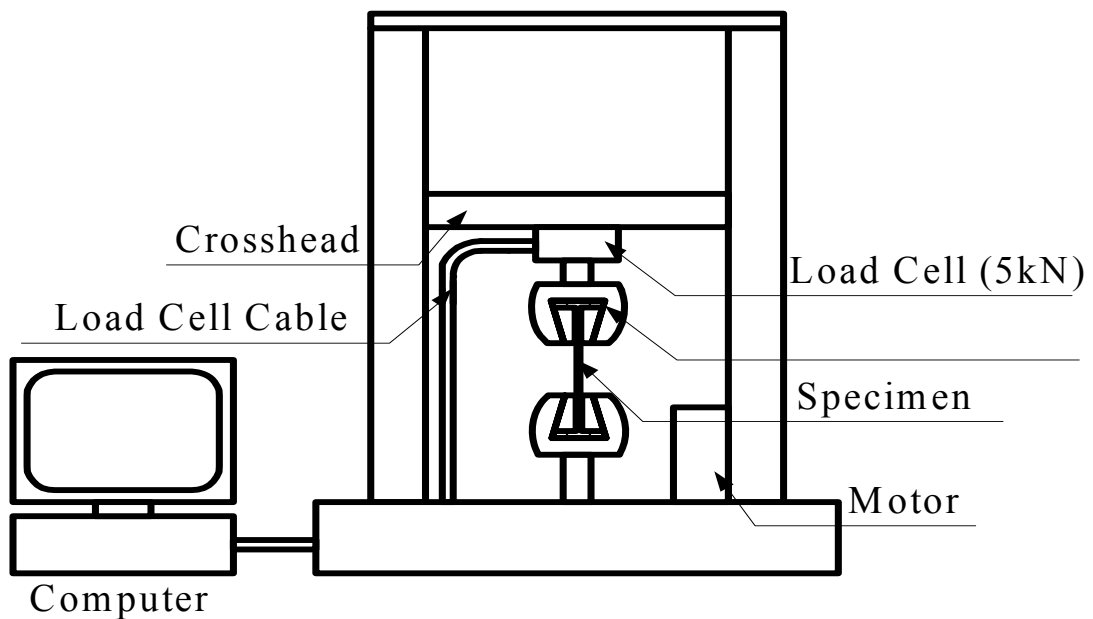


Fig. 2-13 Schematic of tensile test.

The tensile strength and modulus were measured according to JIS K7113 using a universal testing machine (Series 3360, Instron Co., Ltd., Canton, America) with a tensile speed of 10 mm/min. The specimen of tensile test is presented in Fig. 2-15 and the schematic of tensile test is presented in Fig. 2-21. The samples were placed for 48 h at room temperature ($23 \pm 2^\circ\text{C}$) and atmospheric conditions (relative humidity of $50 \pm 5\%$) before test.

2.3.8 Charpy impact test

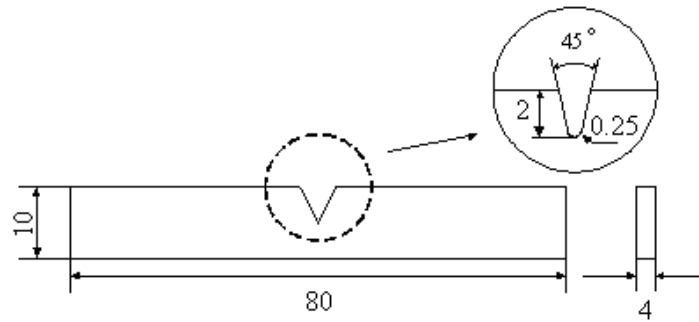


Fig. 2-22 Schematic of Charpy impact test specimens.

The izod impact strength are measured according to JIS K 7111-1:2012 (or ISO 179-1:2010) using a universal testing machine (U-F, Ueshima Seisakusho Co., Ltd., Japan) with a speed of 10 mm/min. The specimen of Charpy impact test is present in Fig. 2-22 and the schematic of bending test is presented in Fig. 2-23. The samples are placed for 48h at room temperature ($23 \pm 2^\circ\text{C}$) and atmospheric conditions (relative humidity of $\approx 50 \pm 5\%$) before test.

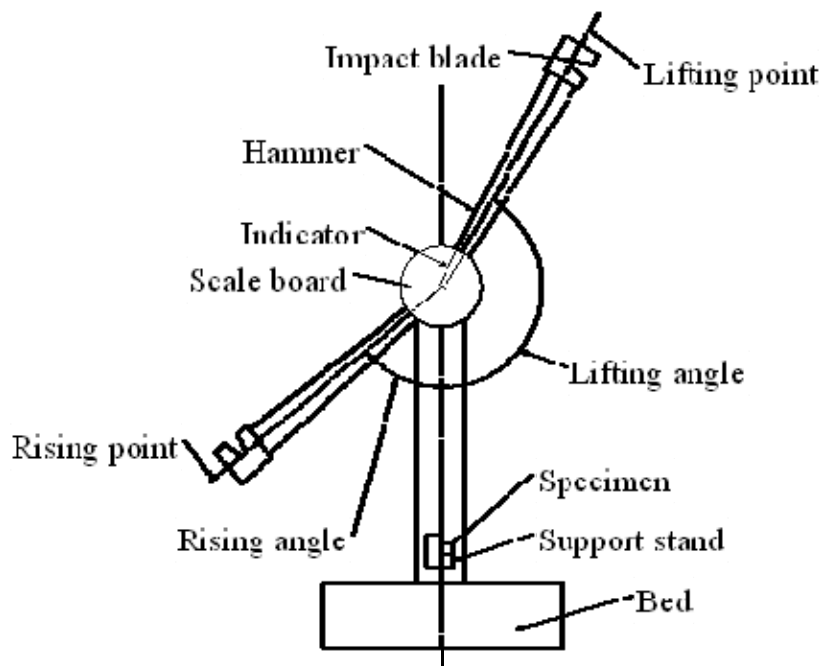


Fig. 2-23 Schematic of Charpy impact test.

The izod impact strength are obtained from formula 2-1. Where, E is the impact energy, b is the width of specimen (mm), t is the thickness of specimen (mm), d is the deepness of V-notch (mm).

$$a_{kc} = E / b(t-d) \quad (2-1)$$

$$E = WR\{(\cos\beta-\cos150^\circ)-(\cos\alpha-\cos150^\circ) [(150^\circ+\beta)/(150^\circ+\alpha)]\} \quad (2-2)$$

2.3.9 Dynamic mechanical analyzer (DMA)

A dynamic mechanical analyzer (RSA-G2, TA Instruments, Wilmington, USA, shown in Fig. 2-24) was used for the DMA of the flame retardant PLA nanocomposites, in which the storage modulus E' , the loss modulus E'' , and $\tan \delta$ (δ is defined as the phase lag between stress and strain) were determined. The clamping mode of the specimen was three-point bending and the span of the girder was 10 mm. The parallel part of the dumbbell shaped specimen was used for the measurements. The specimens were heated from 30 °C to 180 °C, and each specimen was subjected to the temperature scan mode at a programmed heating rate of 2 °C /min and a frequency of 1.0 Hz; the amplitude of strain was 0.1%.



Fig. 2-24 Dynamic mechanical analyzer (DMA) instrument.

2.4 Conclusions

In Chapter 3, three types of flame retardants were characterized by ^1H , ^{13}C and ^{31}P NMR spectroscopy, elemental analysis (EA), Fourier transform infrared (FT-IR) spectroscopy, Raman spectroscopy, X-ray photoelectron spectroscopy (XPS), TGA and TEM. The resultant flame retardants were introduced into epoxy resin and PLA to form flame retardant polymer composites. The performance of those composites were

investigated through non-flammability, thermal behaviors and mechnacial properties.

The experimental procedure was displayed as Fig. 2-25.

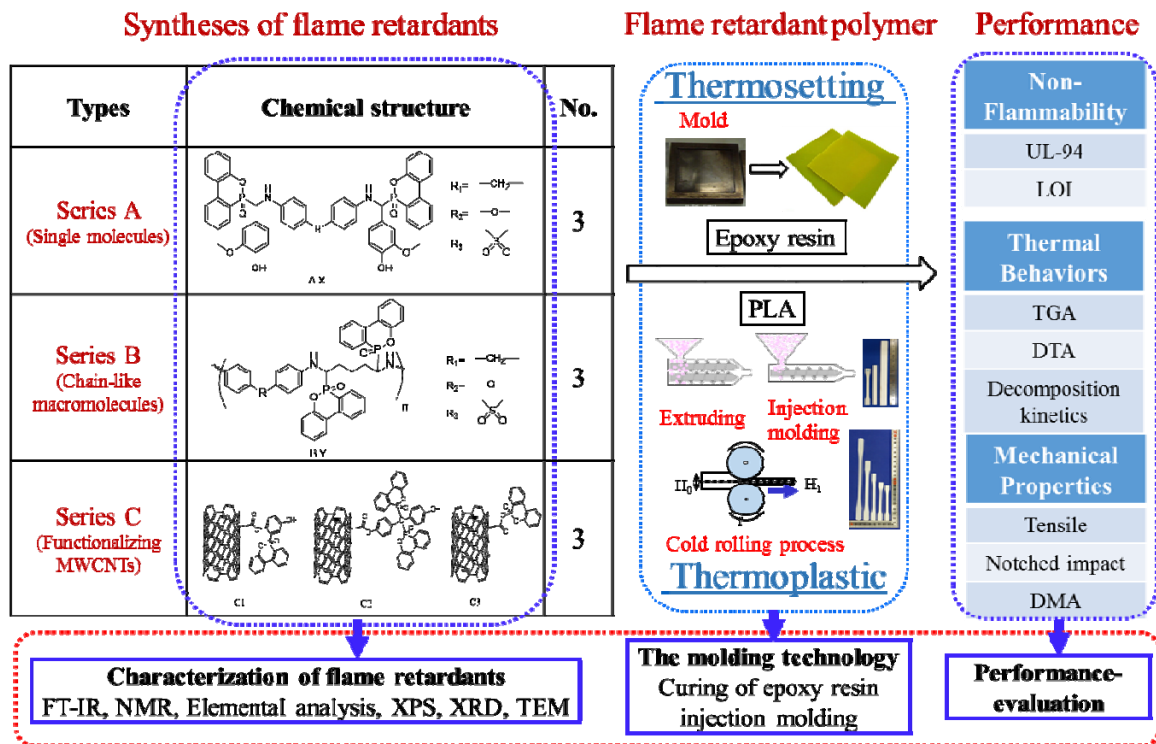


Fig. 2-25 The experimental process.

References

- [1] Wang, C. S., & Shieh, J. Y. Synthesis and properties of epoxy resins containing 2-(6-oxid-6H-dibenz< c, e> < 1, 2> oxaphosphorin-6-yl) 1, 4-benzenediol. *Polymer*, 1998, 39(23), 5819-5826.
- [2] Salmeia, K. A., & Gaan, S. (2015). An overview of some recent advances in DOPO-derivatives: chemistry and flame retardant applications. *Polymer Degradation and Stability*, 113, 119-134.
- [3] Gu, L., Chen, G., Yao, Y. Two novel phosphorus-nitrogen-containing halogen-free flame retardants of high performance for epoxy resin. *Polymer Degradation and Stability*, 2014, 108, 68-75.
- [4] Hariharasubramanian, A., Ravichandran, Y. D., Rajesh, R., Rajkumari, R., Selvan, G. K., & Arumugam, S. (2014). Functionalization of multi-walled carbon nanotubes with 6-aminobenzothiazole and their temperature-dependent magnetic studies. *Fullerenes, Nanotubes and Carbon Nanostructures*, 22(10), 874-886.
- [5] D. Tasis, N. Tagmatarchis, A. Bianco, and M. Prato, Chemistry of carbon nanotubes, *Chemical Reviews*, 106 (2006) 1105-1136.
- [6] Engel R. Synthesis of carbon-phosphorus bonds. CRC press, 2003.
- [7] Ma, H. Y., Tong, L. F., Xu, Z. B., & Fang, Z. P. Functionalizing carbon nanotubes by grafting on intumescent flame retardant: nanocomposite synthesis, morphology, rheology, and flammability. *Advanced functional materials*, 2008, 18(3), 414-421.
- [8] <http://www.westsystem.com/ss/epoxy-chemistry/>.
- [9] JIS C60695-11-10: 2006 or IEC 60695-11-10: 1999.
- [10] JIS K 7201-2: 2007 or ISO 4589-2: 1996.

Chapter 3 Three Types of Novel Flame Retardants: Syntheses and Characterization

3.1 Introduction

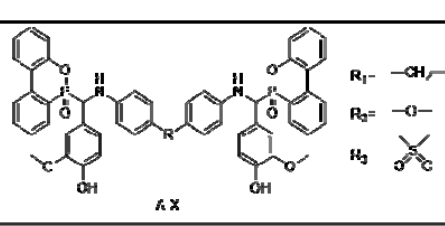
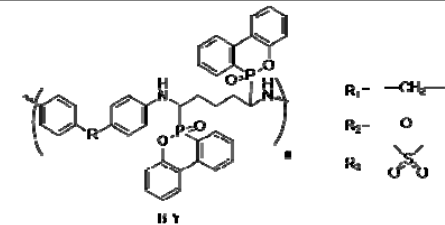
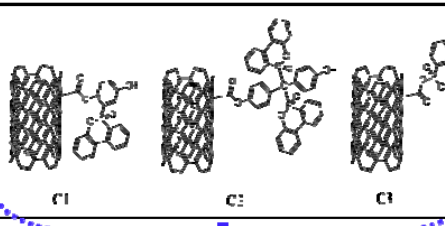
Driven by the urgent need of environmental protection, halogen-free flame retardant (HFFR) has been being developed rapidly since 1970s [1]. As an important branch of HFFR family, phosphorus-containing flame retardants (PFRs), since reported by French chemist Gay-Lussac at the beginning of the nineteenth century [2], have been developed greatly by advantage of that: effective at low concentration-organic types; easy incorporation and processing; relatively little detrimental effect on physical properties and so on [3]. Today, PFRs are among the "workhorse" products in the flame-retardant field, and research have focused on searching for high efficiently phosphorus sources.


Among them, 9,10-dihydro-9-oxa-10-phosphaphenanthrene 10-oxide (DOPO) group has been drawing intense research interest. Based on the active P—H bond, chemically introducing DOPO into various monomers has become a strategy for preparing HFFRs [4]. Since the late 1990s, a series of flame retardants and hardeners covalently boned with DOPO group have been prepared and tested in epoxy resins by Wang[5-7], among which one reactive monomer containing DOPO group displayed the highest phosphorus resource efficiency to our knowledge: an epoxy thermoset using this HFFR reached UL 94 V-0 flammability rating, when the phosphorus content is as low as 0.81 wt.% [8]. Lin reported a one-pot reaction of DOPO, amine and dehyde with high yields [9]. Following this invention as well as earlier work by Lin [10-12], we synthesized three HFFRs by introducing DOPO to Schiff base via a two-step procedure, and obtained epoxy thermosets meeting UL-94 V-0 flammability rating with LOI value as high as 35.6, when the phosphorus content was 1.0 wt.% [13], and found that the sites of hydroxyl in these HFFRs significantly affected LOI values of the as-prepared thermosets with identical phosphorus contents. To sum up, optimizing the flame-retarding performance

and resource efficiency by selecting functional groups and adjusting their sites of DOPO-based reactive monomer is feasible.

In this chapter, three types of DOPO-containing flame retardants (Series A: single molecules; Series B: chain-like macromolecules; Series C: functionalizing MWCNTs) were synthesized based on the Pudovik reactions. Flame retardants series A were characterized by ^1H , ^{13}C and ^{31}P NMR spectroscopy, elemental analysis (EA) and Fourier transform infrared (FT-IR) spectroscopy. For series B, FT-IR and X-ray photoelectron spectroscopy (XPS) were taken to confirm their compositions. The structures and compositions of flame retardants series C were confirmed by FT-IR, Raman, XPS, transmission electron microscope (TEM) and Thermogravimetric analyses (TGA). The synthesis and characterization of flame retardants in this work are shown in Fig. 3-1.

Syntheses of flame retardants

Types	Chemical structure	No.
Series A (Single molecules)		3
Series B (Chain-like macromolecules)		3
Series C (Functionalizing MWCNTs)		3



Characterization of flame retardants
FT-IR, Raman, NMR, Elemental analysis, XPS, TEM

Fig. 3-1 Synthesis and characterization of flame retardants.

3.2 Experimental

3.2.1 Materials

For flame retardant series A:

4,4'-Methylenedianiline (DDM), 4,4'-oxydianiline (DDE), 4,4'-diaminodiphenylsulfone (DDS) and 3-methoxy-4-hydroxybenzaldehyde (vanillin) from Tokyo Chemical Industry Co., Ltd., were used as received. 9,10-Dihydro-9-oxa-10-phosphaphenanthrene 10-oxide (DOPO) was purchased from Eutec trading (Shanghai) Co., Ltd.

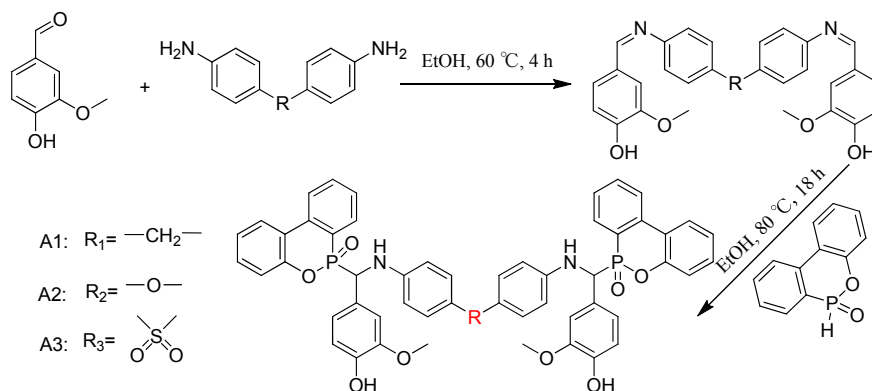
For flame retardant series B:

Glutaraldehyde (24-26% in Water) was purchased from Tokyo Chemical Industry Co., Ltd.

For flame retardant series C:

MWCNTs (Vapor Grown Carbon Fiber (VGCF®-X), average diameter was approximately 10~12 nm) were purchased from Showa Denko Company, Tokyo, Japan. 4-Benzoquinone, 4,4'-dihydroxybenzophenone, hydrogen peroxide solution (H₂O₂, 35% in water), sulfuric acid (H₂SO₄ 98 wt.%), nitric acid (HNO₃, 67 wt.%), tetrahydrofuran (THF), thionyl chloride (SOCl₂), N,N-dimethylformamide (DMF), ethanol (EtOH) and toluene were obtained from Tokyo Chemical Industry Co., Ltd.

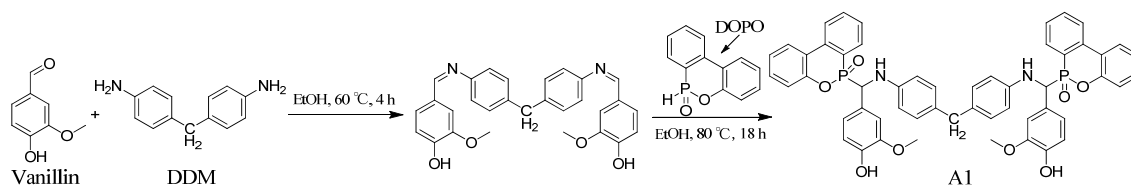
3.2.2 Syntheses of flame retardants-series A base on Pudovik reaction



Scheme 3-1. Syntheses of flame retardant series A.

Scheme 3-1 shows that flame retardants A1, A2 and A3 were respectively prepared by a one-pot procedure based on Pudovik reaction with two steps: synthesis of Schiff base from condensation reaction between DDM (or DDE or DDS) and vanillin; the addition reaction between DOPO and the Schiff base. The whole procedure does not need extraction of solvent.

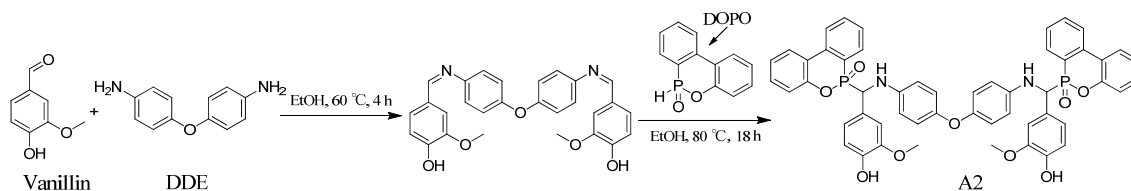
(1) Synthesis of A1



Scheme 3-2. Synthesis of flame retardant A1.

As shown in scheme 3-2, A1 was prepared by a one-pot procedure with two-steps. To a 500 mL three-neck round-bottom glass flask equipped with a reflux condenser and a mechanical stirrer, was charged with the solution of DDM (14.87 g, 0.075 mol) in EtOH (150 mL). The solution of vanillin (22.82 g, 0.15 mol) in EtOH (100 mL) was added dropwise into the flask within 30 min. After this solution had been added completely, the mixture was stirred at 60 °C until there was only one dot left in TLC (about 4 h). Then DOPO (32.43 g, 0.15 mol) was added into the mixture, and 80 mL of EtOH was added at the same time. The reaction mixture was stirred at 80°C for another 18 h. After the reaction completed, the reaction mixture was filtered, leaving a white solid (DP-DDM) which was washed repeatedly with hot EtOH. Flame retardant A1 was collected after drying for more than 8 h in a vacuum oven. (White solid 60.87 g, yield: 90.3%)

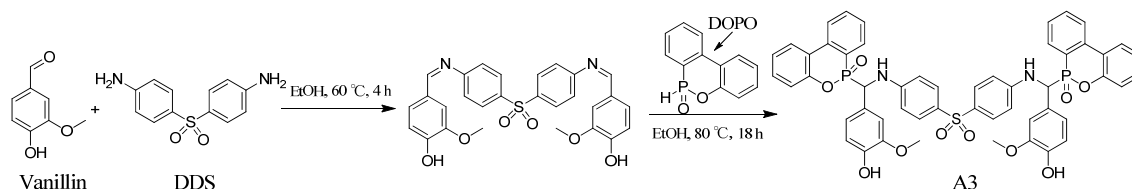
(2) Synthesis of A2



Scheme 3-3. Synthesis of flame retardant A2.

As shown in scheme 3-3, flame retardant A2 was prepared in a similar procedure of A1, using vanillin, DDE and DOPO as starting materials. (White solid 8, yield: 90.8%)

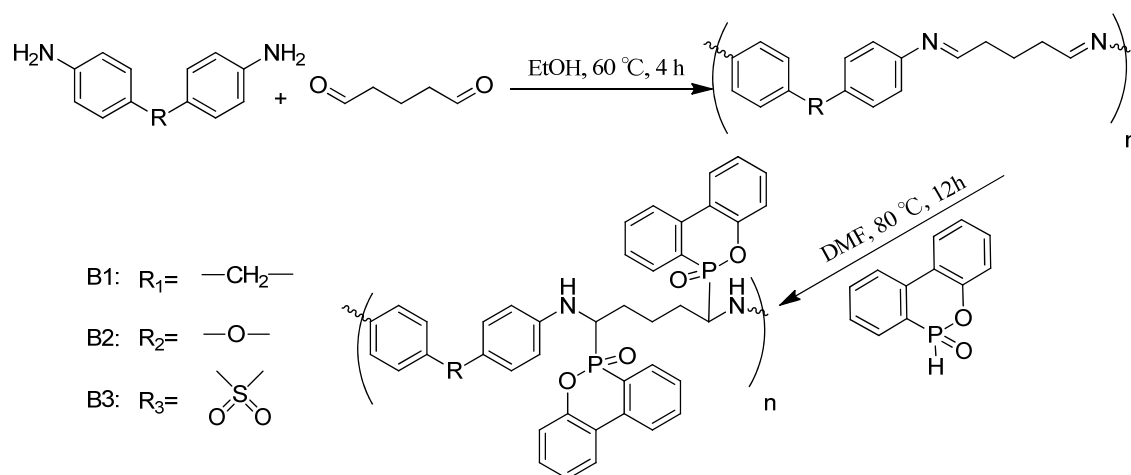
(3) Synthesis of A3



Scheme 3-4. Synthesis of flame retardant A3.

As shown in scheme 3-4, flame retardant A3 was prepared in a similar procedure of A1, using vanillin, DDS and DOPO as starting materials. (White solid, yield: 90.7%)

3.2.3 Syntheses of flame retardants-series B

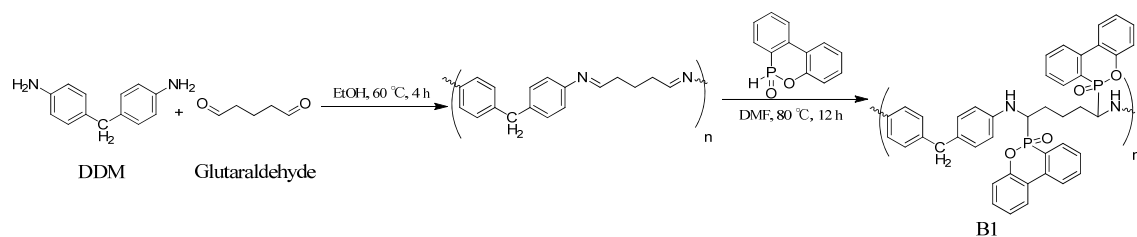


Scheme 3-5. Syntheses of flame retardant series B.

(1) Synthesis of B1

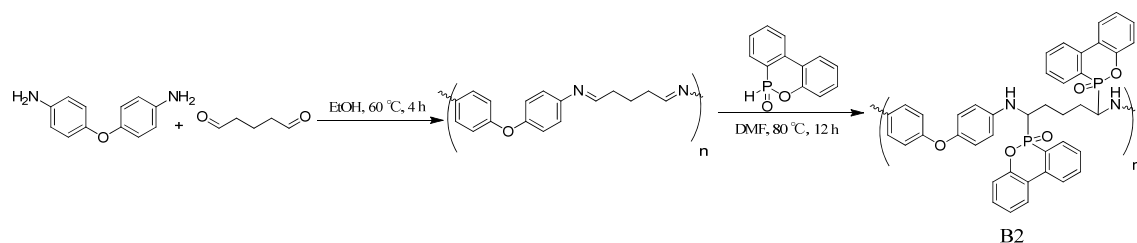
B1 was prepared as follows (was depicted in scheme 3-6): (1) DDM (14.87 g, 0.075 mol), and glutaraldehyde (7.5 g, 0.075 mol) were dissolved in anhydrous EtOH (200 mL) under nitrogen atmosphere. The yellow solution was stirred at 60 °C for 4 h. The reaction mixture was filtered, leaving a yellow solid which was washed repeatedly with hot EtOH. (2) After the yellow solid dissolved in DMF, DOPO (32.43 g, 0.15 mol) was added into the mixture. The reaction mixture was stirred at 80 °C for another 12 h. When the reaction

completed, the solvent was removed by rotary evaporation leaving yellow liquid (flame retardant B1).



Scheme 3-6. Synthesis of flame retardant B1.

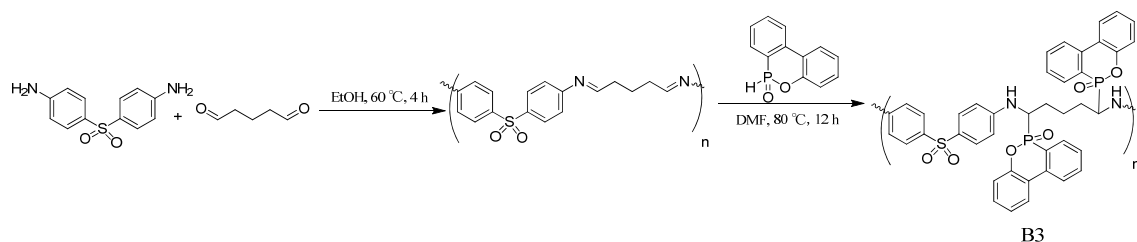
(2) Synthesis of B2



Scheme 3-7. Synthesis of flame retardant B2.

As shown in scheme 3-7, flame retardant B2 was prepared in a similar procedure of B1, using DDE, glutaraldehyde and DOPO as starting materials.

(3) Synthesis of B3



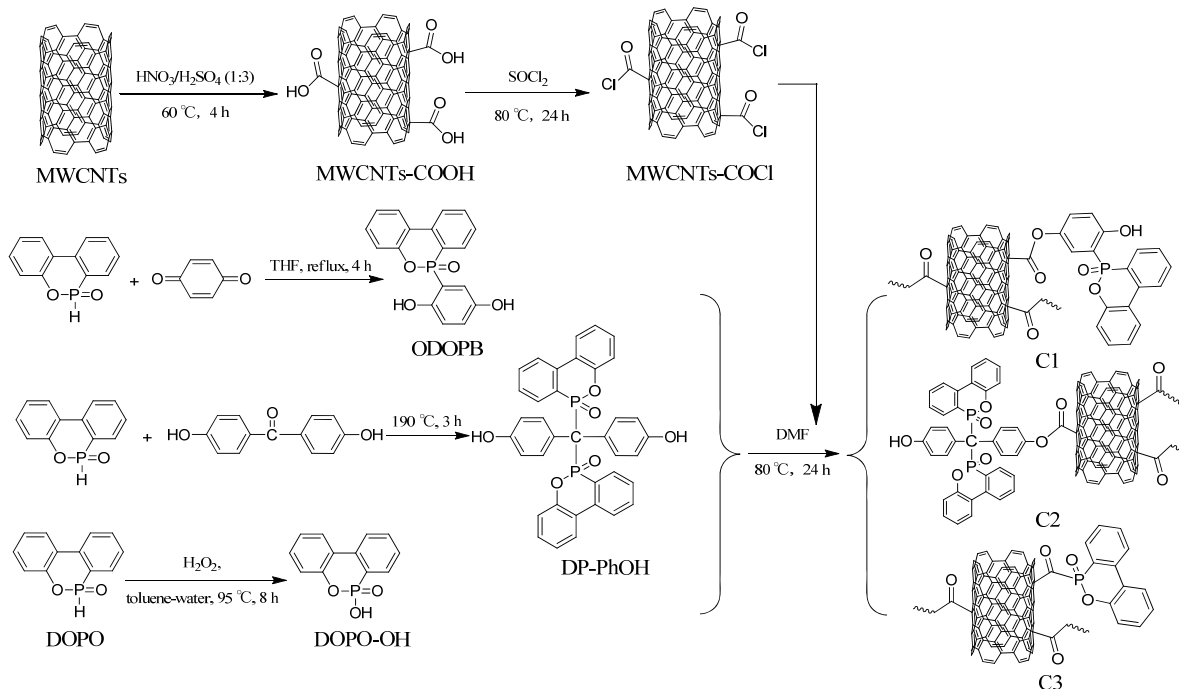
Scheme 3-8. Synthesis of flame retardant B3.

As shown in scheme 3-8, flame retardant B3 was prepared in a similar procedure of B1, using DDS, glutaraldehyde and DOPO as starting materials.

3.2.4 Flame retardants-series C of functionalizing MWCNTs

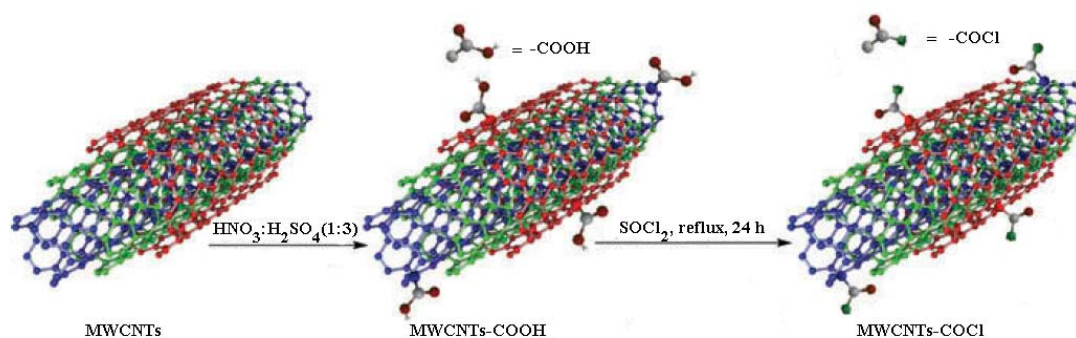
As shown in scheme 3-9, core-shell nanostructured MWCNT-DOPO-OH with MWCNTs as hard core and DOPO-OH as shell was prepared by three steps: (1) Synthesis

of MWCNTs-COCl. (2) Synthesis of flame retardant molecules. (3) The formation of flame retardant series C by grafting flame retardant molecules onto the surface of MWCNTs.



Scheme 3-9. Syntheses of flame retardant series C.

(1) Synthesis of MWCNTs-COCl

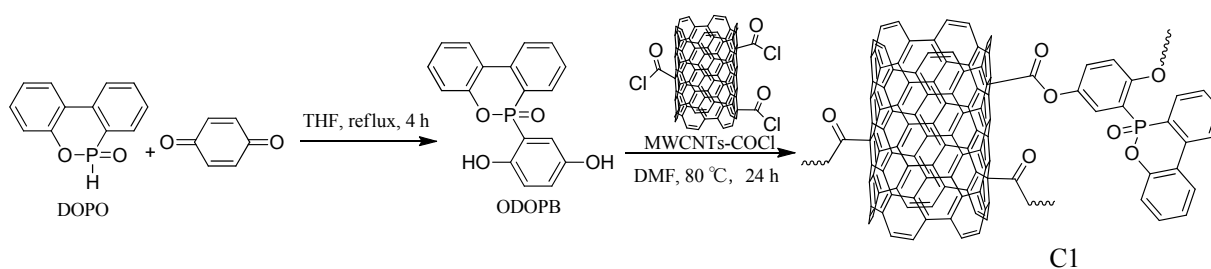


Scheme 3-10. Synthesis of MWCNTs-COCl.

MWCNTs-COCl was prepared following the reported procedure [14-16]. MWCNTs was acid-treated with a mixture of nitric acid and sulfuric acid (1:3 by volume) in ultrasonic bath at $50\text{--}60\text{ }^\circ\text{C}$ for 4 h. The acid-treated MWCNTs (MWCNT-COOH) was washed to neutral ($\text{pH} = 7.0$), and dried at $80\text{ }^\circ\text{C}$ in a vacuum oven overnight. The mixture

of MWCNT-COOH, SOCl₂ and DMF (with the ratio of 200 mg : 50 ml : 1 ml) was dispersed in ultrasonic bath for about 2 h and refluxed at 80 °C for 24 h. Then unreacted SOCl₂ was removed by distillation and the remained MWCNT-COCl was dried at room temperature under vacuum.

(2) Synthesis of C1



Scheme 3-11. Synthesis of flame retardant C1.

Step 1: ODOPB was synthesized according to the reported process [17]. 10-(2,5-dihydroxyphenyl)-10-hydrogen-9-oxa-10-phosphoryl phenanthrene-10-oxide (ODOPB), was synthesized using 9,10-dihydro-9-oxa-10-phospha-phenanthrene-10-oxide (DOPO) and benzoquinone as the starting materials and THF as the solvent.

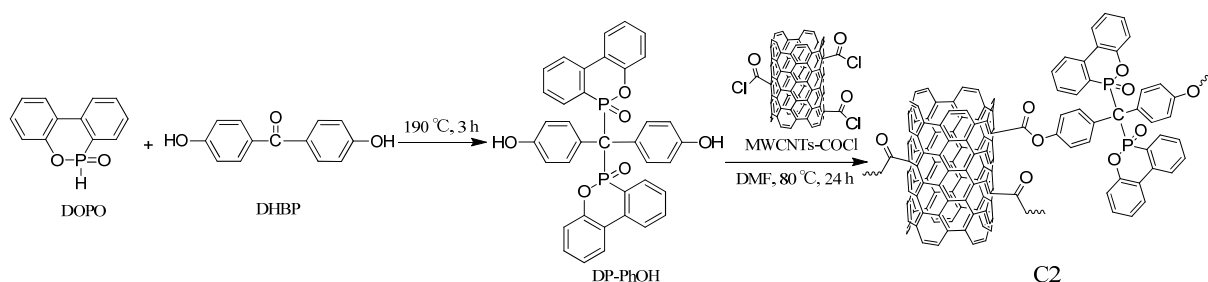
In a multi-necked flask equipped with a stirrer, reflux condenser and thermometer, DOPO was suspended in THF and heated to 80 °C. Then benzoquinone was added to the mixture within 8 h. As the suspension was cooled to room temperature, the remained ODOPB was filtered, washed with water and recrystallized from THF.

Step 2: The calculated amounts of MWCNT-COCl, ODOPB and one drop of pyridine as catalyst were added in a glass flask and dispersed by DMF. Then the mixtures were stirred at 80 °C for 12 h under nitrogen atmosphere. The products (flame retardant C1) was filtered, washed with DMF and then dried to constant weight at 80 °C under vacuum.

(3) Synthesis of C2

Step 1: DP-PhOH was synthesized according to the reported procedure [18]. DOPO and DHBP were mixed together in a round-bottomed flask. The mixture was heated to 190 °C and stirred for 3 h. The reaction mixture then became thick. After being cooled to 100 °C, 10 ml toluene was added to the flask. The pale yellow precipitate was filtered and washed

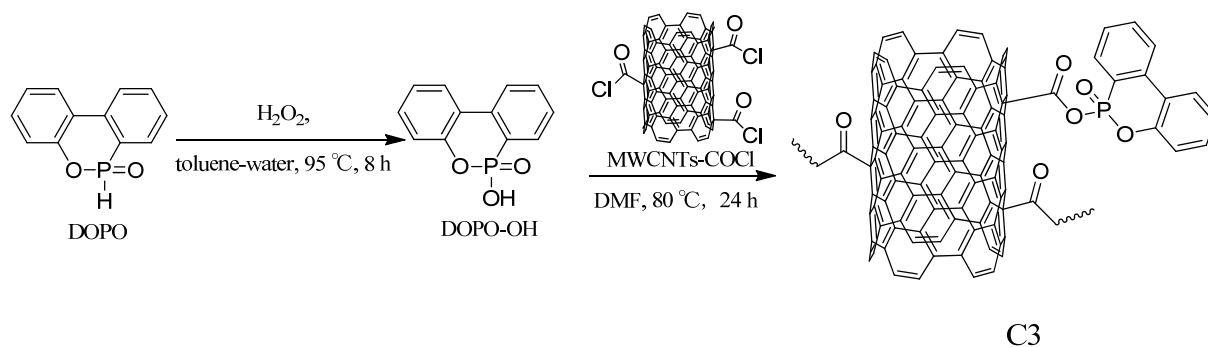
with toluene. The as-synthesized DOPO-PhOH was dissolved in boiling N,N-dimethylacetamide (DMAc) in nitrogen atmosphere, followed by filtration of the hot solution which was then precipitated in tetrahydrofuran (THF) and diethyl ether(Et₂O), filtered off and recrystallized two times to achieve high purity. The received white powder product was dried in vacuum to remove residual solvents.



Scheme 3-12. Synthesis of flame retardant C2.

Step 2: The calculated amounts of MWCNT-COCl, DP-PhOH and one drop of pyridine as catalyst were added in a glass flask and dispersed by DMF. Then the mixtures were stirred at 80 °C for 12 h under nitrogen atmosphere. The products (flame retardant C2) was filtered, washed with DMF and then dried to constant weight at 80 °C under vacuum.

(4) Synthesis of C3



Scheme 3-13. Synthesis of flame retardant C3.

Step 1: DOPO-OH was synthesized according to the reported US patent [19]. In a multi-necked flask equipped with a stirrer, reflux condenser and thermometer, DOPO was suspended in toluene-water mixture and heated to 95 °C. Then hydrogen peroxide was added to the mixture within 8 h. As the suspension was cooled to room temperature, the remained DOPO-OH was filtered, washed with water and recrystallized from acetic acid.

Step 2: The calculated amounts of MWCNT-COCl, DOPO-OH and one drop of pyridine as catalyst were added in a glass flask and dispersed by DMF. Then the mixtures were stirred at 80 °C for 12 h under nitrogen atmosphere. The products (MWCNT-DOPO-OH) was filtered, washed with DMF and then dried to constant weight at 80 °C under vacuum.

2.3.5 Instruments and measurements

Fourier transform infrared (FT-IR) spectra were recorded on a Bruker Vertex 70 infrared spectrophotometer by KBr disc method with optical range of 400~4000 cm^{-1} . ^1H NMR (400 MHz), ^{13}C NMR (101 MHz) and ^{31}P (162 MHz) NMR spectra were registered with a Bruker AV-400 spectrometer by using DMSO- d_6 as solvent and TMS as an internal standards. The elemental analyses were performed with a CHNOS Elemental Analyzer-vario EL cube. Raman spectra were recorded on the laser Raman spectrometer (Horiba JY HR800, HORIBA, Ltd., France) at 532 nm radiation with range of 1000~2000 cm^{-1} . X-ray photoelectron spectroscopy (XPS) analyses were performed on PHI Quantum 5000 (Physical Electronics Division, Perkin-Elmer Corp., USA) equipped with an Al $K\alpha$ radiation source. Thermal gravimetric analyses (TGA) of samples were carried out with Shimadzu DTG-60/60H from 30 °C to 600 °C at heating rates of 10 °C· min^{-1} , whereas the flow of nitrogen was maintained at 50 $\text{mL}\cdot\text{min}^{-1}$. Transmission electron microscopy (TEM) images were obtained on a Model H-8100 transmission electron microscope (Hitachi Ltd., Japan).

3.3 Results and discussion

3.3.1 Characterization of flame retardants-series A

The syntheses and yields of flame retardants-series A were shown in Fig. 3-2. The chemical structures and compositions of flame retardant A1, A2 and A3 were confirmed by FT-IR, elemental analysis, ^1H NMR, ^{13}C NMR and ^{31}P NMR spectroscopy.

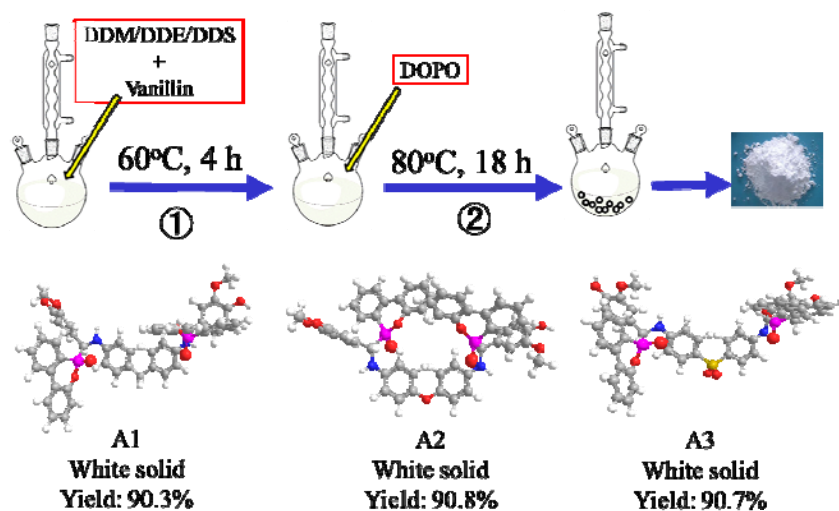


Fig. 3-2 Syntheses and yields of flame retardant series A.

(1) FT-IR spectra

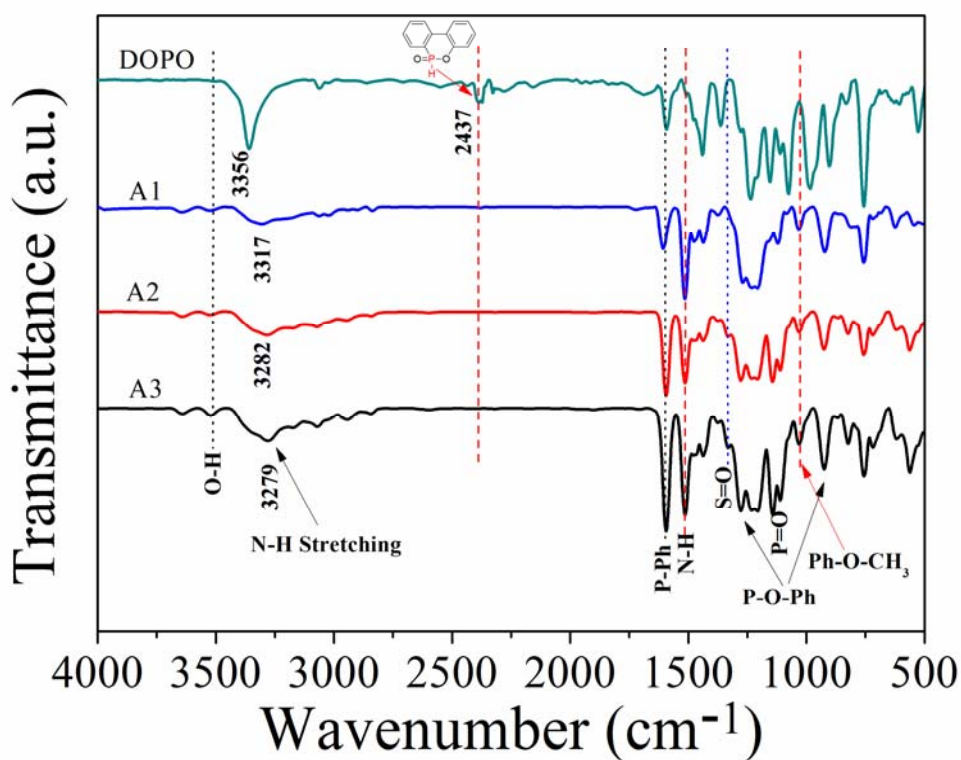


Fig. 3-3 FT-IR spectra of DOPO and A1, A2, A3.

Figure 3-3 shows the FT-IR spectra of DOPO and flame retardant A1, A2, A3. The disappearance of P—H stretching vibration at 2437 cm⁻¹ demonstrates that DOPO has been essentially converted [20-24].

The absorption-peaks at 758 cm^{-1} , 925 cm^{-1} and 1231 cm^{-1} corresponds to the P—O—Ph linkage of DOPO groups in flame retardant A1 (or A2, A3). Ph—O—C and —CH₃ stretching vibrations at 1032 cm^{-1} , 2842 cm^{-1} and 2946 cm^{-1} indicate the existence of vanillin groups in A1 (or A2, A3). The peaks at 1032 cm^{-1} , 2842 cm^{-1} and 2946 cm^{-1} of A1 (or A2, A3) are attributed to the stretching vibrations of Ph—O—C and —CH₃ of vanillin group. The peaks at 1514 cm^{-1} and $3282\sim 3279\text{ cm}^{-1}$ are ascribed to N—H bending vibrations and N—H stretching vibrations. For A3, the peak at 1331 cm^{-1} corresponds to the characteristic stretching vibration of S=O. These FTIR data were summarized in Tab. 3-1.

These FTIR data and their analyses of flame retardant A1 (or A2, A3) are self-consistent with the results of NMR described below and element analysis results.

Tab. 3-1 FTIR data of flame retardant A1, A2 and A3.

No.	FT-IR (KBr)
A1	925 cm^{-1} , 1234 cm^{-1} (P-O-Ph); 1033 cm^{-1} (Ph-O-C); 1207 cm^{-1} (P=O); 1514 cm^{-1} , 3317 cm^{-1} (N-H); 1596 cm^{-1} (P-Ph); 3511 cm^{-1} (O-H).
A2	925 cm^{-1} , 1234 cm^{-1} (P-O-Ph); 1033 cm^{-1} (Ph-O-C); 1206 cm^{-1} (P=O); 1514 cm^{-1} , 3282 cm^{-1} (N-H); 1594 cm^{-1} (P-Ph); 3510 cm^{-1} (O-H).
A3	926 cm^{-1} , 1236 cm^{-1} (P-O-Ph); 1034 cm^{-1} (Ph-O-C); 1207 cm^{-1} (P=O); 1514 cm^{-1} , 3279 cm^{-1} (N-H); 1595 cm^{-1} (P-Ph); 3514 cm^{-1} (O-H).

(2) ¹H, ¹³C and ³¹P NMR spectra

As shown in Fig. 3-4, figure A1-(a), figure A2-(a) and figure A3-(a) respectively show the ¹H NMR spectra of flame retardant A1, A2 and A3. The chemical shifts at 7.9~7.2 ppm are attributed to the aromatic protons on DOPO group in A1 (or A2, A3) (labeled a-h). A strong resonance signal around 3.67~3.42 ppm is characteristic of the protons (labeled r) of methyl groups, whose aromatic protons are shown by the inset of Fig. 3-4(a). The chemical shifts of H^q (H^q) display germinal couplings resulting from chiral electron effects, generated from the configuration of P*—(C⁷*—H^q)—N* and possible interactions including two sets of intra-hydrogen bonds built up from N*—H and O=P*—O, where * denotes that the labeled atoms provide chiral electron effect. This phenomenon is reported previously [25-27].

Tab. 3-2 NMR data of flame retardant of A1, A2 and A3.

NMR	A1	A2	A3
¹ H NMR	δ 8.90 (d, $J = 11.4$ Hz, 2H), 8.16 (dd, $J = 16.3, 9.5$ Hz, 4H), 8.01 – 7.94 (m, 1H), 7.79 – 7.63 (m, 3H), 7.52 (t, $J = 6.7$ Hz, 1H), 7.47 – 7.34 (m, 3H), 7.29 (t, $J = 7.6$ Hz, 2H), 7.14 (d, $J = 8.0$ Hz, 1H), 7.04 (d, $J = 8.1$ Hz, 1H), 6.91 (s, 2H), 6.82 – 6.46 (m, 12H), 6.44 – 6.36 (m, 1H), 6.03 (d, $J = 4.8$ Hz, 1H), 5.23 (dd, $J = 14.4, 10.0$ Hz, 1H), 4.92 – 4.81 (m, 1H), 3.73 – 3.54 (m, 6H), 3.42 (d, $J = 11.0$ Hz, 2H).	δ 9.02 – 8.92 (m, 2H), 8.12 (t, $J = 7.3$ Hz, 4H), 7.87 (dd, $J = 9.8, 6.0$ Hz, 1H), 7.66 (dd, $J = 14.4, 4.6$ Hz, 3H), 7.48 – 7.18 (m, 12H), 7.11 (d, $J = 8.1$ Hz, 1H), 6.99 (dd, $J = 7.8, 3.1$ Hz, 1H), 6.91 (d, $J = 18.2$ Hz, 2H), 6.76 (dt, $J = 13.7, 7.8$ Hz, 6H), 6.66 – 6.60 (m, 2H), 5.44 (dd, $J = 16.5, 9.5$ Hz, 1H), 5.17 – 5.07 (m, 1H), 3.67 – 3.59 (m, 6H).	δ 9.02 – 8.92 (m, 2H), 8.11 (dd, $J = 11.5, 4.7$ Hz, 4H), 7.85 (d, $J = 8.4$ Hz, 1H), 7.75 – 7.59 (m, 3H), 7.47 – 7.18 (m, 12H), 7.11 (d, $J = 8.1$ Hz, 1H), 7.01 – 6.96 (m, 1H), 6.91 (d, $J = 17.9$ Hz, 2H), 6.74 (dd, $J = 15.1, 10.4$ Hz, 6H), 6.62 (dd, $J = 8.0, 2.2$ Hz, 2H), 5.43 (dd, $J = 16.2, 9.6$ Hz, 1H), 5.11 (dd, $J = 13.7, 10.3$ Hz, 1H), 3.62 (d, $J = 3.7$ Hz, 6H).
¹³ C NMR	δ 149.54 (C16, C16', dd, $J = 20.5, 8.8$ Hz), 147.72 (C13, C13', s), 146.63 (C7, C7', s), 145.55 (C14, C14', t, $J = 11.7$ Hz), 135.86 (C22, C22', dd, $J = 10.9, 5.9$ Hz), 134.10 (C2, C2', s), 133.76 (C9, C9', s), 132.24 (C24, C24', d, $J = 9.1$ Hz), 131.28 – 130.82 (C18, C18', m), 129.15 (C3, C3', C4, C4', s), 128.72 (C26, C26', dd, $J = 21.1, 12.4$ Hz), 126.36 – 125.77 (C25, C25', m), 125.07 (C20, C20', d, $J = 8.8$ Hz), 124.71 (C19, C19', s), 124.34 (C23, C23', dd, $J = 15.8, 8.0$ Hz), 123.57 (C27, C27', s), 123.13 (C21, C21', s), 122.42 – 121.91 (C10, C10', m), 121.68 (C12, C12' dd, $J = 19.1, 5.4$ Hz), 120.53 (C17, C17', dd, $J = 22.2, 5.7$ Hz), 115.50 (C5, C5' and C6, C6', s), 114.31 (C1, d, $J = 7.3$ Hz), 113.32 (C11, C11', d, $J = 11.2$ Hz), 57.61 – 56.26 (C8, C8', m), 56.07 (C15, C15', s).	δ 151.34 (C1, C1', t, $J = 9.1$ Hz), 149.53 (C15, C15', dd, $J = 35.1, 8.9$ Hz), 147.73 (C12, C12', s), 146.83 (C13, C13', s), 136.34 – 135.76 (C6, C6', m), 134.14 (C21, C21', d, $J = 33.4$ Hz), 132.21 (C8, C8', d, $J = 8.9$ Hz), 131.09 (C23, C23', s), 129.98 (C17, C17', s), 128.79 (C25, C25', d, $J = 12.8$ Hz), 128.53 (C2, C2', C3, C3', s), 127.02 (C26, C26', d, $J = 18.5$ Hz), 126.06 (C24, C24', d, $J = 11.4$ Hz), 125.39 – 124.87 (C19, C19', m), 124.33 (C18, C18', t, $J = 8.8$ Hz), 123.81 (C22, C22', d, $J = 9.6$ Hz), 122.67 (C20, C20', d, $J = 12.3$ Hz), 122.12 – 121.66 (C9, C9', m), 121.53 (C11, C11', d, $J = 5.1$ Hz), 120.74 – 119.99 (C16, C16', m), 115.58 (C10, C10', s), 113.28 (C4, C4', C5, C5', dd, $J = 14.3, 6.2$ Hz), 54.62-56.80 (C7, C7', q), 56.06 (C14, C14', s).	δ 151.31 (C1, C1', t, $J = 9.4$ Hz), 149.52 (C15, C15', dd, $J = 35.1, 9.1$ Hz), 147.70 (C12, C12', s), 146.81 (C13, C13', s), 136.02 (C6, C6', dd, $J = 27.4, 5.9$ Hz), 134.12 (C21, C21', d, $J = 33.6$ Hz), 132.20 (C8, C8', d, $J = 7.4$ Hz), 131.08 (C23, C23', s), 129.95 (C17, C17', s), 128.77 (C25, C25', d, $J = 14.1$ Hz), 128.51 (C2, C2', C3, C3', s), 127.01 (C26, C26', d, $J = 18.7$ Hz), 126.06 (C24, C24', d, $J = 11.7$ Hz), 125.14 (C19, C19', dd, $J = 7.9, 6.2$ Hz), 124.33 (C18, C18', t, $J = 8.8$ Hz), 123.82 (C22, C22', d, $J = 10.0$ Hz), 122.68 (C20, C20', d, $J = 12.5$ Hz), 121.92 (C9, C9', dd, $J = 10.1, 5.0$ Hz), 121.63 (C11, C11', dd, $J = 25.3, 5.4$ Hz), 120.35 (C16, C16', dd, $J = 35.2, 5.6$ Hz), 115.55 (C10, C10', s), 113.55 – 113.05 (C4, C4', C5, C5', m), 56.75-55.70 (C7, C7', m), 56.04 (C14, C14', s).
³¹ P NMR	δ 34.45 (s), 31.72 (s).	δ 33.16 (s), 31.46 (s).	δ 33.10 (s), 31.38 (t, $J = 8.1$ Hz).

A strong resonance signal around 3.67~3.42 ppm is characteristic of the protons (labeled r) of methyl groups, whose aromatic protons are shown by the inset of Fig. 3-4(a). The chemical shifts of H^q (H^{q'}) display germinal couplings resulting from chiral electron effects, generated from the configuration of P*—(C^{7*}—H^q)—N* and possible interactions including two sets of intra-hydrogen bonds built up from N*—H and O=P*—O, where * denotes that the labeled atoms provide chiral electron effect. This phenomenon is reported previously [25-27].

Fig. 3-4 (b) (A1-(b), A2-(b) and A3-(b)) respectively show ¹³C NMR spectrum of flame retardant A1, A2 and A3. Out of the same reason, C^{8*} in A1 atom (or C^{7*} in A2, A3) displays quadra-split peaks ranging from 54.62 to 57.61 ppm. The other peaks were well assigned to the chemical structure of flame retardant A1, A2 and A3 (Tab. 3-2). The other resonance peaks ranging from 151 to 113 ppm for carbon atoms have been attributed as shown in Figure 1(b) and Figure 2(b).

The two peaks observed in ³¹P NMR spectrum (Fig. A1-(c), A2-(c) and A3-(c)) are consistent of with the chiral configuration mentioned above.

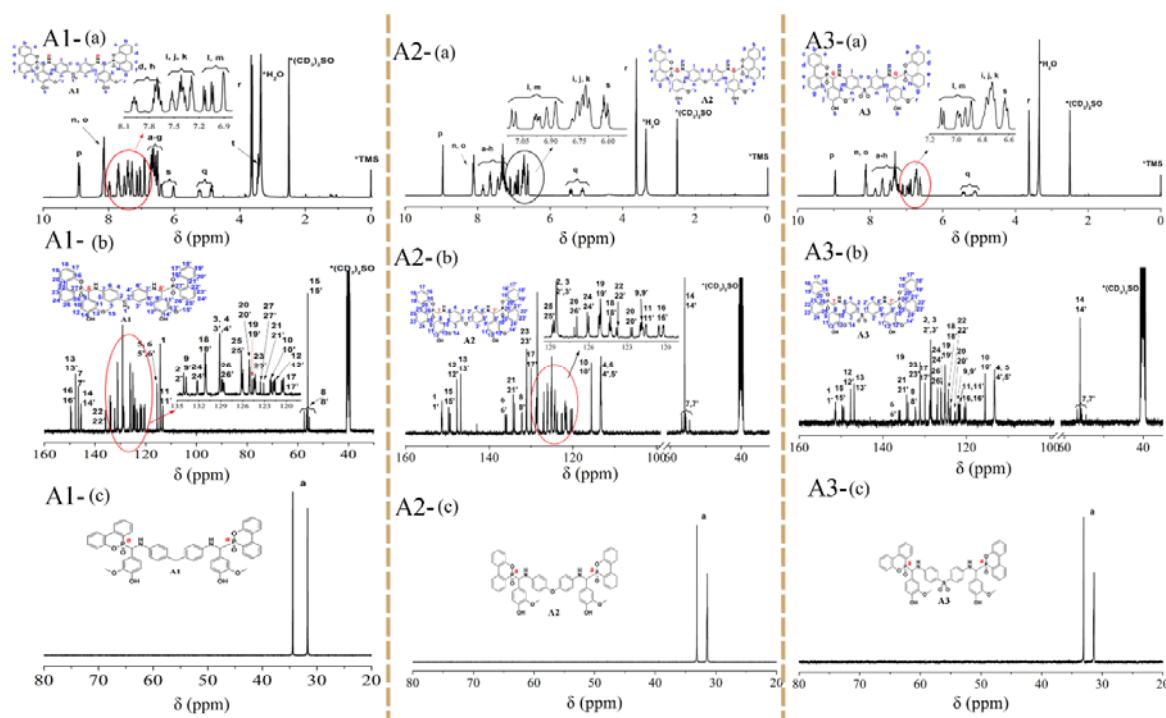


Fig. 3-4 NMR spectra of A1, A2 and A3: (a) ¹H NMR; (b) ¹³C NMR; (c) ³¹P NMR.

Taking the two chiral P and two chiral C (P*—(C^{7*}—H^q)—N*) into account in each

chemical scheme, there are eight groups of diastereomers in A1 (or A2, A3).

The ^1H , ^{13}C and ^{31}P NMR spectrum of A1, A2 and A3 are all consistent with the assigned structure presented in Fig. 3-4, and the results are summarized in Tab. 3-2. The chemical structures of those novel flame retardant were well monitored by ^1H , ^{13}C , and ^{31}P NMR spectroscopy

(3) Elemental Analysis

Element analysis data also confirm the structures of flame retardant A1, A2 and A3. The elemental analysis results (Tab. 3-3) are in good agreement with the data calculated in light of the expected formula of flame retardant. These characterization data further indicated that flame retardant A1, A2 and A3 were successfully synthesized, and no side products were detected.

Tab. 3-3 Elemental analysis data.

No.	Molecular Formula	C (%)		H (%)		N (%)		S (%)	
A1	$\text{C}_{53}\text{H}_{44}\text{N}_2\text{O}_8\text{P}_2$	69.54	70.82	5.018	4.93	2.87	3.12	0.089	0
A2	$\text{C}_{52}\text{H}_{42}\text{N}_2\text{O}_9\text{P}_2$	69.22	69.33	4.614	4.70	2.72	3.11	0.083	0
A3	$\text{C}_{52}\text{H}_{42}\text{N}_2\text{O}_{10}\text{P}_2\text{S}$	64.25	65.82	4.634	4.46	2.69	2.95	3.006	3.38

Experimental values
 Calculated values

3.3.2 Characterization of flame retardants-series B

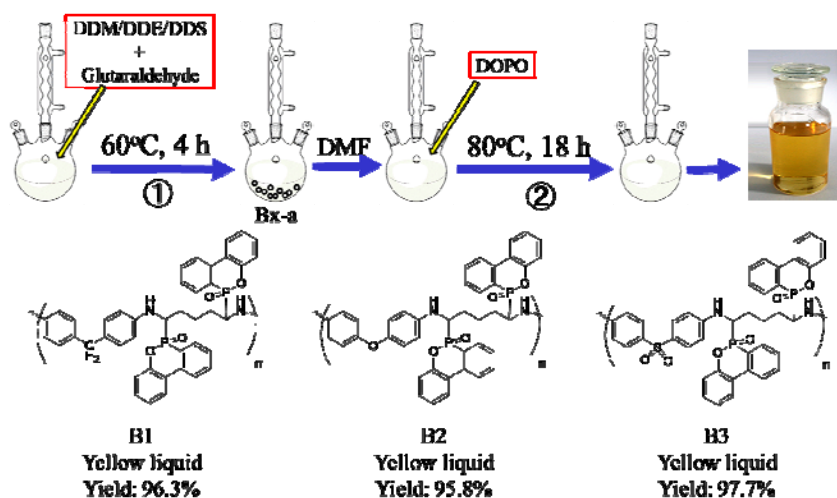


Fig. 3-5 Syntheses and yields of flame retardant series B.

The syntheses and yields of flame retardants-series B were shown in Fig. 3-5. The chemical structures and compositions of flame retardant B1, B2 and B3 were confirmed by FT-IR and XPS spectroscopy.

(1) FT-IR spectra

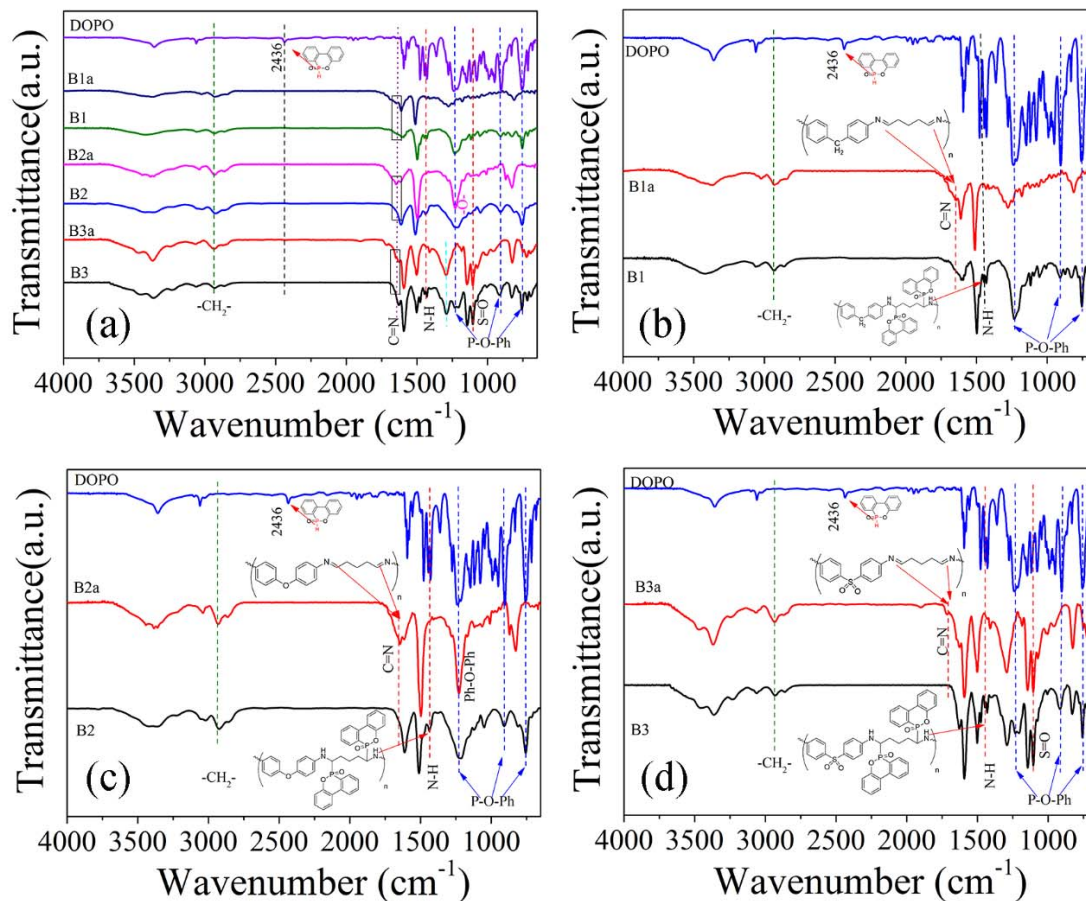


Fig. 3-6 FT-IR spectra of DOPO and flame retardants B1, B2, B3.

Fig.3-6 shows FT-IR spectra of DOPO and flame retardants B1, B2, B3. The absorption peaks in the spectrum of DOPO corresponded to the reported association that: 758 cm^{-1} , 906 cm^{-1} and 1238 cm^{-1} (P—O—Ph); 1206 cm^{-1} (P=O); 1594 cm^{-1} (P—Ph); 2436 cm^{-1} (P—H) [28-29]. Comparing with the FT-IR spectrum of DOPO, it is also found that the absorption peak at 2436 cm^{-1} for P—H stretching vibration disappeared from the spectrum of flame retardants (B1, B2 and B3) and their synthesis intermediates (B1a, B2a and B3a).

Additionally, a broad peak at 3230 cm^{-1} for hydroxyl-association and a new peak

around 2930~2850 cm^{-1} attributing to $\text{—CH}_2\text{—}$ stretching vibration appeared, indicating that glutaraldehyde has been connected to DDM, DDE or DDS by condensation reaction. For the spectrum of both flame retardants and their synthesis intermediates, the characteristic absorption peaks associated with DOPO at 754 cm^{-1} , 944 cm^{-1} and 1202 cm^{-1} are attributed to the P—O—Ph stretching vibrations. Moreover, a new absorption peak for N—H stretching vibration indicates that P—H groups of DOPO have reacted with C=N groups of the Schiff base (synthesis intermediates B1a, B2a or B3a). These results provide an evidence for the formation of such chain-like macromolecules flame retardants.

(2) XPS

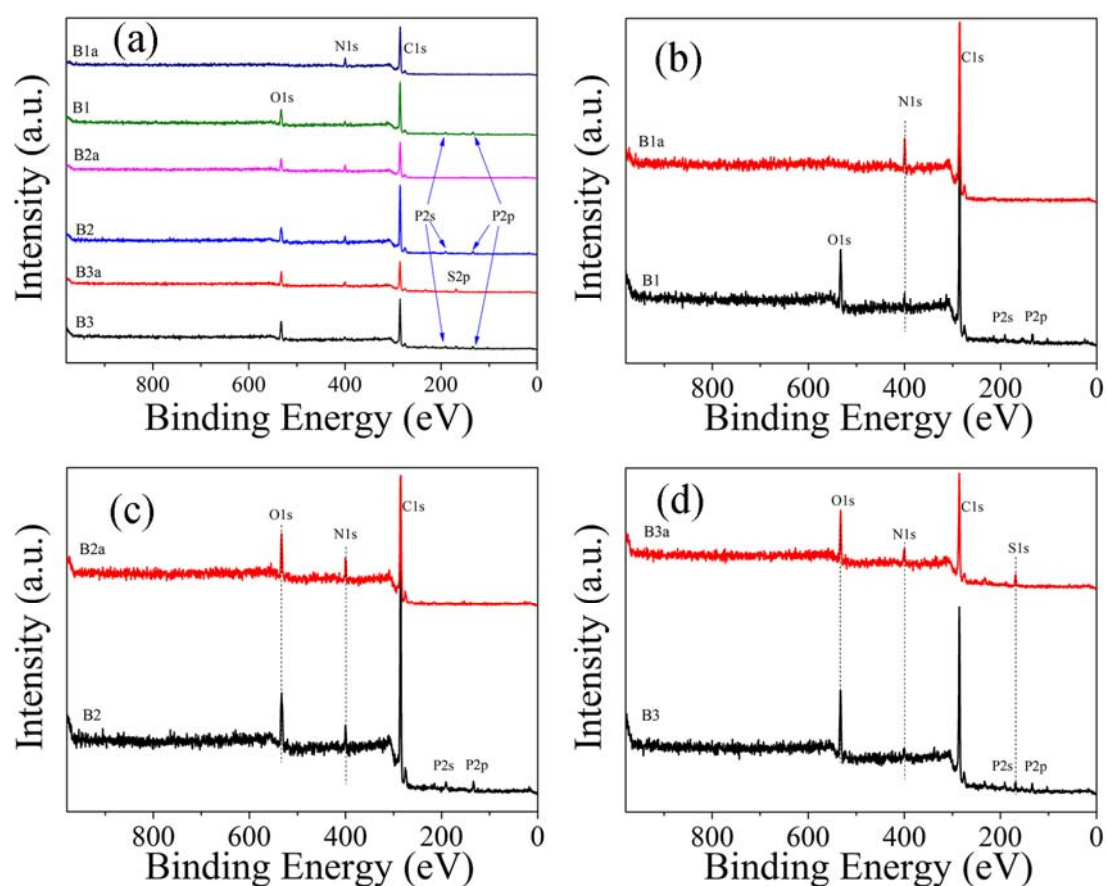


Fig. 3-7 The XPS survey spectra of flame retardants (B1, B2 and B3) and their synthesis intermediates (B1a, B2a and B3a).

XPS analysis was performed to understand the chemical composition of flame

retardants (B1, B2 and B3) and their synthesis intermediates (B1a, B2a and B3a). The spectra are shown in Figure 3-7.

The survey spectra (Fig. 3-7b) show that besides the C1s (285 eV), N1s (399.5 eV) and peaks of synthesis intermediates B1a, new peak can be observed at 533.5 eV (O1s) for chain-like macromolecules B1, which can apparently be attributed to the Pudovik reaction with DOPO (Scheme 3-6). The appearance of P2p peaks at 135.5 eV for all flame retardants-series B further confirm the Pudovik reaction between P—H groups with C=N groups according to scheme 3-5. It can thus be concluded that the DOPO groups have been chemically introduced into the chain-like macromolecules flame retardants-series B.

3.3.3 Characterization of flame retardants-series C

(1) FT-IR

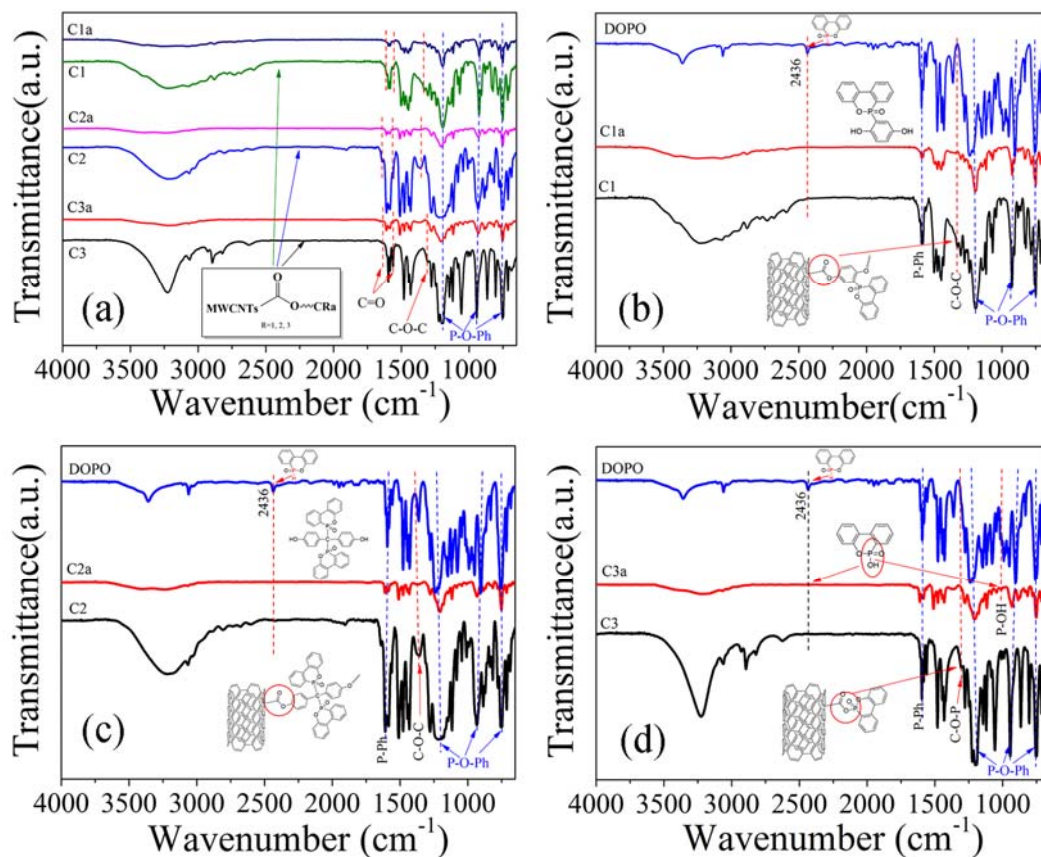


Fig. 3-8 FT-IR spectra of DOPO and flame retardants C1, C2, C3.

Fig. 3-8 shows FT-IR spectra of DOPO, flame retardants-series C and their synthesis intermediates. The FT-IR spectrum of DOPO can be associated as follows: 758 cm^{-1} , 906 cm^{-1} and 1238 cm^{-1} (P—O—Ph); 1206 cm^{-1} (P=O); 1594 cm^{-1} (P—Ph); 2436 cm^{-1} (P—H) [30-32]. Comparing with the FT-IR spectrum of DOPO, it is found that the absorption peak at 2436 cm^{-1} for P—H stretching vibration disappeared from the spectrum of flame retardants-series C (C1, C2 and C3) and their synthesis intermediates (C1a, C2a and C3a).. For flame retardant C3 (Fig. 3-8d), a broad peak at 3230 cm^{-1} for hydroxyl-association and a new peak around 1011 cm^{-1} attributing to P—OH stretching vibration appeared, indicating that DOPO has been essentially converted to synthesis intermediate DOPO-OH. From the spectrum of C3, the characteristic absorption peaks associated with DOPO-OH at 754 cm^{-1} , 944 cm^{-1} and 1202 cm^{-1} are attributed to the P—O—Ph stretching vibrations. Moreover, a new absorption peak at 1305 cm^{-1} for C—O—P stretching vibration indicates that the hydroxyl groups of DOPO-OH have reacted with the acyl chloride groups on the surface of MWCNT. These results provide an evidence for the formation of such functionalized multi-walled carbon nanotube C3.

(2) Raman

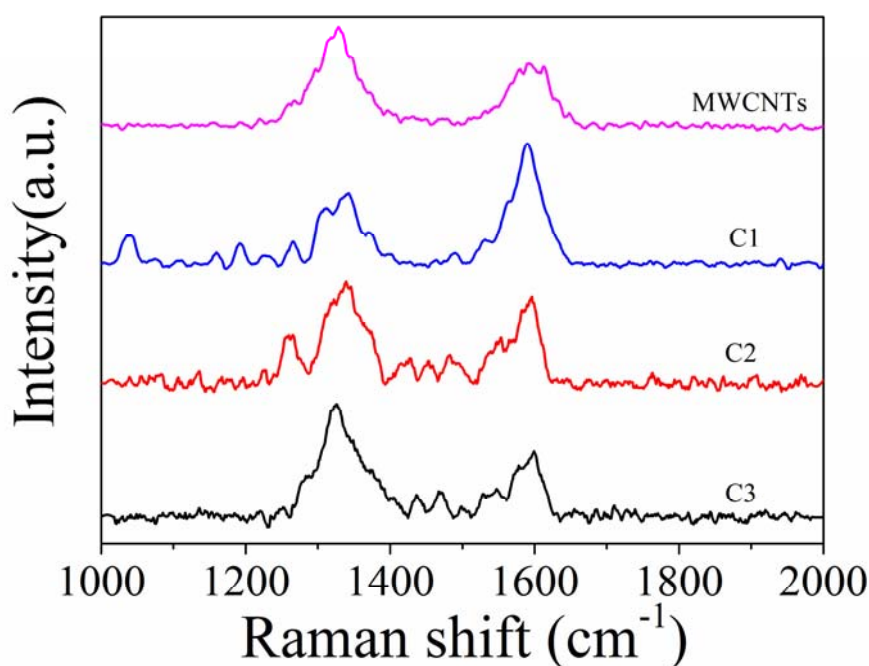


Fig. 3-9 Raman spectra of MWCNTs and flame retardants-series C (C1, C2 and C3).

Raman spectra for MWCNTs and flame retardants-series C (C1, C2 and C3) are presented in Fig. 3-9, and the data are summarized in Tab. 3-4. According to the reported literatures, the typical peaks for MWCNT at ca. 1329 cm^{-1} (peak D, sp^3 hybridization of carbon) relates to the disordered graphite structure, and 1593 cm^{-1} (peak G, sp^2 hybridization of carbon) corresponds to a splitting of the E_{2g} stretching mode of graphite [33-35]. Therefore, the value of I_G/I_D can represent the degree of functionalization on the side walls of carbon nanotubes. And more generally, the decrease in I_G/I_D reflects the increase in disordered amorphous domain or content of sp^3 -hybridized carbons. As the data shown in Tab. 3-4, I_G/I_D of MWCNT is 0.52, while, that for flame retardants C1, C2 and C3 is 2.01, 0.81 and 0.47, respectively. That results clearly indicates the chemical graft of DOPO groups on the MWCNTs surfaces.

Tab. 3-4 Data of Raman spectra of pristine MWCNTs, C1, C2 and C3.

	X_G	X_D	$R = I_G/I_D$
MWCNTs	1593	1329	0.52
C1	1590	1343	2.01
C2	1596	1339	0.81
C3	1599	1326	0.47

(3) XPS

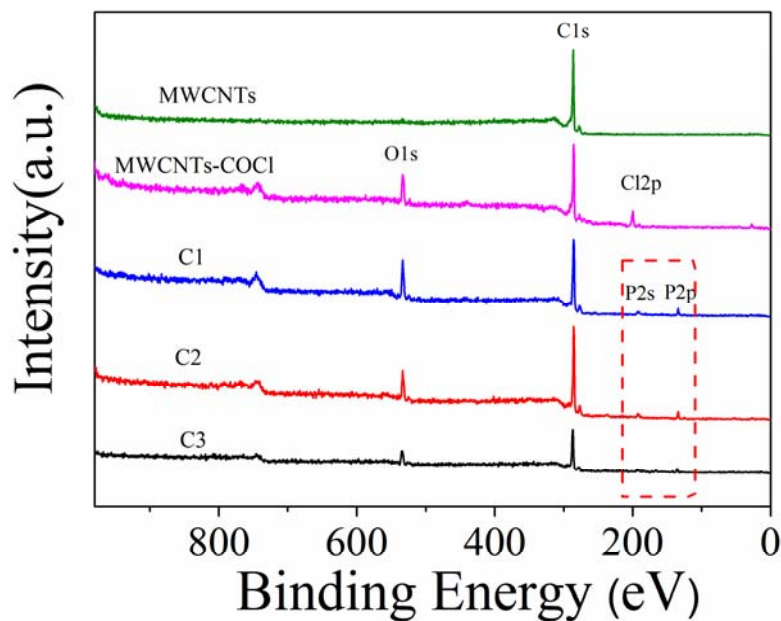


Fig. 3-10 The XPS survey spectra of MWCNTs and flame retardants-series C.

XPS analysis was performed to understand the chemical composition and structure of flame retardants-series C, and the spectra are shown in Fig. 3-10. The survey spectra show that besides the C1s (285 eV), a new peak can be observed at 200 eV (Cl2p) for MWCNTs-COCl, which can apparently be attributed to the chloroformylation reaction on the surface of MWCNTs (Scheme 3-10). The appearance of P2p peaks at 135.5 eV for all flame retardants-series C further confirm that the DOPO groups have been chemically introduced into the nano-core-shell flame retardants-series C.

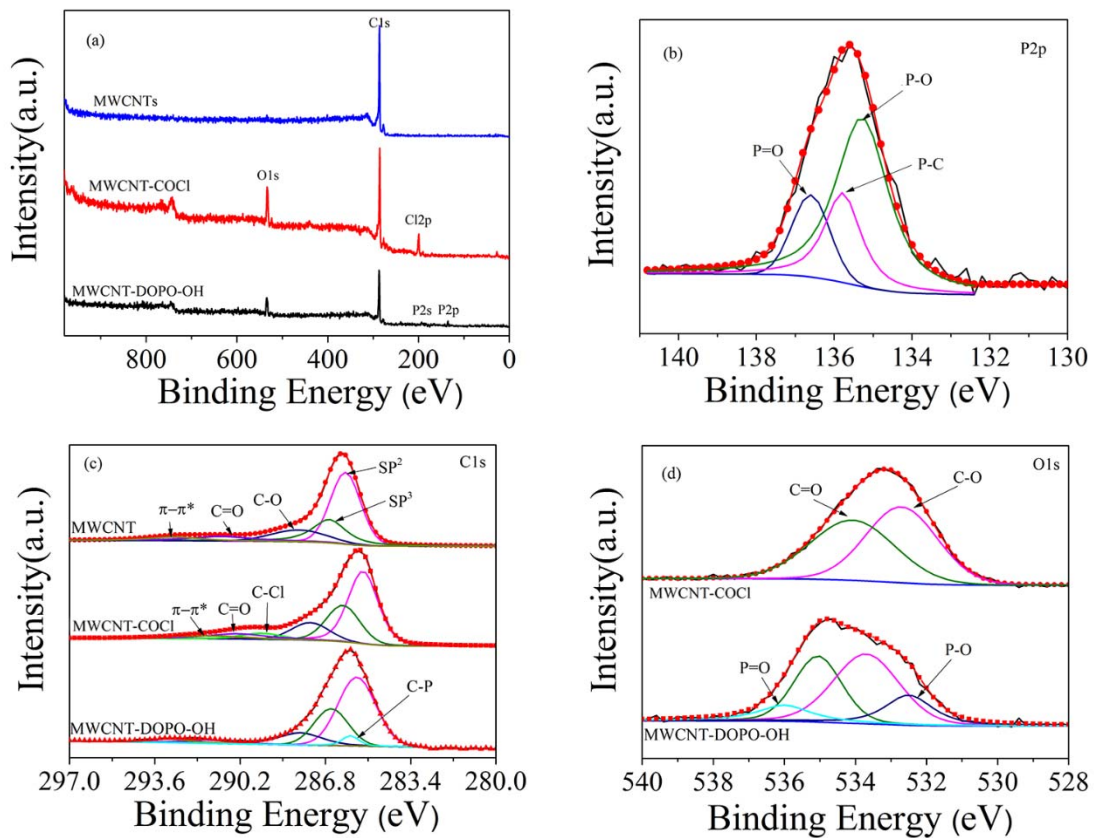


Fig. 3-11 The XPS (a) survey spectra of MWCNTs, MWCNT-COCl and C3; high-resolution XPS spectra of (b) P2p for C3; (c) C1s for MWCNTs, MWCNT-COCl and C3; (d) O1s for MWCNT-COCl and C3.

Take flame retardant C3 as an instance. The survey spectra (Fig. 3-11a) show that besides the deconvolution of the C1s peak at 286 eV of the as-received MWCNTs, new peaks are observed at 200 eV (Cl2p) and 533 eV (O1s) for MWCNT-COCl, which can apparently be attributed to the acylation reaction on the surface of MWCNTs (Scheme

3-10) [36-37]. The disappearance of Cl2p peak and appearance of P2p peaks at 135.5 eV for C3 further confirm the chemically grafting reaction of DOPO-OH groups on MWCNTs-COCl surfaces, according with the *Step 2* in Scheme 3-13. The high-resolution XPS P2p spectra for C3 (Fig. 3-11b) show three relatively well-resolved peaks of P—O (135.3 eV), P—C (135.8 eV) and P=O (136.6 eV) with the ratio of 2 : 1 : 1, corresponding to that three kinds of phosphorus species in C3 [38]. From Fig. 3-11c and d, the detailed analyses of XPS spectra provide clear evidence that the MWCNTs have been surface chemically modified following the three steps shown in Scheme 1. As seen in Fig. 3-11c, the following bonds for MWCNTs are assigned: sp² C=C (286 eV), sp³ C—C (286.7 eV), C—O (287.8 eV), C=O (290.8 eV), π — π^* (292.8 eV) [39-41]. The C—Cl bond at 289.4 eV for MWCNT-COCl confirms the acylation reaction. While its disappearance as well as the appearance of new C—P bond (286.8 eV) demonstrate the following nucleophile substitution reaction. Comparing the high-resolution XPS O1s spectra for MWCNT-COCl with MWCNT-DOPO-OH (Fig. 3-11d), the nucleophile substitution reaction between MWCNT-COCl and DOPO-OH is further evidenced by the appearance of peak at 532.4 eV (P—O) and 536 eV (P=O) represented phosphorus element [42]. It can thus be concluded that the DOPO-OH groups have been chemically grafted onto the MWCNTs surfaces to form flame retardant C3.

(4) TEM

As more direct evidence for the covalent functionalization of DOPO-containing flame retardant onto MWCNTs, pristine MWCNTs and flame retardants-series C (C1, C2 and C3) were analyzed by TEM and the results are shown in Fig. 3-12. For pristine MWCNTs (Fig. 3-12a), the hollow core and the open end can be found as well as the surface seems to be smooth and clear without any extra phase adhering to it. In contrast, a 5 nm-thin layer covered on the surface of MWCNTs is observed in flame retardants-series C (Fig. 3-12b). Such core-shell structured flame retardants-series C with the DOPO-containing flame retardant layer as the shell and MWCNTs at the center shows an increased diameter about 19~20 nm comparing to that (10~11nm) of pristine MWCNTs, which indicates that

DOPO-containing flame retardant have been successfully grafted onto the MWCNT surface.

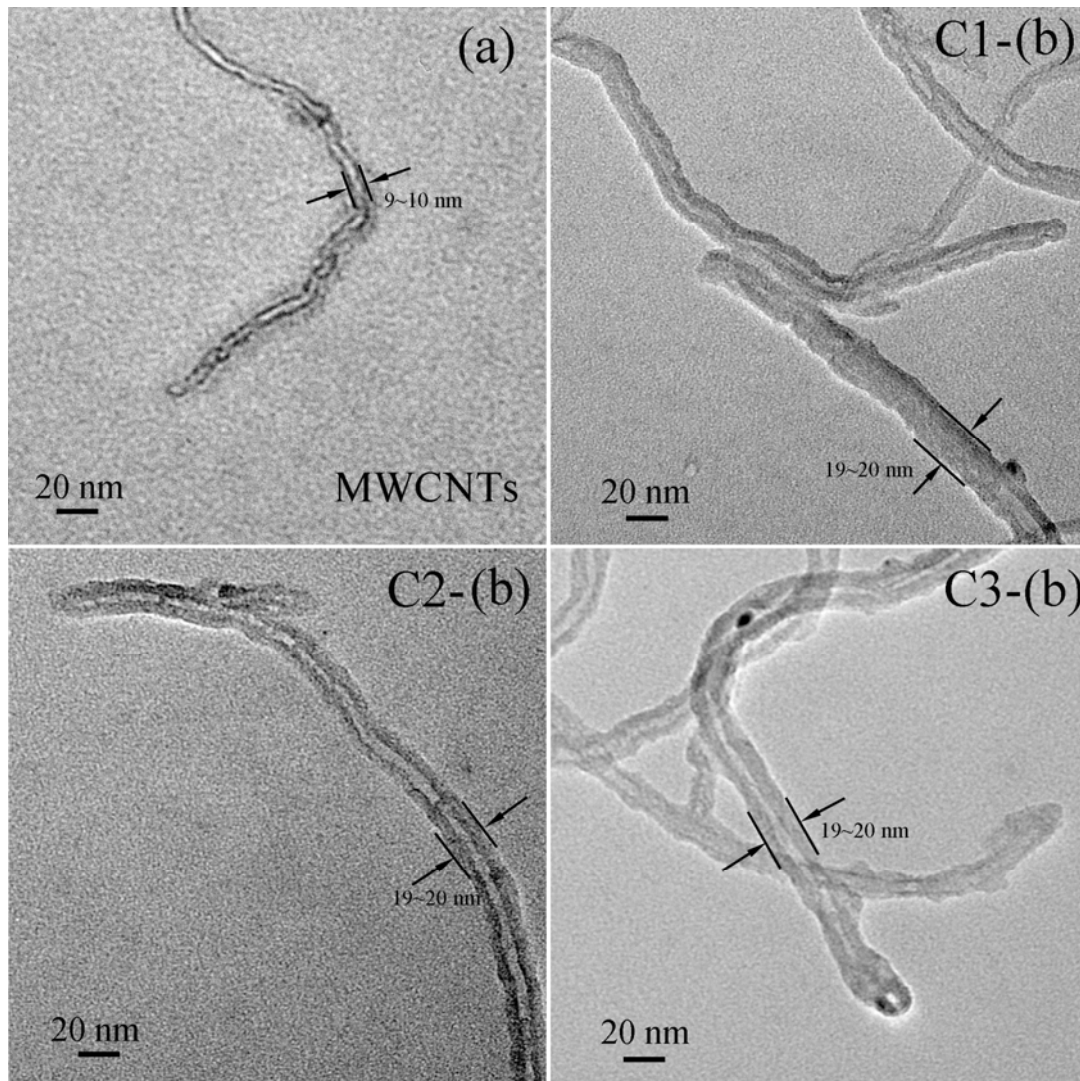


Fig. 3-12 TEM images of (a) MWCNTs and flame retardants C1-(b), C2-(b), C3-(b).

(5) TGA

Thermal stability of pristine MWCNT, flame retardants-series C (C1, C2 and C3) and their synthesis intermediates (DOPO-containing flame retardants C1a, C2a and C3a) were investigated by TGA under N₂ atmosphere at a heating rate of 10 °C/min, and the results are shown in Fig. 3-13. Pristine MWCNTs hardly decomposes at temperature below 600 °C, and the residue is about 96.6 wt.%, whereas DOPO-containing flame retardants C1a, C2a and C3a remain about 4.2 wt.%, 28.5 wt.% and 7.9 wt.% residue char after thermal degradation, respectively. The weight loss of flame retardants-series C

increases rapidly at 350~450 °C, which is due to the decomposition of shell flame retardants, as well as 69.3 wt.%, 58.1 wt.% and 60.8 wt.% residue char is left at the end of the test (600 °C), respectively. It is due to the attachment of DOPO-containing shells on the MWCNTs surface which causes the decrease in the thermal stability of MWCNTs. According to previous study by Ma *et al.* [14] the relative amounts of grafted DOPO-containing shell can be determined by TGA through such thermal decomposition test. Take flame retardant C3 as instance, the difference in the residue weight loss between pristine MWCNTs and C3 (35.8 wt%) at 600 °C divides that between pristine MWCNTs and C3a (88.7 wt.%) resulting the grafting amount of C3a (about 40.4 wt. %). For flame retardants C1 and C2, 29.55 wt.% of C1a and 56.5 wt.% of C2a are grafted onto the surface of MWCNTs, respectively.

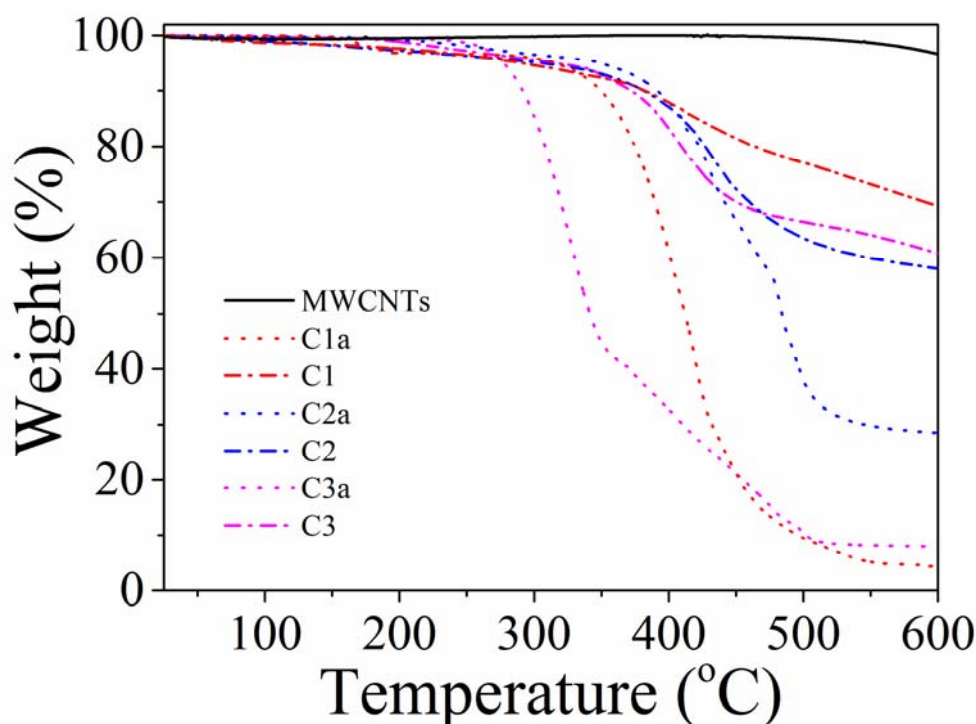


Fig. 3-13. TGA curves of MWCNTs, flame retardants-series C (C1, C2 and C3) and their synthesis intermediates (DOPO-containing flame retardants C1a, C2a and C3a).

3.4 Conclusions

In summary, three types of novel DOPO-containing flame retardants (Series A: single

molecules; Series B: chain-like macromolecules; Series C: Functionalizing MWCNTs) were successfully synthesized in good yields based on the Pudovik reactions. Flame retardants series A were characterized by ^1H , ^{13}C and ^{31}P NMR spectroscopy, elemental analysis (EA) and Fourier transform infrared (FT-IR) spectroscopy. For series B, FT-IR and X-ray photoelectron spectroscopy (XPS) were taken to confirm their compositions. Core-shell nanostructured flame retardants-series C with MWCNTs as the hard core and molecule flame retardant (C1a, C2a or C3a) as shell were successfully synthesized. The results from FTIR, Raman, XPS, TGA and TEM proved that high density with about 29.5 wt% C1a, 56.5 wt% C2a or 40.4 wt% C3a was covalently grafted on the surface of MWCNTs, respectively.

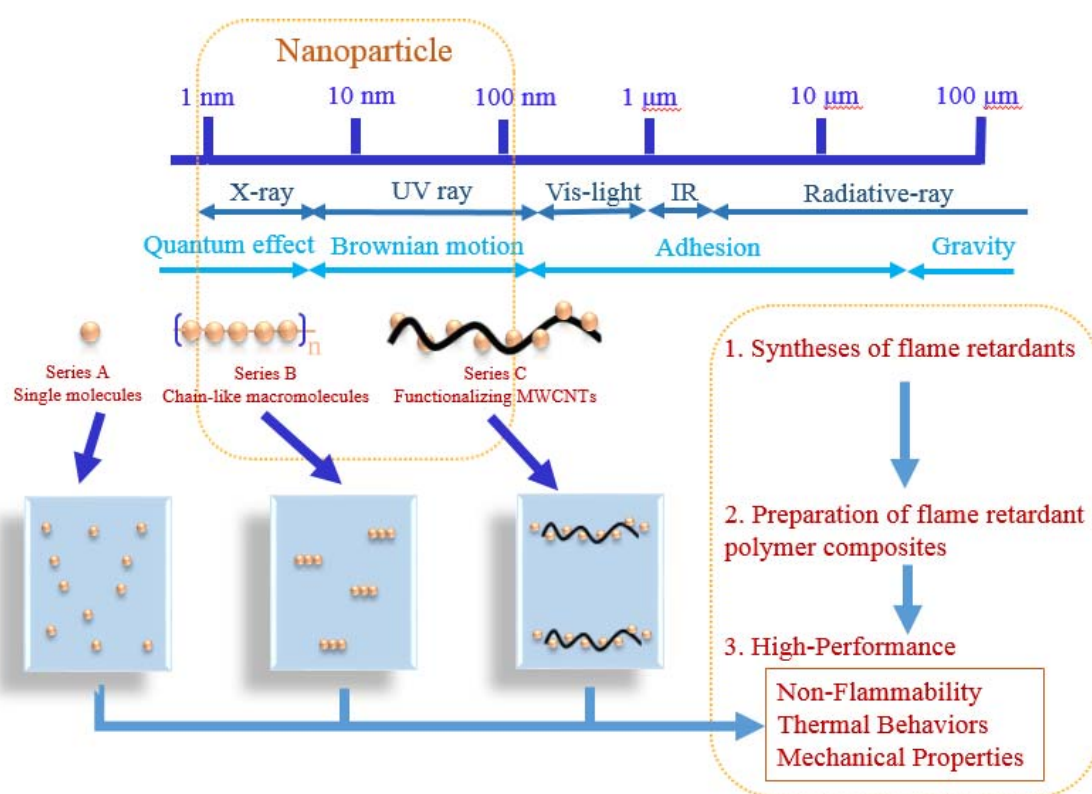


Fig. 3-14 The overall structure of the present study.

References

- [1] Fisk P, Girling A, Wildey R. Prioritisation of flame retardants for environmental risk assessment. Wallingford, UK: Environment Agency, 2003.
- [2] Gay-Lussac, J. L. Note on the properties of salts for making fabrics incombustible. *Ann. chim*, 1821, 2(18), 211-217.
- [3] Papazoglou, E. S. Flame retardants for plastics. *Handbook of building materials for fire protection*, 2004, 1-88.
- [4] Andrae, N. J. Durable and environmentally friendly flame retardants for synthetics, 2008.
- [5] Lee, K., Yoon, K., Kim, J., Bae, J., Yang, J., Hong, S. Effect of novolac phenol and oligomeric aryl phosphate mixtures on flame retardance enhancement of ABS. *Polymer Degradation and Stability*, 2003, 81(1), 173-179.
- [6] Min, H. J., & Yu, C. R. Studies of Quinazolone Analogues Containing Phosphorus and Their Reaction with Aldehydes. *Chemical Research In Chinese Universities*, 2000, 10, 056.
- [7] Bourbigot, S., Fontaine, G., Gallos, A., Bellayer, S. Reactive extrusion of PLA and of PLA/carbon nanotubes nanocomposite: processing, characterization and flame retardancy. *Polymers for Advanced Technologies*, 2011, 22(1), 30-37.
- [8] Levchik, S. V., Weil, E. D. A review of recent progress in phosphorus-based flame retardants. *Journal of Fire Sciences*, 2006, 24(5), 345-364.
- [9] Chiang, C. L., Ma, C. C. M. Synthesis, characterization and thermal properties of novel epoxy containing silicon and phosphorus nanocomposites by sol-gel method. *European polymer journal*, 2002, 38(11), 2219-2224.
- [10] Sun, D., Yao, Y. Synthesis of three novel phosphorus-containing flame retardants and their application in epoxy resins. *Polymer Degradation and Stability*, 2011, 96(10), 1720-1724.
- [11] Wang, X., Hu, Y., Song, L., Xing, W., Lu, H., Lv, P., Jie, G. Flame retardancy and

thermal degradation mechanism of epoxy resin composites based on a DOPO substituted organophosphorus oligomer. *Polymer*, 2010, 51(11), 2435-2445.

[12] Xu, M. J., Xu, G. R., Leng, Y., Li, B. Synthesis of a novel flame retardant based on cyclotriphosphazene and DOPO groups and its application in epoxy resins. *Polymer Degradation and Stability*, 2016, 123, 105-114.

[13] Wang, C. S., & Shieh, J. Y. Synthesis and properties of epoxy resins containing 2-(6-oxid-6H-dibenz< c, e> < 1, 2> oxaphosphorin-6-yl) 1, 4-benzenediol. *Polymer*, 1998, 39(23), 5819-5826.

[14] Ma, H. Y., Tong, L. F., Xu, Z. B., & Fang, Z. P. Functionalizing carbon nanotubes by grafting on intumescent flame retardant: nanocomposite synthesis, morphology, rheology, and flammability. *Advanced functional materials*, 2008, 18(3), 414-421.

[15] Yu, T., Jiang, N., & Li, Y. Functionalized multi-walled carbon nanotube for improving the flame retardancy of ramie/poly (lactic acid) composite. *Composites Science and Technology*, 2014, 104, 26-33.

[16] Deng, X., Jia, G., Wang, H., Sun, H., Wang, X., Yang, S., ... & Liu, Y. Translocation and fate of multi-walled carbon nanotubes in vivo. *Carbon*, 2007, 45(7), 1419-1424.

[17] Ho, T. H., Hwang, H. J., Shieh, J. Y., & Chung, M. C. Thermal, physical and flame-retardant properties of phosphorus-containing epoxy cured with cyanate ester. *Reactive and Functional Polymers*, 2009, 69(3), 176-182.

[18] Chen, H., Zhang, K., & Xu, J. Synthesis and characterizations of novel phosphorous–nitrogen containing poly (ether sulfone)s. *Polymer degradation and stability*, 2011, 96(2), 197-203.

[19] Eberstaller, R., & Hintermeier, G. Flame-retardant expandable polymers: U.S. Patent Application No. 14/112,913, 2012.

[20] Lin C H, Cai S X, Lin C H. Flame-retardant epoxy resins with high glass-transition temperatures. II. Using a novel hexafunctional curing agent: 9,10-dihydro-9-oxa-10-phosphaphenanthrene 10-yl-tris (4-aminophenyl) methane. *Journal of Polymer Science Part A: Polymer Chemistry*, 2005, 43(23): 5971-5986.

-
- [21] Sun J, Wang X, Wu D. Novel spirocyclic phosphazene-based epoxy resin for halogen-free fire resistance: synthesis, curing behaviors, and flammability characteristics. *ACS Applied Materials & Interfaces*, 2012, 4(8): 4047-4061.
- [22] Sun D, Yao Y. Synthesis of three novel phosphorus-containing flame retardants and their application in epoxy resins. *Polymer Degradation and Stability*, 2011, 96(10): 1720-1724.
- [23] Zhang R, Xiao X, Tai Q, et al. Preparation of lignin-silica hybrids and its application in intumescent flame-retardant poly (lactic acid) system. *High Performance Polymers*, 2012: 0954008312451476.
- [24] Gu L, Chen G, Yao Y. Two novel phosphorus-nitrogen-containing halogen-free flame retardants of high performance for epoxy resin. *Polymer Degradation and Stability*, 2014, 108: 68-75.
- [25] Lin C H, Lin H T, Chang S L, et al. Benzoxazines with tolyl, p-hydroxyphenyl or p-carboxyphenyl linkage and the structure-property relationship of resulting thermosets. *Polymer*, 2009, 50(10): 2264-2272.
- [26] Lin C H, Lin H T, Sie J W, et al. Facile, one-pot synthesis of aromatic diamine-based phosphinated benzoxazines and their flame-retardant thermosets. *Journal of Polymer Science Part A: Polymer Chemistry*, 2010, 48(20): 4555-4566.
- [27] Wang C S, Shieh J Y. Synthesis and properties of epoxy resins containing bis(3-hydroxyphenyl) phenyl phosphate. *European polymer journal*, 2000, 36(3): 443-452.
- [28] Gu, L., Qiu, J., & Sakai, E. A novel DOPO-containing flame retardant for epoxy resin Synthesis, nonflammability, and an optimized curing procedure for high performance. *High Performance Polymers*, 2016, DOI: 0954008316664123.
- [29] Gu, L., Qiu, J., & Sakai, E. Thermal stability and fire behavior of aluminum diethylphosphate-epoxy resin nanocomposites. *Journal of Materials Science: Materials in Electronics*, 2016, DOI: 0954008316664123.
- [30] Deng, X., Jia, G., Wang, H., Sun, H., Wang, X., Yang, S., ... & Liu, Y. Translocation

and fate of multi-walled carbon nanotubes in vivo. *Carbon*, 2007, 45(7), 1419-1424.

[31] Wang, X., Hu, Y., Song, L., Xing, W., Lu, H., Lv, P., & Jie, G. Flame retardancy and thermal degradation mechanism of epoxy resin composites based on a DOPO substituted organophosphorus oligomer. *Polymer*, 2010, 51(11), 2435-2445.

[32] Perret, B., Schartel, B., Stöß, K., Ciesielski, M., Diederichs, J., Döring, M., ... & Altstädt, V. Novel DOPO-based flame retardants in high-performance carbon fibre epoxy composites for aviation. *European Polymer Journal*, 2011, 47(5), 1081-1089.

[33] Xu, M. J., Xu, G. R., Leng, Y., & Li, B. Synthesis of a novel flame retardant based on cyclotriphosphazene and DOPO groups and its application in epoxy resins. *Polymer Degradation and Stability*, 2016, 123, 105-114.

[34] Eswaraiah, V., Sankaranarayanan, V., & Ramaprabhu, S. Inorganic nanotubes reinforced polyvinylidene fluoride composites as low-cost electromagnetic interference shielding materials. *Nanoscale Res Lett*, 2011, 6(1), 137.

[35] Zhao, Y., Yang, X., Zhan, L., Ou, S., & Tian, J. High electrocatalytic activity of PtRu nanoparticles supported on starch-functionalized multi-walled carbon nanotubes for ethanol oxidation. *Journal of Materials Chemistry*, 2011, 21(12), 4257-4263.

[36] Yang, X. H., Guo, J. W., Yang, S., Hou, Y., Zhang, B., & Yang, H. G. A free radical assisted strategy for preparing ultra-small Pt decorated CNTs as a highly efficient counter electrode for dye-sensitized solar cells. *Journal of Materials Chemistry A*, 2014, 2(3), 614-619.

[37] Roy, S., Das, T., Ming, Y., Chen, X., Yue, C. Y., & Hu, X. Specific functionalization and polymer grafting on multiwalled carbon nanotubes to fabricate advanced nylon 12 composites. *Journal of Materials Chemistry A*, 2014, 2(11), 3961-3970.

[38] Paraknowitsch, J. P., Zhang, Y., Wienert, B., & Thomas, A. Nitrogen-and phosphorus-co-doped carbons with tunable enhanced surface areas promoted by the doping additives. *Chemical Communications*, 2013, 49(12), 1208-1210.

[39] Okpalugo, T. I. T., Papakonstantinou, P., Murphy, H., McLaughlin, J., & Brown, N. M. D. High resolution XPS characterization of chemical functionalised MWCNTs and

SWCNTs. *Carbon*, 2005, 43(1), 153-161.

[40] Dubal, D. P., Gund, G. S., Lokhande, C. D., & Holze, R. Decoration of spongelike Ni(OH)₂ nanoparticles onto MWCNTs using an easily manipulated chemical protocol for supercapacitors. *ACS applied materials & interfaces*, 2013, 5(7), 2446-2454.

[41] Bao, J., Dou, M., Liu, H., Wang, F., Liu, J., Li, Z., & Ji, J. Composition-Dependent Electrocatalytic Activity of Palladium–Iridium Binary Alloy Nanoparticles Supported on the Multiwalled Carbon Nanotubes for the Electro-Oxidation of Formic Acid. *ACS applied materials & interfaces*, 2015, 7(28), 15223-15229.

[42] Andreiadis, E. S., Jacques, P. A., Tran, P. D., Leyris, A., Chavarot-Kerlidou, M., Josselme, B., ... & Artero, V. Molecular engineering of a cobalt-based electrocatalytic nanomaterial for H₂ evolution under fully aqueous conditions. *Nature Chemistry*, 2013, 5(1), 48-53.

Chapter 4 Flame Retardant Epoxy Resins: Non-Flammability, Thermal Stability and Mechanical Properties

4.1 Introduction

Flame-retarding epoxy resin has become one of the basic materials in the electronic industry. For example, brominated epoxy resins are used as main materials for the copper clad laminate, because of their good flame retardancy, low cost, excellent physical and mechanical properties.[1] The poor fire resistance of epoxy composites is one of the major concerns in their applications as basic materials in the electronic industry [2]. The subject of flame retardant epoxy resins and their composites has attracted considerable interest. For example, brominated epoxies are widely available for commercial use because of their good flame retardancy, low cost, as well as excellent physical and mechanical properties [3]. However, halogenated epoxy resins or halogen-containing flame retardants cause serious environmental problems, i.e., the release of toxic and corrosive gases associated with burning during combustion, such as hydrogen halides, which are a potential health hazard [4-6]. In recent years, driven by the urgent need of environmental protection, researches on halogen-free flame retardant (HFFR) of environment friendly, so called “green flame retardant”, have received considerable attention.[7] As an important branch of HFFR family, phosphorus-containing flame retardants impart significant flame-retarding property to epoxy resins through phosphorylation.[8] The condensed phase mechanism and vapor phase mechanism are mainly suggested to explain the phosphorylation.[9] A lot of studies based on these two mechanisms have been carried out to predict the composite properties of fire-retardancy and develop efficient phosphorus-containing fire-retardant composites, of which three main strategies was recommended.[10-12] The first one relies on the expectation of forming carbonaceous chars or barrier layers of polyphosphoric acid during combustion

in the condensed phase.[13] The second strategy suggests the reactive types of flame retardants. Reactive types of flame retardants exhibit much better flame retardancy and overcome several drawbacks associated with physical blends of epoxy to the additive types.[14] The third strategy involves the synergistic property. Such synergistic property probably occurs due to the formation of the P—N bonded intermediates, which gives better phosphorylating agents than those of the related phosphorus compounds without nitrogen [15]. Nevertheless, there are still many challenges for phosphorus-containing flame retardant epoxy resins to encounter (or risk) such as: phosphorus resource efficiency, potential eutrophication from phosphorous, as well as the flame-retarding performance in terms of UL 94 V-0 rating [16].

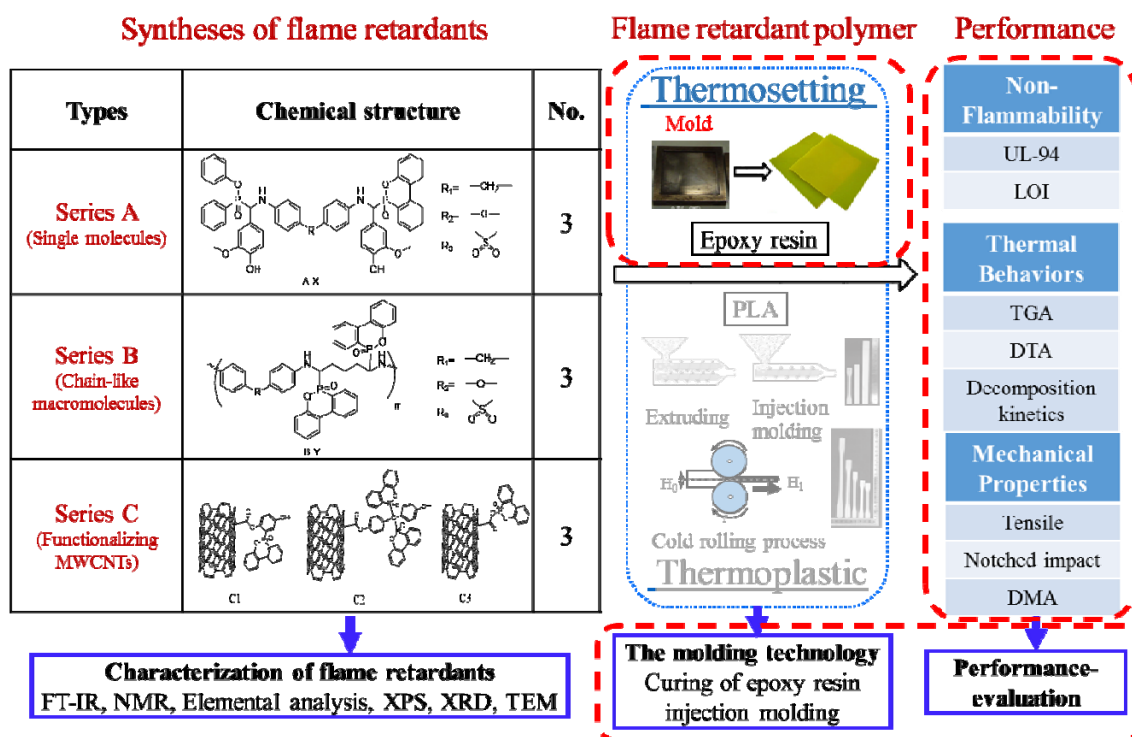


Fig. 4-1 Preparation and performance-evaluation of flame retardant epoxy resin composites.

In this work, three types of DOPO-containing flame retardants (Series A: single molecules; Series B: chain-like macromolecules; Series C: Functionalizing MWCNTs) were well dispersed into epoxy resin to form flame-retardant epoxy resin composites. Such epoxy resin composites showed high performance that: meeting UL 94 V-0

flammability rating; high LOI values of more than 34.5; higher T_g than that of neat epoxy resin; excellent mechanical properties. The preparation and performance-evaluation of flame retardant epoxy resin composites in this work are shown in Fig. 4-1.

4.2 Experimental

4.2.1 Materials

Flame retardants Ax, Bx and Cx were synthesized following Chapter 3. According to the supplier (Clariant Chemicals Ltd., Germany.), the average particle size for nano-aluminum diethylphosphinate (AlPi) is about 300 nm. It was dried at 80 °C for 12 h in a vacuum oven before adding into epoxy resin. 2, 2-Bis (4-glycidyloxyphenyl) propane (another name as diglycidyl ether of bisphenol A, short for DGEBA, epoxy equivalent = 0.51 mol/100 g) from Wuxi Diaisheng Epoxy Co., Ltd., were used as received.

4.2.2 Instruments and measurements

The Underwriter Laboratories 94 vertical tests (UL-94) were performed according to IEC 60695-11-10:1999 using a horizontal and vertical burning instrument (FZ-5401, Dongguan Hanyang electronic instrument Co., Ltd, China). The LOI test was performed according to the testing procedure of ISO 4589-2:1996 with the dimensions $80 \times 6 \times 3$ mm³ of each sample. Thermal gravimetric analyses (TGA) of samples were carried out with Shimadzu DTG-60/60H from 30 °C to 600 °C at heating rates of 10 °C·min⁻¹, whereas the flow of nitrogen was maintained at 50 mL·min⁻¹. Differential thermal analyses (DTA) were taken with the same instrument from 30 °C to 200 °C at heating rates of 5 °C·min⁻¹. The scanning electron microscope (SEM) observation was performed on a Hitachi S-4300 scanning electron microscope in high vacuum mode with 5 kV acceleration voltage. Dynamic mechanical analysis (DMA) was performed by using a TA Instrument RSA-G2 with a sample size of $20 \times 5 \times 2$ mm³ by 3-Point Bending mode with an amplitude of 30 μm. The storage modulus E' and $\tan \delta$ were determined as the sample

was subjected to the temperature scan mode at a programmed heating rate of 3 °C·min⁻¹ and a frequency of 1 Hz.

4.2.3 Preparation of flame retardant epoxy resins

(1) Curing procedure of flame retardants-series A or B modified epoxy resin.

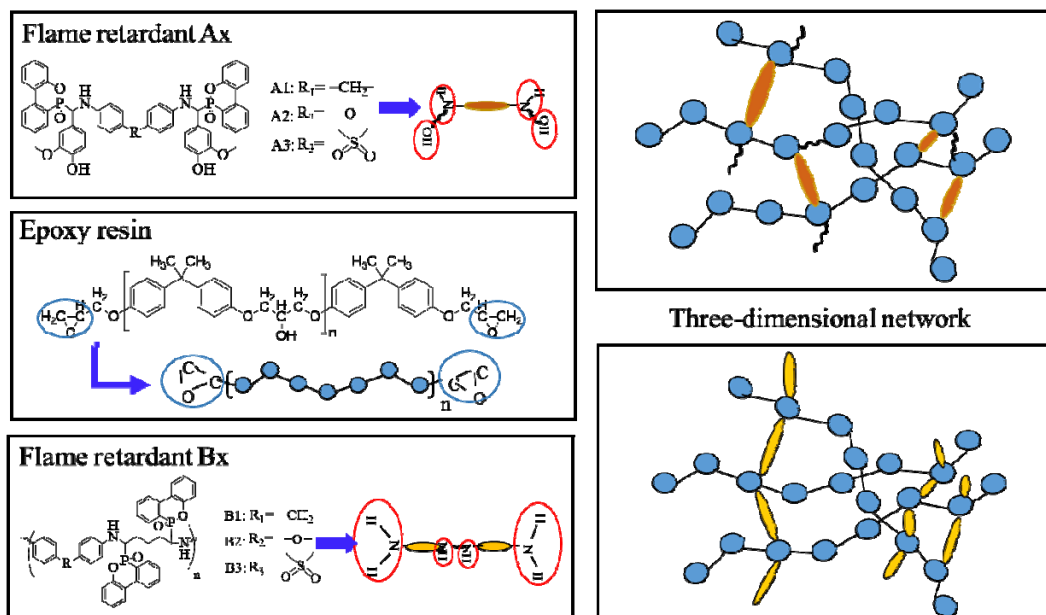


Fig. 4-2 Curing reaction of flame retardants-series A or B with epoxy resin.

The flame retardants-series A (A1, A2 or A3) or B (B1, B2 or B3) modified epoxy resins with phosphorus content 0.75 wt%, 1.0 wt%, 1.5wt% were cured using DDM as hardener. As shown in Fig.4-2, due to the same active proton numbers of A1 (or A2, A3, B1, B2, B3) and DDM, flame retardants-series A (or series B) were used as co-curing agents of DDM.

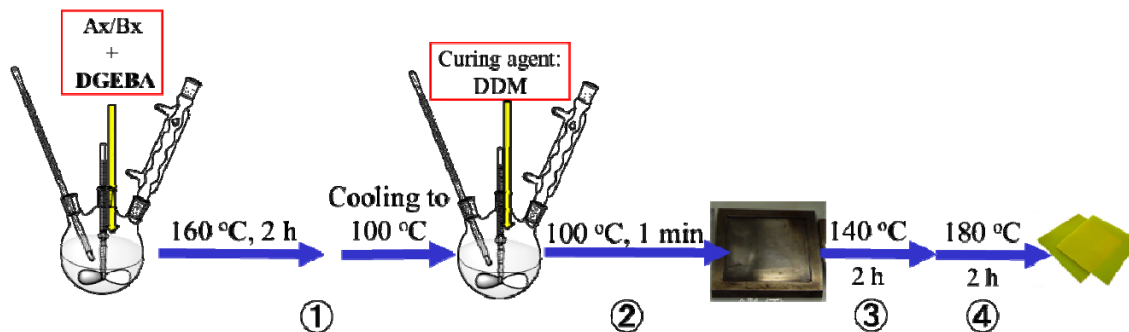


Fig. 4-3 Preparation of flame retardant epoxy resin composites with flame retardants-series A and B.

The curing agents and epoxy resins were added at a 1:1 equivalent ratio of active proton to epoxy group. The flame retardants-series A (or series B) and epoxy resin were mixed and stirred at 160°C for 2 h, then DDM was added when the mixtures were cooled to 100°C. The products were cured at 140°C for 2 h and then 180°C for 2 h. Thereafter, the epoxy thermosets were cooled slowly to room temperature, in order to prevent cracking. The preparation of flame retardant epoxy resin composites (labeled as shown in Tab. 4-1) with flame retardants-series A and B are shown in Fig 4-3.

(2) Curing procedure of flame retardants-series C modified epoxy resin.

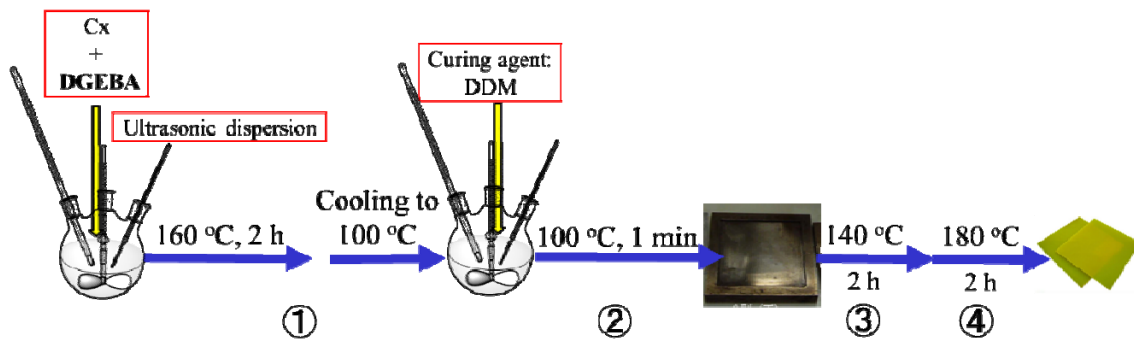


Fig. 4-4 Preparation of flame retardant epoxy resin composites with flame retardants-series C.

The flame retardants-series C (1 wt%)-modified epoxy resins with phosphorus content of 0.75 wt%, 1.00 wt% and 1.50 wt% were cured using DDM as hardeners, which were labeled as shown in Tab. 4-1. The preparation of flame retardant epoxy resin composites with flame retardants-series C are shown in Fig. 4-4. Curing procedure: 1 wt% C1 (or C2, C3), ALPi and Epoxy resin were mixed and stirred by a mechanical stirrer at 20 rpm, accompanied with dispersing through ultrasonication technique (600 W) at 30 °C for 2 h. Then the appropriate amount of DDM (EP/DDM =100/25, w/w) was added when the mixtures were heated to 100 °C. After degasification, the prepared mixture was poured into the mold. The systems were cured at 140°C for 2 h and then 180°C for 2 h. Thereafter, the flame retardants-series C modified epoxy resin composites were allowed to cool slowly to room temperature, in order to prevent cracking.

4.3 Results and discussion

4.3.1 Non-flammability and residual char analysis

In this work, the flame retardancy of flame retardants-series A (or series B, series C)-modified epoxy resin composites were evaluated by Underwriter Laboratories 94 vertical tests (UL 94) and LOI test.

(1) Non-flammability

For flame retardants-series A modified epoxy resin composites, the *LOI* values and UL-94 vertical burning grades of thermosets, $A_x/(P^0\%-Y)$ ($x=1, 2, 3$ and $Y=0.75, 1.0, 1.5$), are summarized in Tab.4-1. The *LOI* values of $A_x/(P^0\%-0.75)$ ($x=1, 2, 3$) are 34.5, 33.3 and 34.8, respectively. All the three epoxy resin composites with phosphorus content of 0.75 wt% arrive UL-94 V-0 grade. To the best of our knowledge, this is the highest flame-retarding efficiency based on phosphorus content. The *LOI* values of those flame retardants-series A modified epoxy resin composites increase with the addition of A_x ($x=1, 2, 3$) increasing, which may result from nitrogen-phosphorus synergistic effect. Take flame retardant A3 as instance, further assessment of the flammability of the $A_3/(P^0\%-Y)$ epoxy resin composites are provided in Tab. 4-1. When flame retardant A3 is added, the *LOI* value of $A_3/(P^0\%-1.00)$ is increased to 35.8, which can reach UL 94 V-0 rating. $B_2/(P^0\%-1.50)$ achieves a higher *LOI* value of 37.5 and the UL 94 V-0 rating.

For flame retardants-series B modified epoxy resin composites, the flame-retardant performance of the $B_x/(P^0\%-Y)$ ($x=1, 2, 3$ and $Y=0.75, 1.0, 1.5$) composites have been investigated in terms of UL-94 vertical burning tests, and the results are also summarized in Tab. 4-1. It is clear that UL 94 V-0 flammability rating can be reached for $B_x/(P^0\%-0.75\%)$ ($x=1, 2, 3$) and meanwhile the *LOI* value reached over 35.5. The flame retardancy of $B_x/(P^0\%-Y)$ epoxy resin composites increase with the phosphorus content increasing.

Tab. 4-1 Thermal properties and flame retardancy of epoxy resin composites.

Series	Flame retardant	Thermoset ID	T_g (°C) ^a	T_g (°C) ^b	T_g (°C) ^c	Char Yield ^d	UL-94 grade	LOI
A	A1	A1/(P%-0.75)	157	159	168	27.3	V-0	34.5
		A1/(P%-1.00)	151	155	164	30.6	V-0	36.5
		A1/(P%-1.50)	143	146	156	30.1	V-0	37.0
	A2	A2/(P%-0.75)	145	143	154	22.8	V-0	33.3
		A2/(P%-1.00)	141	142	154	24.3	V-0	34.8
		A2/(P%-1.50)	135	137	151	22.8	V-0	35.0
	A3	A3/(P%-0.75)	140	142	150	24.4	V-0	34.8
		A3/(P%-1.00)	138	138	146	22.5	V-0	35.8
		A3/(P%-1.50)	134	137	147	25.9	V-0	37.5
B	B1	B1/(P%-0.75)	154	158	167	27.8	V-0	36.5
		B1/(P%-1.00)	147	154	162	26.7	V-0	37.8
		B1/(P%-1.50)	143	150	157	31.0	V-0	40.2
	B2	B2/(P%-0.75)	149	161	168	25.8	V-0	35.6
		B2/(P%-1.00)	154	162	169	27.2	V-0	38.5
		B2/(P%-1.50)	149	154	163	27.0	V-0	40.0
	B3	B3/(P%-0.75)	152	159	166	25.5	V-0	35.5
		B3/(P%-1.00)	151	162	170	29.2	V-0	38.2
		B3/(P%-1.50)	145	152	159	26.1	V-0	39.6
C	C1	C1/AlPi/(P%-0.75)	160	165	173	23.3	V-1	36.5
		C1/AlPi/(P%-1.00)	156	163	169	24.1	V-0	39.5
		C1/AlPi/(P%-1.50)	174	171	180	27.5	V-0	41.2
	C2	C2/AlPi/(P%-0.75)	169	169	176	22.0	V-1	37.2
		C2/AlPi/(P%-1.00)	170	173	180	24.5	V-0	40.2
		C2/AlPi/(P%-1.50)	162	169	177	30.3	V-0	43.5
	C3	C3/AlPi/(P%-0.75)	166	168	179	23.9	V-1	37.5
		C3/AlPi/(P%-1.00)	175	174	177	28.4	V-0	41.2
		C3/AlPi/(P%-1.50)	174	173	179	27.6	V-0	42.4

^a Measured by DTA.

^b Measured by DMA (Loss modulus).

^c Measured by DMA (Tan delta).

^d Residual weight percentage at 600 °C.

When flame retardant B2 is added, the LOI value of B2/(P%-1.00) is increased to 38.5, which can reach UL 94 V-0 rating. B2/(P%-1.50) achieves a higher LOI value of 40.0 and the UL 94 V-0 rating. According to the above results, a significant improvement of the flame retardancy for those Bx-modified epoxy resin composites by well dispersion of Bx into epoxy resin matrix.

For flame retardants-series C modified epoxy resin composites, the flammability of Cx/AlPi/(P%-Y) (x=1, 2, 3 and Y=0.75, 1.0, 1.5) composites with Cx content of 1 wt% have been investigated by UL 94 vertical burning tests and *LOI* tests. As shown in Tab. 4-1, the addition of C3 to AlPi/Epoxy resin flame retardant system can markedly increase the *LOI* values to 37.5, 41.2 and 42.4, respectively. It is expected that the flame retardancy of these epoxy resin nanocomposites improve better with the presence of 1 wt% Cx. As expected, the *LOI* values increase greatly for Cx/AlPi//Epoxy nanocomposites with only 1 wt% flame retardants-series C loading, demonstrating that the flame retardancy improved with adding Cx. Generally, when the LOI value is more than 26, materials could be considered to have flame retardancy. More importantly, Cx/AlPi/(P%-1.00) nanocomposites with 1 wt% Cx and phosphorus content of 1.00 wt% can achieve UL 94 V-0 rating, which can be attribute to the excellent char formation-promoting properties of nano-core-shell structured Cx. Take flame retardant C3 as instance, further assessment of the flammability of the C3/AlPi/(P%-Y) epoxy resin nanocomposites with 1 wt% C3 are provided in Tab. 4-1. Keeping the phosphorus-amount of 0.75 wt%, 1.00 wt%, 1.50 wt%, C3/AlPi/(P%-Y) nanocomposites show increasing *LOI* values of 37.5, 41.2 and 42.4, respectively.

This means these Cx/AlPi/(P%-Y) nanocomposites should almost be nonflammable in air. It could be concluded that the incorporation of 1 wt% Cx into the flame retardant AlPi/Epoxy resin systems is very effective for the enhancement of flame retardancy and makes those flame retardants-series C modified-epoxy resin nanocomposites becoming nonflammable functional polymers.

(2) Residual char analysis

It has been observed that the physical structure of the charring layer plays a very important role in preventing of heat transfer, flame spreading and droplet generation during combustion [17-19]. The morphologies of the residual chars collected from the vertical burning tests were investigated by SEM.

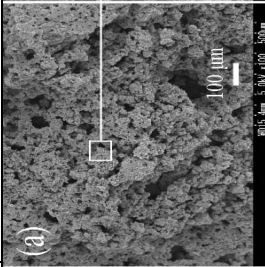
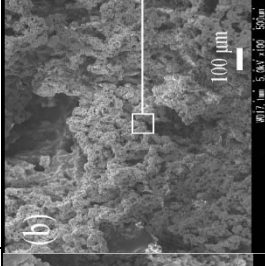
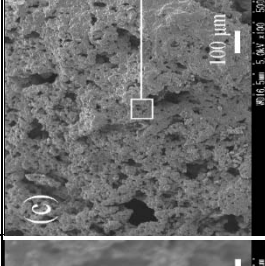
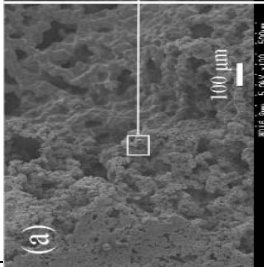
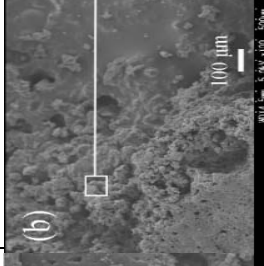
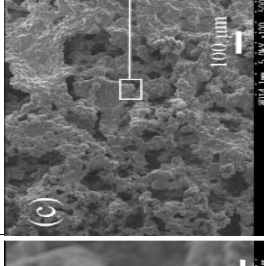
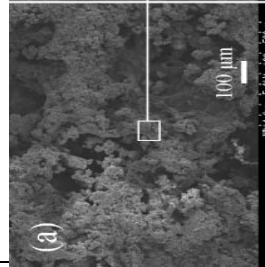
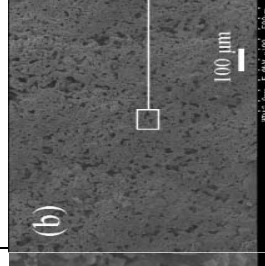
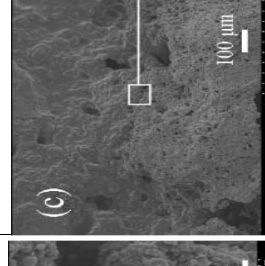
The outside of $A_x/(P\%-0.75)$'s ($x=1, 2, 3$) residual char is constructed by irregular-shaped bulks. Multiporous bulks that the pore density of $A_3/(P\%-0.75)$'s char outside is higher than that of $A_2/(P\%-0.75)$. This gassy surface is suggested to form with gas generation during combustion of thermoset. In addition, the char residual insides of $A_x/(P\%-0.75)$ are constructed by fussy and porous char bulks separated by irregular solid bulks [20].

For flame retardants-series B modified epoxy resin composites, irregular-shaped bulks were observed in all composites. Such a structural form prevents heat transfer and protects the matrix inside. It can be concluded that the addition of Bx enhanced the char formation during combustion, which serves as a barrier against heat and oxygen [21].

With a view to further clarify the combustion mechanism, morphologies of the residual chars of $C_x/AlPi/(P\%-Y)$ epoxy resin nanocomposites were collected from the vertical burning tests and investigated by SEM as shown in Tab. 4-2. All these residual chars exhibit a non-smooth carbonaceous charring layer with uneven distributing irregular-shaped pores. According to high magnification photo of each samples, the char show a foam structure indicating a typical morphology after the intumescent char formation.

For $C_x/AlPi/(P\%-0.75)$, a loose expansion surface adhering with some irregular-shaped and multiporous particles are observed, which may be resulted from the gas-products degraded during combustion. Such gas-generating process provide nonflammable gas as well as quenching effective phosphorus free radical to impede combustion according to the vapor phase mechanism and free radical quenching mechanism [22].

Tab. 4-2 SEM images of the residual chars obtained from UL 94 vertical burning tests.

Flame retardant	P%-0.75	P%-1.00	P%-1.50
C1	  	  	  

4.3.2 The thermal stability of epoxy resin composites

The thermal stability of epoxy-based functional materials establishes their service environment. For instance, as an important parameter of the thermal property of epoxy thermosets, T_g gives information about the crosslinking density, below which the epoxy thermosets can be used well in most cases. In this chapter, the thermal stability of flame retardant epoxy resin composites were investigated by TGA and DTA under nitrogen atmospheres at a heating rate of $10\text{ }^\circ\text{C}\cdot\text{min}^{-1}$.

(1) The thermal stability of Ax-modified epoxy resin composites

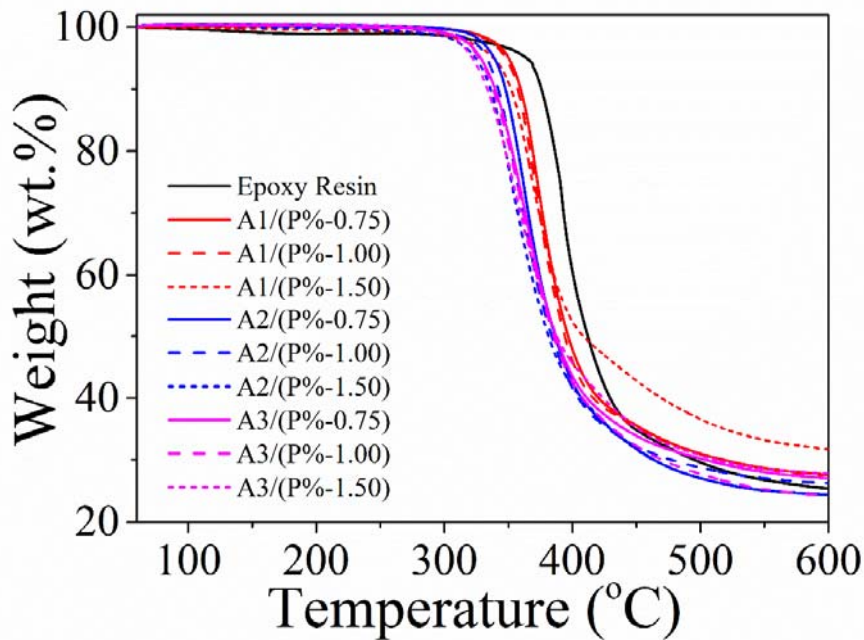


Fig. 4-5 TGA curves of flame retardants-series A modified epoxy resin composites measured at a heating rate of $10\text{ }^\circ\text{C}/\text{min}$.

The TGA curves of epoxy resin and flame retardants-series A modified epoxy resin composites under nitrogen are respectively shown in Fig. 4-5, and the analysis results are summarized in Tab. 4-1. Under nitrogen atmospheres, there is only a one-sharp weight loss stage for all the samples. Taking A2-modified epoxy resin composites as instance, the onset decomposition temperature of 5% weight loss ($T_{5\%}$) at a heating rate of $10\text{ }^\circ\text{C}\cdot\text{min}^{-1}$ is 366, 363 and $365\text{ }^\circ\text{C}$ for A2/(P%-0.75), A2/(P%-1.00) and A2/(P%-1.50), respectively, significantly lower than that ($377.79\text{ }^\circ\text{C}$) of epoxy resin. The decreasing

trend of $T_{5\%}$ can be attributed to the fact that the O=P-O bond in Ax-modified epoxy resin is more active than common C-C bond, which is also suggested to form phosphorus-containing radical stabilizers by the quenching mechanism in combustion. Additionally, Ax-modified epoxy resin composites show slower weight loss rate than that of neat epoxy resin. It is noteworthy that higher char yield can be obtained accompany with the addition of Ax, as charring layer plays a very important role in the performance of flame retardancy.

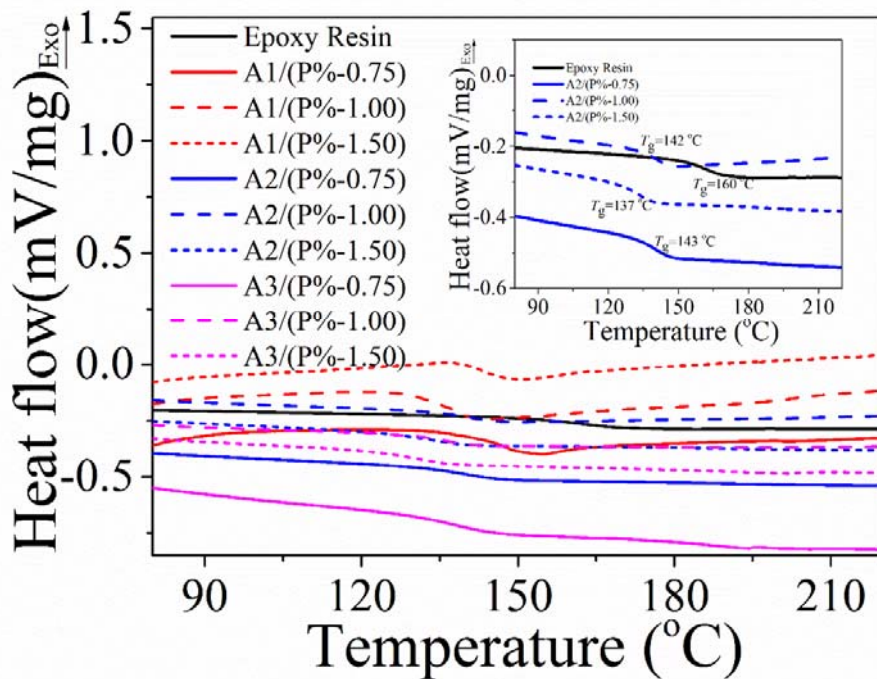


Fig. 4-6 DTA curves of flame retardants-series A (inset flame retardant A2) modified epoxy resin composites measured at a heating rate of 10 °C/min.

Fig. 4-6 shows DTA thermograms of epoxy resin and Ax-modified epoxy resin composites. Obtained from that, T_g s are summarized in Tab. 4-1. It is expected that all Ax-modified epoxy resin composites show a high- T_g , indicating an excellent thermal stability. Moreover, T_g s of all Ax/(P%-Y) epoxy resin composites with different flame retardant amount show a slight change to each other. Taking A2-modified epoxy resin composites as instance, T_g s of all the A2/(P%-Y) epoxy resin composites show just a slight change to each other of 137 to 143 °C, while, lower than that (160 °C) of neat

epoxy resin, which can be attributed to the poor chemical combination.

(2) The thermal stability of Bx-modified epoxy resin composites

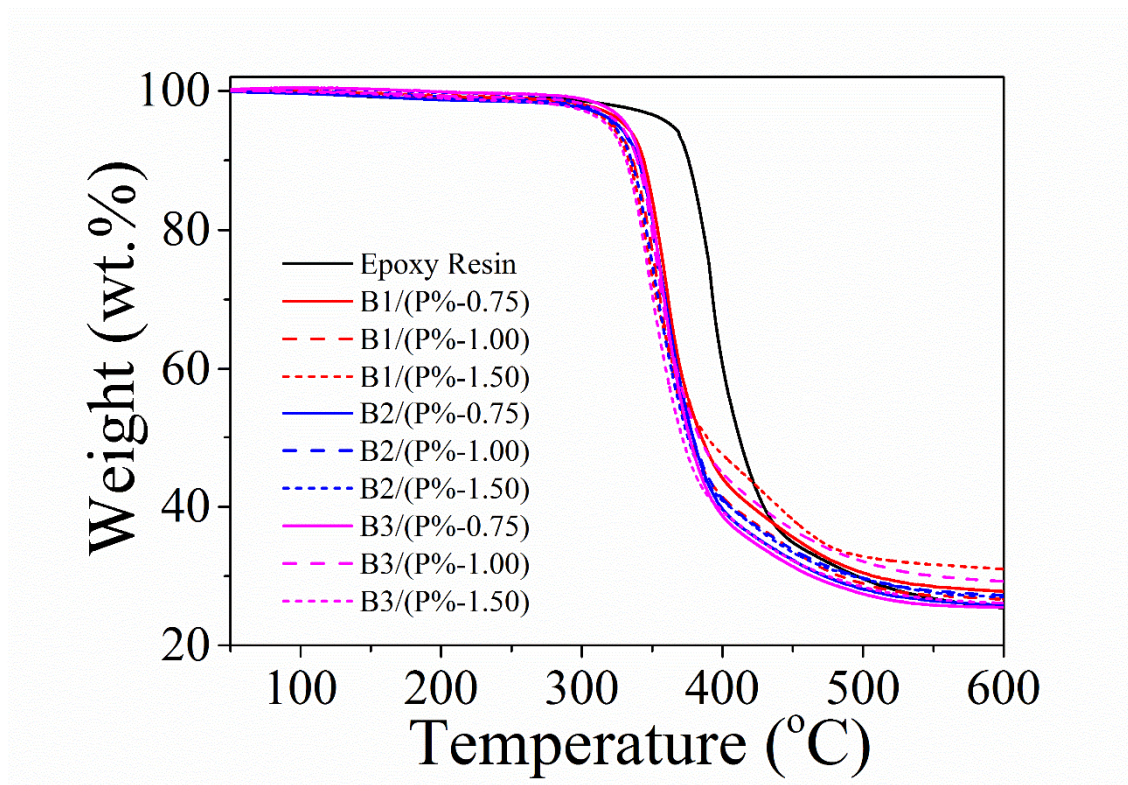


Fig. 4-7 TGA curves of flame retardants-series B modified epoxy resin composites measured at a heating rate of 10 °C/min.

The TGA curves of epoxy resin and flame retardants-series B modified epoxy resin composites under nitrogen are respectively shown in Fig. 4-7, and the analysis results are also summarized in Tab. 4-1. Under nitrogen atmospheres, there is only a one-sharp weight loss stage for all the samples. The decreasing trend of $T_{5\%}$ also can be attributed to the fact that the O=P-O bond in Bx is more active than common C-C bond, which is suggested to form phosphorus-containing radical stabilizers by the quenching mechanism in combustion. Flame retardant Bx-modified epoxy resin composites show slower weight loss rate than that of neat epoxy resin. As charring layer plays a very important role in the performance of flame retardancy, higher char yield obtained accompany with the addition of Bx, indicating high flame retardancy with the addition of flame retardants-series B.

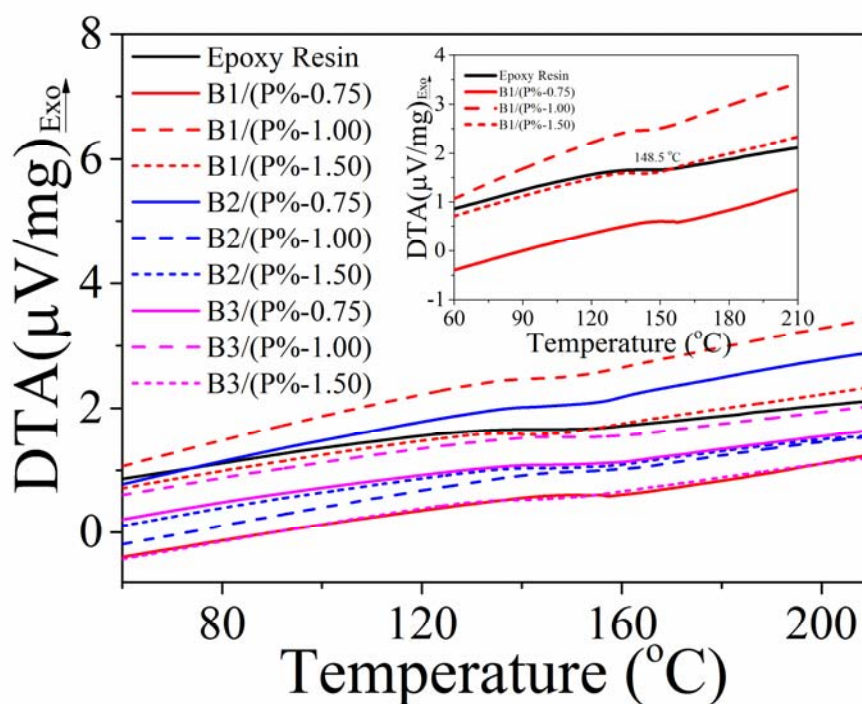


Fig. 4-8 DTA curves of flame retardants-series B (inset flame retardant B1) modified epoxy resin composites measured at a heating rate of 10 °C/min.

Fig. 4-8 shows DTA thermograms of epoxy resin and flame retardants-series B-modified epoxy resin composites. Obtained from that, T_g s of Bx-modified epoxy resin composites are summarized in Tab. 4-1. It is expected that all Bx-modified epoxy resin composites show a high- T_g , indicating an excellent thermal stability. Moreover, T_g s of all Bx/(P%-Y) epoxy resin composites with different flame retardant amount show a slight change to each other. Taking B1-modified epoxy resin composites as instance, T_g s of all the B1/(P%-Y) epoxy resin composites show just a slight change to each other of 143 to 154 °C, while, lower than that (160 °C) of neat epoxy resin, which also can be attributed to the poor chemical combination of Bx with epoxy resin.

(3) The thermal stability of Cx-modified epoxy resin nanocomposites

The thermal stability of pure-epoxy resin and flame retardants-series C modified epoxy resin nanocomposites were investigated by TGA under nitrogen atmospheres at a heating rate of 10 °C·min⁻¹. Fig. 4-9 shows the TGA curves of the thermal decomposition

process. For all the samples, there is only a one-sharp weight loss stage. Taking flame retardant C1-modified epoxy resin composites as instance, the onset decomposition temperatures of 5% weight loss ($T_{5\%}$) are 352.8, 350.1 and 347.1 °C for C1/AlPi/(P%-0.75), C1/AlPi/(P%-1.00) and C1/AlPi/(P%-1.50), respectively, which are significantly lower than that of pure-epoxy resin. In previous work, the decreasing trend of $T_{5\%}$ for DOPO-containing flame retardant epoxy resin composites have been explained that the O=P—O bond in is more active than common C—C bond [23].

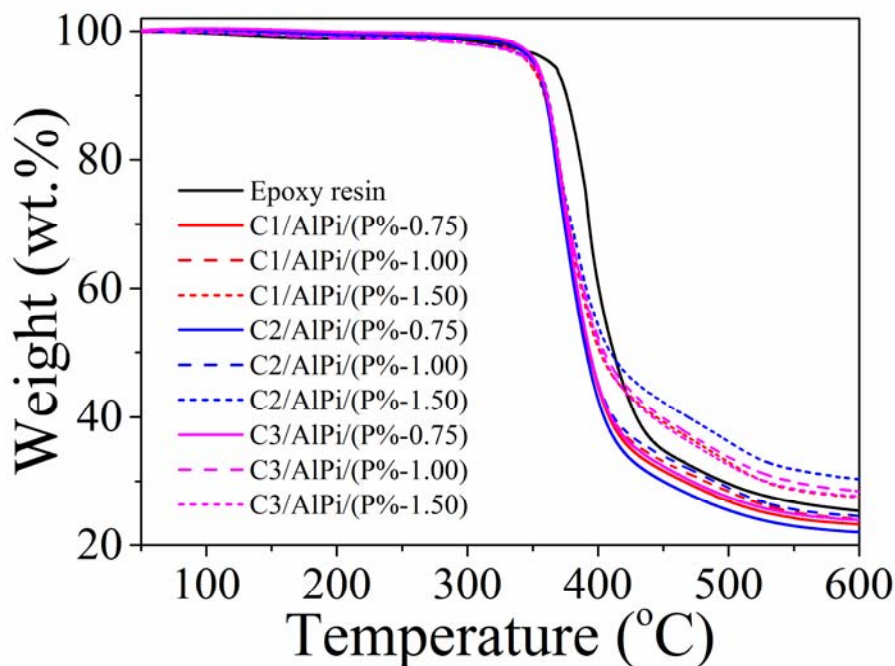


Fig. 4-9 TGA curves of flame retardants-series C modified epoxy resin composites measured at a heating rate of 10 °C/min.

In this work, C_x/AlPi/(P%-Y) nanocomposites show lower values of $T_{5\%}$ to that of AlPi/(P%-Y) composites, probably resulting from aluminum-phosphorus synergistic effect. The anti-fractured O=P—O bond may result in forming phosphorus-containing radical stabilizers by the quenching mechanism in combustion. Additionally, flame retardants-series C modified epoxy resin nanocomposites show slower weight loss rate than that of pure epoxy resin. It is noteworthy that higher char yield can be obtained with simultaneously adding AlPi and C_x, as charring layer plays a very important role in the

performance of flame retardancy.

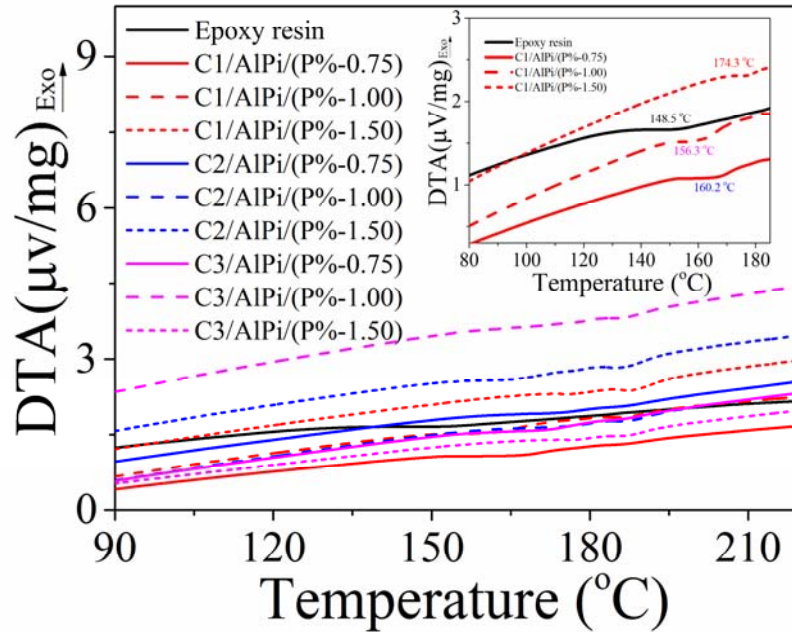


Fig. 4-10 DTA curves of flame retardants-series C (inset flame retardant C1) modified epoxy resin composites measured at a heating rate of 10 °C/min.

Fig. 4-10 shows DTA thermograms of pure-epoxy resin and $C_x/AlPi/(P\%-Y)$ epoxy resin nanocomposites. Obtained from that, values of T_g obtained from Fig. 4-10 are summarized in Tab. 4-1. Taking $C_3/AlPi/(P\%-Y)$ nanocomposites as instance, the value of T_g increase to 166 °C with addition of 1 wt% Cx into epoxy resin matrix. It can be explained by the fact that the addition of functionalized MWCNTs shows influence on epoxy resin molecular chain configuration. Moreover, the values of T_g for $C_3/AlPi/(P\%-Y)$ nanocomposites show a slight increase from 166 to 174 °C with the increasing of phosphorus amount, higher than that of neat epoxy resin (160 °C), which can be attributed to the well chemical compatibility of Cx to epoxy resin.

4.3.3 Mechanical properties of Cx-modified epoxy resin nanocomposites

The notched impact strength and dynamic mechanical analysis (DMA) were taken to evaluate the mechanical properties of $C_x/AlPi/(P\%-Y)$ ($x=1, 2, 3$ and $Y=0.75, 1.00, 1.50$) epoxy resin nanocomposites.

(1) Izod notched impact strength of Cx-modified epoxy resin nanocomposites

The notched impact strengths were determined to evaluate the mechanical properties of Cx- modified epoxy resin nanocomposites. Fig. 4-11 presents the changes in notched impact strengths of these nanocomposites with 1 wt% of Cx and phosphorus content varying from 0 wt%, 0.75wt%, 1.00 wt% to 1.50 wt%. Pure-epoxy resin showed a high notched impact strength of $2.34 \pm 0.16 \text{ kJ}\cdot\text{m}^{-2}$. It was obvious that notched impact strength increased with phosphorus content of 0.75 wt%. However, the notched impact strength slightly decreased when the phosphorus content is over 0.75 wt%. With the addition of Cx into AlPi/Epoxy resin flame retardant system, the notched impact strength slightly increased. Taking C3/AlPi/(P%-Y) nanocomposites as instance, C3/AlPi/(P%-0.75), C3/AlPi/(P%-1.00) and C3/AlPi/(P%-1.50) nanocomposites showed notched impact strengths of 2.90 ± 0.22 , 2.38 ± 0.27 , and $2.23 \pm 0.15 \text{ kJ}\cdot\text{m}^{-2}$, respectively.

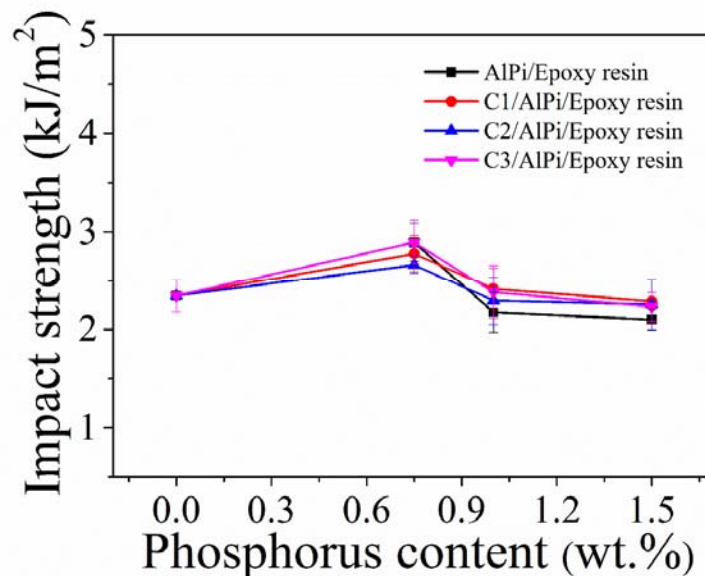


Fig. 4-11 Notched impact strength of AlPi- and flame retardants-series C-modified epoxy resin nanocomposites.

To further investigate the relationships between the impact strengths and the amounts of flame retardant Cx added, the fractographs from impact test specimens were studied. The morphologies and distributions of flame retardants in epoxy resin matrix played an

important role in mechanical properties as well as flame retardancy. It was obvious that there were no clearly visible bulk aggregates of flame retardant Cx in all the C3/AlPi/(P%-Y) nanocomposites. This indicated good dispersibility of the nano-structured flame retardant Cx in epoxy resin matrix.

(2) DMA of flame retardants-series C modified epoxy resin nanocomposites

The dynamic mechanical and thermogravimetric properties of flame retardants-series C modified epoxy resin nanocomposites were also investigated. The storage modulus and loss factors obtained from DMA tests are plotted in Fig. 4-12, and the data is presented in Tab. 4-1. It was evident that the addition of different kinds of flame retardants, Cx, into AlPi/Epoxy resin flame retardant system impacted the storage modulus. T_g s obtained from loss modulus showed good agreement with DTA results. It is noteworthy that T_g s of Cx/AlPi/(P%-Y) epoxy resin nanocomposites obtained from $\tan \delta$ values showed slight variations, following the addition of Cx. This phenomenon for Cx-modified epoxy resin nanocomposites could be attributed to the nano-core-shell structure of Cx, based on the typical mechanical properties and thermal behaviors.

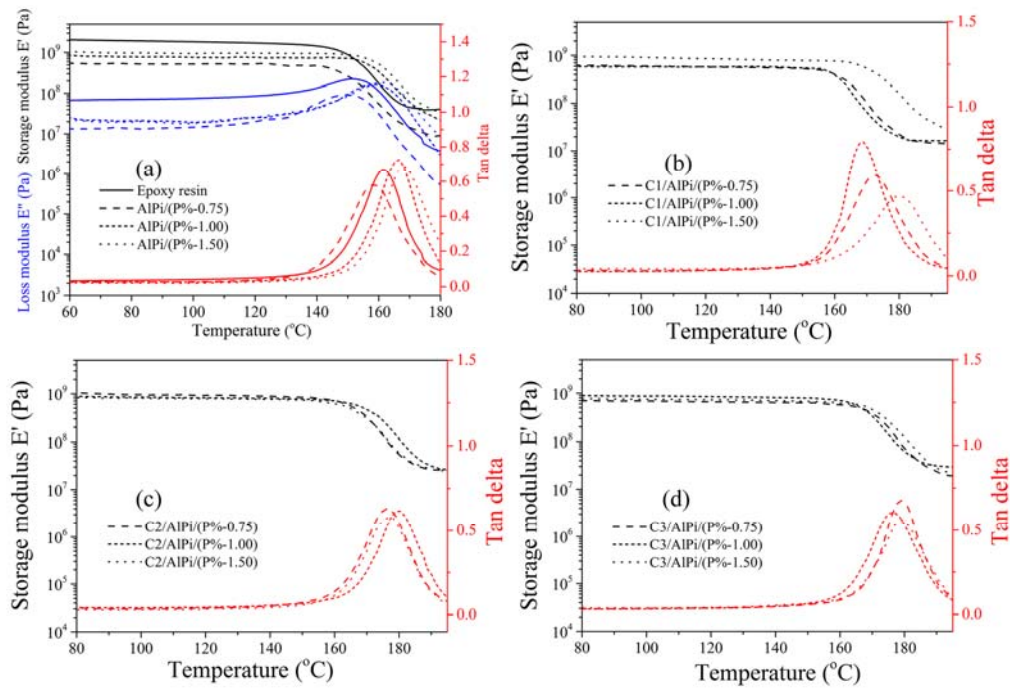


Fig. 4-12 DMA thermograms of modified epoxy resin nanocomposites with flame retardant of (a) AlPi, (b) C1/AlPi, (c) C2/AlPi and (d) C3/AlPi.

4.4 Conclusions

Three types of DOPO-containing flame retardants, Ax (Series A: single molecules), Bx (Series B: chain-like macromolecules) and Cx (Series C: Functionalizing MWCNTs), were well dispersed into epoxy resin matrix with DDM as harder forming flame-retardant epoxy resin composites. Flame retardancy tests indicated that Ax/Bx-modified epoxy resin composites with phosphorus content of 0.75 wt% could reach UL 94 V0 flammability rating, with high *LOI* values. Meanwhile, Cx/AlPi/(P%-Y) epoxy resin nanocomposite with 1 wt% Cx and phosphorus content of 1.00 wt% can reach UL 94 V0 rating. Moreover, TGA results showed that all those flame retardant epoxy resin composites produced high char yields. The mechanical properties of Cx-modified epoxy resin nanocomposites deteriorated slightly with addition of Cx, with notched impact strengths from 2.23 ± 0.15 to 2.90 ± 0.22 kJ·m⁻². Despite this, Cx/AlPi/(P%-Y) epoxy resin nanocomposites showed satisfactory mechanical properties for applications with high storage modulus and *T_g*s.

References

- [1] Feih S, Mathys Z, Gibson A G, *et al.* Modelling the tension and compression strengths of polymer laminates in fire. *Composites science and technology*, 2007, 67(3): 551-564.
- [2] Ratna, Debdatta. Epoxy composites: impact resistance and flame retardancy, Vol. 16, iSmithers Rapra Publishing, 2007.
- [3] Krishnadevi K, Selvaraj V. Biowaste material reinforced cyanate ester based epoxy composites for flame retardant applications. *High Performance Polymers*, 2015: 0954008315605554.
- [4] J, Zhou X, Ye C, *et al.* Thermal Stability and Mechanical Property of Polyvinyl Chloride/Intercalated Hydrotalcite. *Journal of the Chinese Ceramic Society*, 2013, 41(4): 516-520.
- [5] Xiao L, Sun D, Niu T, Yao Y. Syntheses and characterization of two novel 9,10-dihydro-9-oxa-10-phosphaphenanthrene-10-oxide-based flame retardants for epoxy resin. *High Performance Polymers*, 2013: 0954008313495064.
- [6] Lin C H, Cai S X, Lin C H. Flame-retardant epoxy resins with high glass-transition temperatures. II. Using a novel hexafunctional curing agent: 9,10-dihydro-9-oxa-10-phosphaphenanthrene 10-yl-tris (4-aminophenyl) methane. *Journal of Polymer Science Part A: Polymer Chemistry*, 2005, 43(23): 5971-5986.
- [7] Xu J, Liu J, Li K. Application of functionalized graphene oxide in flameretardant polypropylene. *Journal of Vinyl and Additive Technology*, 2015, 21(4): 278-284.
- [8] Wu C S, Liu Y L, Chiu Y S. Epoxy resins possessing flame retardant elements from silicon incorporated epoxy compounds cured with phosphorus or nitrogen containing curing agents. *Polymer*, 2002, 43(15): 4277-4284.
- [9] Wang X, Xing W, Feng X, *et al.* The effect of metal oxide decorated graphene hybrids on the improved thermal stability and the reduced smoke toxicity in epoxy resins. *Chemical Engineering Journal*, 2014, 250: 214-221.
- [10] Wang M, Xu J, Wu H, *et al.* Effect of pentaerythritol and organic tin with

calcium/zinc stearates on the stabilization of poly (vinyl chloride). *Polymer degradation and stability*, 2006, 91(9): 2101-2109.

[11] Benoit V, Cédric L, Alexis C. Post fire behavior of carbon fibers Polyphenylene Sulfide-and epoxy-based laminates for aeronautical applications: A comparative study. *Materials & Design*, 2014, 63: 56-68.

[12] Ye S, Feng J, Wu P. Highly elastic graphene oxide–epoxy composite aerogels via simple freeze-drying and subsequent routine curing. *Journal of Materials Chemistry A*, 2013, 1(10): 3495-3502.

[13] Mauerer O. New reactive, halogen-free flame retardant system for epoxy resins. *Polymer Degradation and Stability* 2005, 88: 70-73.

[14] Müller P, Bykov Y, Döring M. New star-shaped phosphorus-containing flame retardants based on acrylates for epoxy resins. *Polymers for Advanced Technologies* 2013, 24(9): 834-840.

[15] Liu Y L, Hsu C Y, Wei W L, et al. Preparation and thermal properties of epoxy-silica nanocomposites from nanoscale colloidal silica. *Polymer*, 2003, 44(18): 5159-5167.

[16] Green J. A review of phosphorus-containing flame retardants. *Journal of fire sciences*, 1992, 10(6): 470-487.

[17] Wei, L. L., Wang, D. Y., Chen, H. B., Chen, L., Wang, X. L., Wang, Y. Z. Effect of a phosphorus-containing flame retardant on the thermal properties and ease of ignition of poly (lactic acid). *Polymer Degradation and Stability*, 2011, 96(9), 1557-1561.

[18] Cheng, K. C., Lin, Y. H., Guo, W. *et al.* Flammability and tensile properties of polylactide nanocomposites with short carbon fibers. *Journal of Materials Science*, 2015, 50(4): 1605-1612.

[19] Morgan, A. B., & Wilkie, C. A. (Eds.). Flame retardant polymer nanocomposites. John Wiley & Sons, 2007.

[20] Yu, T., Jiang, N., & Li, Y. Functionalized multi-walled carbon nanotube for improving the flame retardancy of ramie/poly (lactic acid) composite. *Composites Science and Technology*, 2014, 104, 26-33.

-
- [21] Song, P., Shen, Y., Du, B., Peng, M., Shen, L., & Fang, Z. Effects of reactive compatibilization on the morphological, thermal, mechanical, and rheological properties of intumescent flame-retardant polypropylene. *ACS applied materials & interfaces*, 2009, 1(2), 452-459.
- [22] Carosio, F., & Alongi, J. Ultra-Fast Layer-by-Layer Approach for Depositing Flame Retardant Coatings on Flexible PU Foams within Seconds. *ACS applied materials & interfaces*, 2016, 8(10), 6315-6319.

Chapter 5 Flame Retardant PLA Composites: Preparation, Non-Flammability, Thermal Behaviors and Mechanical Properties

5.1 Introduction

Poly(lactic acid) (PLA) has been promoted to be one of the most widely used biodegradable polymers in packaging engineering, biomedical fields, household and automobile engineering, electricity industry and so on, because of their outstanding properties and renewable resources (mainly starch and sugar) [1-5]. However, the need for high level of thermal, mechanical and flame retardant properties greatly promotes the research on PLA and its composites for further application and development [6]. The above improvement of properties could be met by addition of nano-sized particles as well as optimization of plastic processing [7-8].

It has been demonstrated that incorporation of small quantities of carbon nanotubes (CNTs) can dramatically improve the thermal and mechanical properties of polymers [9-11]. More importantly, great numbers of cases that CNTs served candidates as flame retardants have been reported in recent years. Ma *et al.* [12] have covalently grafted an intumescent flame retardant (PDSPB) onto the surfaces of multi-walled carbon nanotubes (MWCNTs). And the threshold value at low loading (0.2 wt.%) of the resultant MWCNT-PDSPB can form network structure in acrylonitrile-butadiene-styrene (ABS) matrix, resulting in improving both the dispersion of MWCNTs and flame retardancy of the composites. Many research groups have focused on the functionalized MWCNTs with various flame retardant, such as vinyltriethoxysilane (VTES), [13] melamine/4,4'-diphenylether dicarboxylic acid, [14] S-valine amino acid, [15] graphitic carbon nitride (g-C₃N₄), [16] γ -aminopropyltriethoxysilane (APTES), [17] which all show excellent flame retardancy. It has been proven that the addition of flame retardant functionalized MWCNTs is a very effective way to impart good flame retardancy and

mechanical properties to nanocomposites as a result of well dispersion of functionalized MWCNTs, since the dispersion of MWCNTs in polymer matrix is consider to be a key point in the flame retardancy performance. Because functionalized MWCNTs with various organic, inorganic or organometallic structures using both non-covalent and covalent approaches improve the compatibility with polymer, which makes them much easier to disperse in polymer matrix [18-20]. In other words, the flame retardant grafted onto MWCNTs plays an important role on the performance of functionalized MWCNTs.

9, 10-dihydro-9-oxa-10-phosphaphanthrene-10-oxide (DOPO) has been reported to be an important strategy for preparing halogen-free flame retardants with high thermal stability, good oxidation resistance as well as excellent flame retardancy [21-23]. Grafting DOPO unit onto the surface of MWCNTs is considered as a good idea to gain a dramatically high flame retardant efficiency. Wang *et al.* [24] have reported that the flammability and mechanical properties of poly(ethylene-co-vinyl acetate) (EVM) composites were improved after the incorporation of 1.0 phr flame retardant spirocyclic pentaerythritol bisphosphate disphosphorylchloride/9,10-dihydro-9-oxa-10-phosphaphanthrene-10-oxide/vinylmethyl dimethoxysilane (SPDV) grafted MWCNTs. Yu *et al.* [25] have grafted DOPO-CH₂OH on the surfaces of MWCNTs (MWCNT-DOPOs) to improve the flame retardancy of ramie/PLA composite with UL 94 V-0 class and LOI value of 26.4 when the content of MWCNT-DOPOs and ramie was 5 wt.% and 10 wt.%, respectively. However, there are still some problems with the insolubility and tending to aggregate as well as cost limit the manipulation and processing of higher quantities functionalized MWCNTs in polymer matrix [26]. In most cases, the addition of small quantities of functionalized MWCNTs, usually less than 1 wt.%, can dramatically improve the thermal and mechanical properties of polymers, but still fails to pass the traditional flame retardancy such as UL 94 tests [27-30]. Currently, a great interest is focusing on the synergistically flame retarding effect of novel flame retardant with traditional metal (aluminum, magnesium and calcium, etc.) hydroxide [30-32]. So it is desirable to use this synergistic approach to obtain novel flame retardant PLA systems

with small quantities of functionalized MWCNTs and high flame retardant efficient aluminum hypophosphite (AHP), presenting high performance.

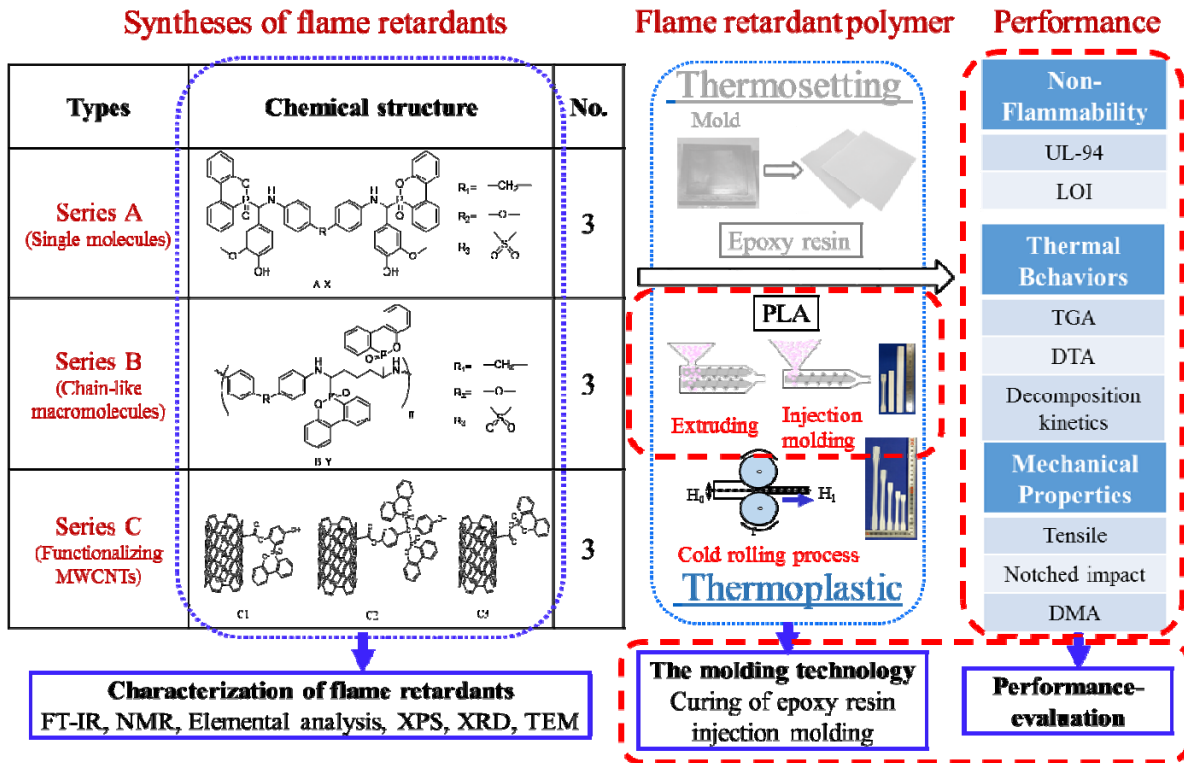


Fig. 5-1 Preparation and performance-evaluation of flame retardant PLA composites.

In the present study, three types of DOPO-containing flame retardants, Ax (Series A: single molecules), Bx (Series B: chain-like macromolecules) and Cx (Series C: Functionalizing MWCNTs), were well dispersed into PLA matrix by melt blending through twin-screw extruder and injection-molding process. Such flame retardant PLA composites showed high performance that: meeting UL 94 V-0 flammability rating; high *LOI* values; high *T_g*; excellent mechanical properties. The preparation and performance-evaluation of flame retardant PLA composites in this work are shown in Fig. 5-1.

5.2 Experimental

5.2.1 Materials

Flame retardant Ax, Bx and Cx were synthesized following Chapter 3. Aluminum

hypophosphite (AHP, the average particle size was about 300 nm) was purchased from Clariant Chemicals Ltd., Germany. Polylactic acid (PLA) (NatureWorks Ingeo 3001D) was provided by NatureWorks LLC., America. PLA and all its fillers were dried at 80 °C for 12 h in a vacuum oven before twin-screw extruder process.

5.2.2 Preparation of PLA-based conductive composites

Twin-screw extruder was used for prior mixing of flame retardant Ax, Bx or Cx and PLA. The extruding temperatures were: C1, 180 °C; C2, 180 °C; C3 and C4, 170 °C. The injection molding machine was used to form the mixture plates into dumbbell (30 mm × 5 mm × 2 mm). The injection temperature was 180 °C, molding temperature was 50 °C, and the injection rate was 17.6 mm/s.

The Underwriter Laboratories 94 vertical tests (UL-94) were performed according to IEC 60695-11-10:1999 using a horizontal and vertical burning instrument (FZ-5401, Dongguan Hanyang electronic instrument Co., Ltd, China). The LOI test was performed according to the testing procedure of ISO 4589-2:1996 with the dimensions 80 × 6 × 3 mm³ of each sample. Thermal gravimetric analyses (TGA) of samples were carried out with Shimadzu DTG-60/60H from 30 °C to 600 °C at heating rates of 10 °C·min⁻¹, whereas the flow of nitrogen was maintained at 50 mL·min⁻¹. Differential thermal analyses (DTA) were taken with the same instrument from 30 °C to 200 °C at heating rates of 5 °C·min⁻¹. The scanning electron microscope (SEM) observation was performed on a Hitachi S-4300 scanning electron microscope in high vacuum mode with 5 kV acceleration voltage. Dynamic mechanical analysis (DMA) was performed by using a TA Instrument RSA-G2 with a sample size of 20 × 5 × 2 mm³ by 3-Point Bending mode with an amplitude of 30 μm. The storage modulus E' and tan δ were determined as the sample was subjected to the temperature scan mode at a programmed heating rate of 3 °C·min⁻¹ and a frequency of 1 Hz. Tensile tests of the composites were carried out on a universal testing machine (Instron Ltd Series 3360) according to JIS K7113 with a crosshead displacement rate of 10 mm·min⁻¹ at 23 ± 1 °C.

5.2.3 Preparation of Ax- or Bx-modified PLA composites

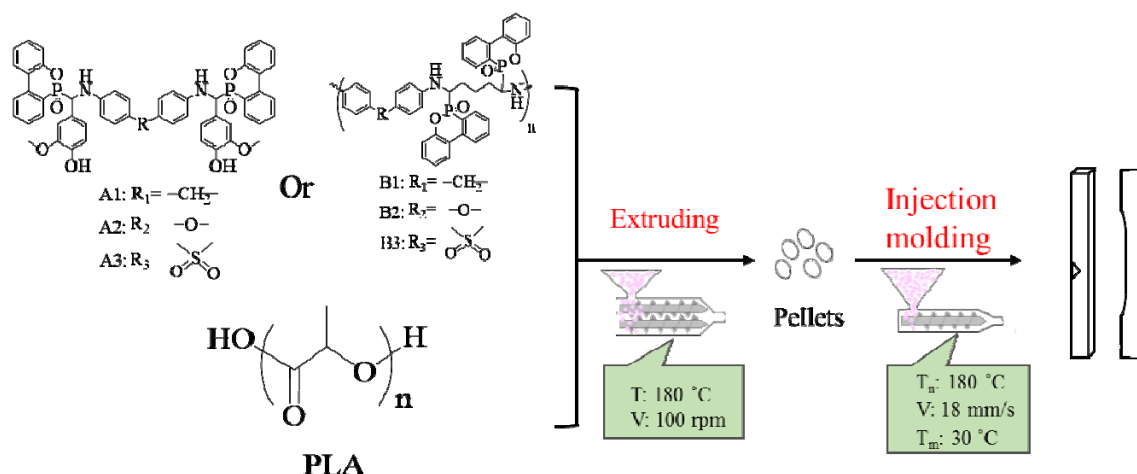


Fig. 5-2 Preparation of flame retardants-series A- or B-based PLA composites.

The flame retardants-series A- or B-modified PLA composites with filler-content of 10 wt%, 20 wt%, 30 wt% and 40 wt% labeled as shown in Tab. 4-1, were prepared by twin-screw extruder (KZW15TW-30MG-NH(-700)-AKTP, Technovel Corporation Co., Ltd., Osaka, Japan) at 180 °C with screw revolving speed 100rpm and coil-feeder revolving speed 22rpm. The modified PLA composites were prepared as specimens using injection molding machine (NP7-1F, Nissei Plastic Industrial Co., Ltd., Nagano, Japan) at 180°C with mold temperature 30°C, cooling time 30s, and injection rate 18 mm/s (Fig. 5-2).

5.2.4 Preparation of Cx-based PLA nanocomposites

Master batch method was adopted to prepare the PC-z/(Cx/AHP-Y) ($x=1, 2, 3$ and denotes the ID of flame retardants-series C; $Y = 10\%, 20\%, 30\%, 40\%$ and denotes the weight percentage content of Cx and AHP; $z=1-12$ and denotes the ID of nanocomposites) nanocomposites. As shown in Fig. 5-3, firstly, the master batches were prepared by mixing 95 wt.% PLA and 5 wt.% Cx using a twin-screw extruder (KZW15TW-30MG-NH(-700)-AKTP, Technovel Corporation Co., Ltd., Osaka, Japan) at 180 °C with a screw revolving speed of 100 rpm and a coil-feeder revolving speed of 20 rpm. Secondly, the master batches, AHP and PLA were mixed using the same extruder

and operated at the same conditions. The nanocomposites consisted of 1 wt.% Cx and various content of AHP with 0 wt.%, 14 wt.%, 19 wt.%, 24 wt.%, were labeled as shown in Tab. 5-2. In order to compare their integrated properties, AHP/PLA composites with AHP-content of 15 wt.%, 20 wt.%, 25 wt.% were also prepared under the same conditions, which were labeled as PC-1/(AHP-15%), PC-2/(AHP-20%) and PC-3/(AHP-25%), respectively. The modified PLA nanocomposites were injected into specimens using injection molding machine (NP7-1F, Nissei Plastic Industrial Co., Ltd., Nagano, Japan) at 180 °C with mold temperature of 40 °C, cooling time of 30s, and injection rate of 18 mm/s.

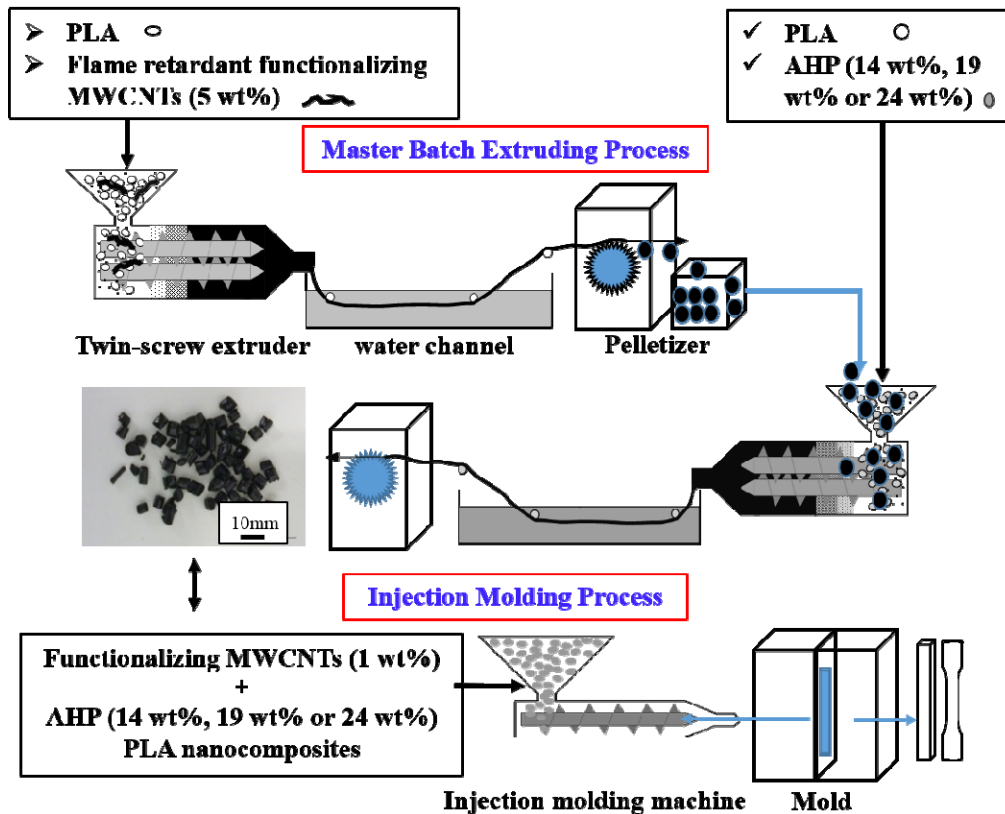


Fig. 5-3 Preparation of flame retardants series C-based PLA nanocomposites.

5.3 Results and discussion

5.3.1 Non-flammability and residual char analysis

In this work, the flame retardancy of flame retardants-series A (or series B, series C)-modified PLA composites were evaluated by Underwriter Laboratories 94 vertical

tests (UL 94) and LOI test. To further understand the process for char formation of flame retardant PLA composites and learn more about the mechanism of their flame retardancy, the morphologies of the residual chars collected from the vertical burning tests were investigated by SEM

(1) Non-flammability

For flame retardants-series A modified PLA composites, the *LOI* values and UL-94 vertical burning grades of PA-z/(Ax-Y) ($x=1, 2, 3$ and denotes the ID of flame retardants-series A; $Y = 10\%, 20\%, 30\%, 40\%$ and denotes the weight percentage content of Ax; $z=1-12$ and denotes the ID of PLA composites), are summarized in Tab.4-1. The *LOI* values of PA-z/(Ax-30%) ($x=1, 2, 3$ and $z=3, 7, 11$) are 36.0, 36.0 and 35.5, respectively. All those three PLA composites with flame retardant content of 30 wt% arrive UL-94 V-0 grade. The *LOI* values of those flame retardants-series A modified PLA composites increase with the addition of Ax ($x=1, 2, 3$) increasing, which may result from nitrogen-phosphorus synergistic effect. Take flame retardant A1 as instance, further assessment of the flammability of the PA-z/(A1-Y) ($Y=10\%, 20\%, 30\%, 40\%$ and $z=1, 2, 3, 4$) PLA composites are provided in Tab. 4-1. When flame retardant A1 is added, the *LOI* value of PA-2/(A1-20%) composite is increased to 36.4, which can only reach UL 94 V-1 rating. PA-3/(A1-30%) composite achieves a higher *LOI* value of 37.2 and the UL 94 V-0 rating.

For flame retardants-series B modified PLA composites, the flame-retardant performance of the PB-z/(Bx-Y) ($x=1, 2, 3$ and denotes the ID of flame retardants-series B; $Y = 10\%, 20\%, 30\%, 40\%$ and denotes the weight percentage content of Ax; $z=1-12$ and denotes the ID of PLA composites) PLA composites have been investigated in terms of UL-94 vertical burning tests, and the results are also summarized in Tab. 4-1. It is clear that UL 94 V-0 flammability rating can be reached for PB-z/(Bx-30%) ($x=1, 2, 3$ and $z=3, 7, 11$) PLA composites and meanwhile the *LOI* value reached over 36.9. The flame retardancy of PB-z/(Bx-Y) PLA composites increase with the flame retardant Bx content increasing. When flame retardant B3 is added, the *LOI* value of PB-9/(B3-10%)

composite is 35.2, which can reach UL 94 V-2 rating. PB-10/(B3-20%) composite increase to a higher LOI value of 36.5 and the UL 94 V-0 rating. According to the above results, a significant improvement of the flame retardancy for those Bx-modified PLA composites by well dispersion of Bx into PLA matrix.

Tab. 5-1 Thermal properties and flame retardancy of Ax-/Bx-modified PLA composites.

Series	Flame retardant	Thermoset ID	T_g (°C) ^a	T_g (°C) ^b	Char Yield ^c	UL-94 grade	LOI
A	A1	PA-1/(A1-10%)	58.2	62.5	4.1	V-2	33.0
		PA-2/(A1-20%)	65.8	64.1	8.2	V-1	35.5
		PA-3/(A1-30%)	66.1	65.3	11.3	V-0	36.0
		PA-4/(A1-40%)	66.7	65.0	11.1	V-0	36.5
	A2	PA-5/(A2-10%)	66.5	61.2	3.9	V-2	33.5
		PA-6/(A2-20%)	66.3	64.4	6.1	V-2	35.0
		PA-7/(A2-30%)	65.6	65.3	9.5	V-0	36.0
		PA-8/(A2-40%)	65.1	65.0	17.7	V-0	37.5
	A3	PA-9/(A3-10%)	66.2	63.1	4.0	V-2	33.0
		PA-10/(A3-20%)	63.4	63.2	7.5	V-1	35.0
		PA-11/(A3-30%)	63.2	63.2	7.2	V-0	35.5
		PA-12/(A3-40%)	61.3	62.9	16.3	V-0	37.0
B	B1	PB-1/(B1-10%)	58.9	63.9	4.1	V-2	35.2
		PB-2/(B1-20%)	62.0	63.5	6.8	V-1	36.8
		PB-3/(B1-30%)	62.9	64.1	14.8	V-0	37.2
		PB-4/(B1-40%)	61.9	63.4	17.4	V-0	38.5
	B2	PB-5/(B2-10%)	61.5	64.2	8.1	V-2	34.5
		PB-6/(B2-20%)	60.6	63.3	8.8	V-2	35.2
		PB-7/(B2-30%)	61.6	64.0	13.5	V-0	36.9
		PB-8/(B2-40%)	62.2	64.1	19.3	V-0	38.6
	B3	PB-9/(B3-10%)	58.1	63.8	7.2	V-2	35.2
		PB-10/(B3-20%)	60.4	63.4	18.2	V-0	36.5
		PB-11/(B3-30%)	59.2	63.5	16.8	V-0	37.2
		PB-12/(B3-40%)	59.5	64.2	16.6	V-0	37.8

^a Measured by DTA.

^b Measured by DMA (Tan delta).

^c Residual weight percentage at 600 °C.

For flame retardants-series C modified PLA nanocomposites, the flammability of PC-z/(Cx/AHP-Y) nanocomposites with Cx content of 1 wt% have been investigated by

UL 94 vertical burning tests and *LOI* tests. As shown in Tab. 4-2, the addition of Cx to AHP/PLA flame retardant system can markedly increase the *LOI* values. It is expected that the flame retardancy of these PLA nanocomposites become better with the presence of 1 wt.% Cx. As expected, the *LOI* values increase greatly for those nanocomposites with only 1 wt. % Cx loading, demonstrating that the flame retardancy improved with the addition of Cx. More importantly, PC-z/(Cx/AHP-15%) nanocomposites with 1 wt.% Cx can achieve UL 94 V-0 rating, which can be attribute to the excellent char formation-promoting properties of nano-structured Cx. It could be concluded that the incorporation of 1 wt.% Cx into the flame retardant AHP/PLA systems is very effective for the enhancement of flame retardancy and makes those flame retardants series C modified-PLA nanocomposites becoming nonflammable functional polymers.

Tab. 5-2 Thermal properties and flame-retardancy of Cx-modified PLA nanocomposites.

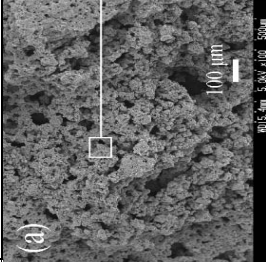
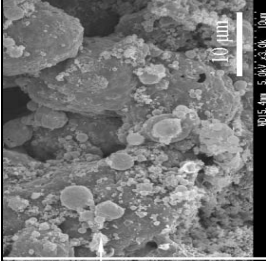
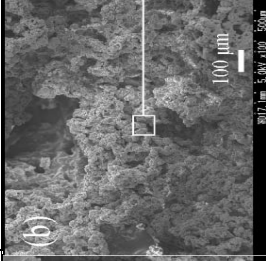
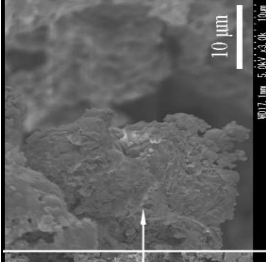

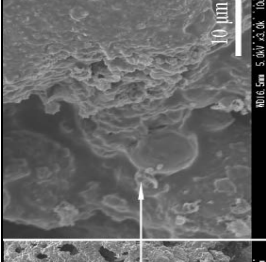
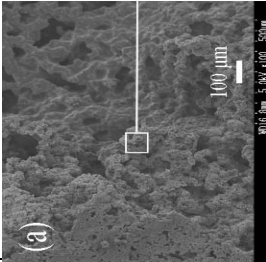
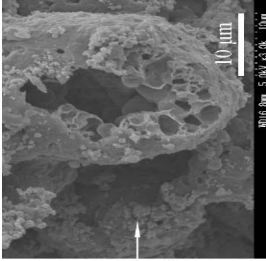
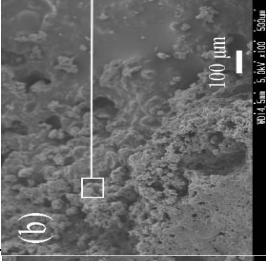
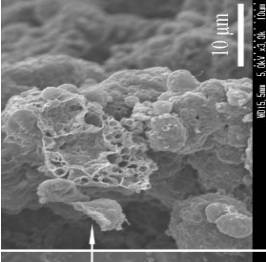
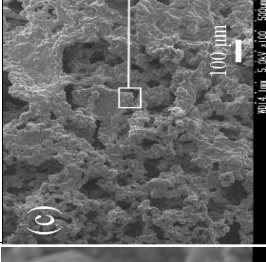
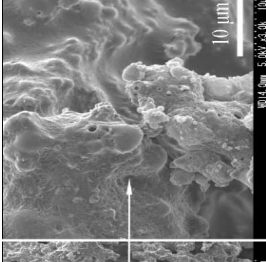
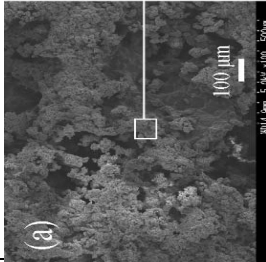
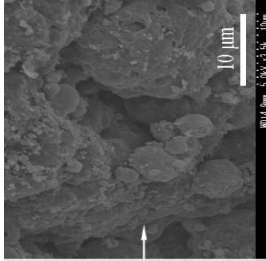
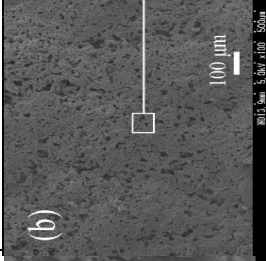
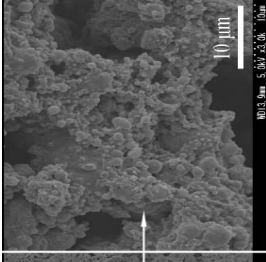
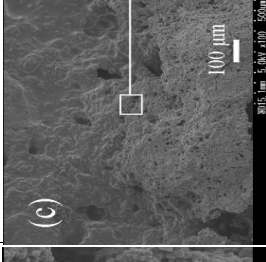
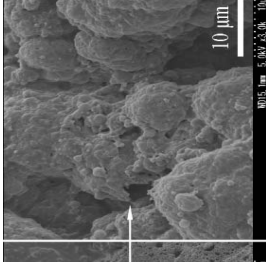
Series	Cx-wt%	AHP wt%	Thermoset ID	T_g (°C) ^a	T_g (°C) ^b	Char Yield ^c	UL-94 grade	<i>LOI</i>
C	--	15	PC-1/(AHP-15%)	56.6	65.1	7.04	V-2	27.5
		20	PC-2/(AHP-20%)	57.6	65.0	15.50	V-0	28.8
		25	PC-3/(AHP-25%)	56.8	64.8	18.69	V-0	29.2
	C1-1%	14	PC-4/(C1/AHP-15%)	58.2	65.5	13.51	V-0	27.8
		19	PC-5/(C1/AHP-20%)	57.2	65.2	14.12	V-0	30.2
		24	PC-6/(C1/AHP-25%)	58.8	65.1	20.16	V-0	31.5
	C2-1%	14	PC-7/(C2/AHP-15%)	58.3	64.3	13.57	V-0	28.2
		19	PC-8/(C2/AHP-20%)	58.4	64.8	15.42	V-0	30.6
		24	PC-9/(C2/AHP-25%)	59.1	64.8	20.62	V-0	31.8
	C3-1%	14	PC-10/(C3/AHP-15%)	57.8	64.8	14.21	V-0	28.6
		19	PC-11/(C3/AHP-20%)	57.9	64.2	20.25	V-0	30.5
		24	PC-12/(C3/AHP-25%)	58.3	64.2	22.90	V-0	32.3

^a Measured by DTA.

^b Measured by DMA (Tan delta).

^c Residual weight percentage at 600 °C.

Tab. 5-3 SEM images of the residual chars obtained from UL 94 vertical burning tests.

Flame retardant	15 wt%	20 wt%	25 wt%
C1 + AHP	 	 	 
C2 + AHP	 	 	 
C3 + AHP	 	 	 

(2) Residual char analysis

It has been observed that the physical structure of the charring layer plays a very important role in preventing of heat transfer, flame spreading and droplet generation during combustion [33-36]. To further understand the process for char formation of Cx-modified flame retardant PLA nanocomposites and learn more about the mechanism of their flame retardancy, the morphologies of the residual chars collected from the vertical burning tests were investigated by SEM. The results are shown in Tab. 4-3. All these residual chars exhibit a non-smooth carbonaceous charring layer with uneven distributing irregular-shaped pores. According to high magnification photo of each samples, the chars show an oolitic structure indicating a typical morphology after the intumescent char formation. Moreover, loose expansion surface adhering with some irregular-shaped and multiporous particles can be observed, which may be resulted from the gas-products degraded from AHP and Cx during combustion. Such gas-generating process provide nonflammable gas as well as quenching effective phosphorus free radical to impede combustion according to the vapor phase mechanism and free radical quenching mechanism.³¹ Furthermore, the special oolitic structure indicates char formation enhancing properties of Cx, resulting in better flame retardancy which is in a good agreement with the results of the *LOI* and UL 94 vertical burning tests.

5.3.2 The thermal stability of PLA composites

In this part, the thermal stability of flame retardant PLA composites were investigated by TGA and DTA under nitrogen atmospheres at a heating rate of 10 °C·min⁻¹.

(1) The thermal stability of Ax-modified PLA composites

Fig. 5-4 shows the TGA curves of the thermal decomposition processes of pure PLA and PA-z/(Ax-Y) PLA composites. All the samples showed only a single-sharp weight loss stage. The onset of decomposition temperature, at which 5% weight loss ($T_{5\%S}$) occurred, decreased with increasing amount of the flame retardant Ax. This was significantly lower (334.29 °C) than that of pure PLA. The decreasing trend of $T_{5\%}$

could be attributed to the fact that the O=P-C bond in DOPO moieties was more active than the common C-C bond. This suggested that phosphorus-containing radical stabilizers were formed by quenching mechanism during combustion. It had been reported that, during combustion, DOPO mainly acted in gas phase as it could vaporize into the gas phase, to yield active radicals, such as $PO_2 \cdot$, $PO \cdot$ and $HPO \cdot$. These radicals acted as scavengers of $H \cdot$ and $OH \cdot$ radicals and thus resulted in suppression of the combustion process [37]. Additionally, PA-z/(Ax-Y) PLA composites showed weight losses at a slower rate following an increase in Ax-content. It is noteworthy that a higher char yield could be obtained, accompanied by an increase in content of the flame retardant Ax. This was due to the fact that the charring layer played a very important role in flame retardancy (inset Fig. 5-4). Moreover, it could be seen in Fig.5-4d that PA-z/(A3-Y) PLA composites had slightly different onset decomposition temperatures compared to that of composites with flame retardant A1 or A2, with higher $T_{5\%}$ s values and slower rates of weight loss.

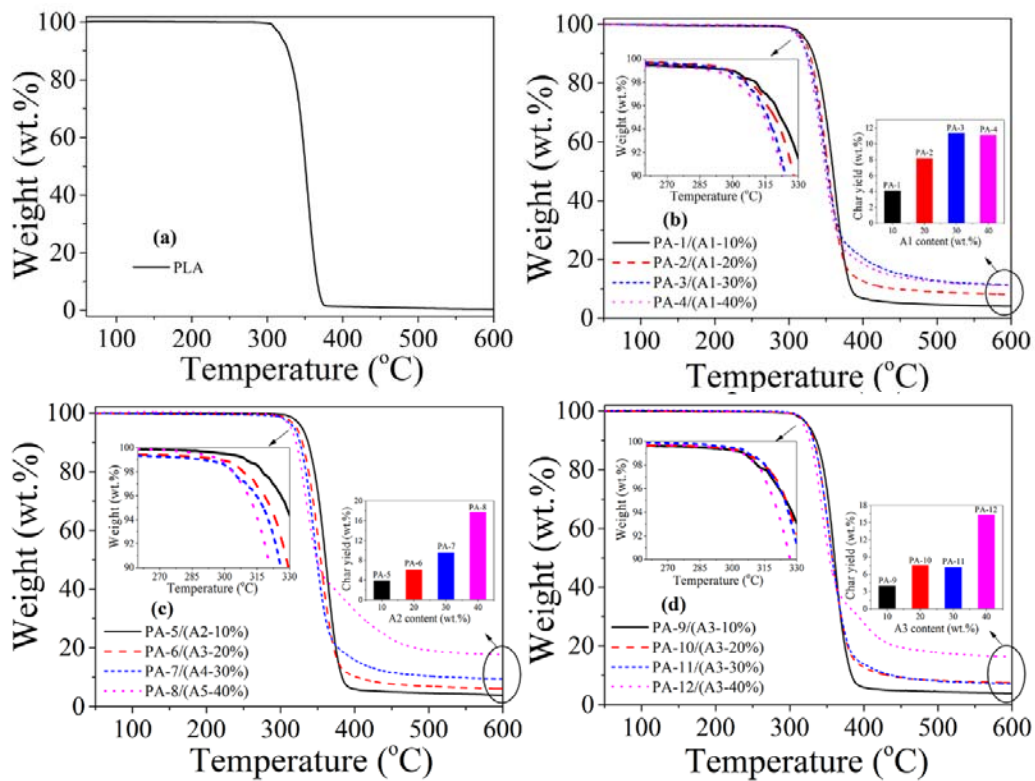


Fig. 5-4 TGA curves of (a) pure-PLA and flame retardants-series A ((b) A1; (c) A2; (d) A3) modified PLA composites measured at a heating rate of 10 °C/min.

Fig. 5-5 shows DTA curves of Ax-modified PLA composites. Values of T_{gs} , obtained from the thermograms are presented in Fig. 5-5(d) and Tab.4-1. It was expected that T_{gs} values of all PA-z/(Ax-Y) PLA composites containing the same flame retardant differed slightly from each other. The decrease of T_{gs} for PA-z/(A3-Y) PLA composites could be attributed to the poor chemical compatibility of A3, due to the rigidity of sulfonyl group ($-\text{SO}_2-$) in its structure.

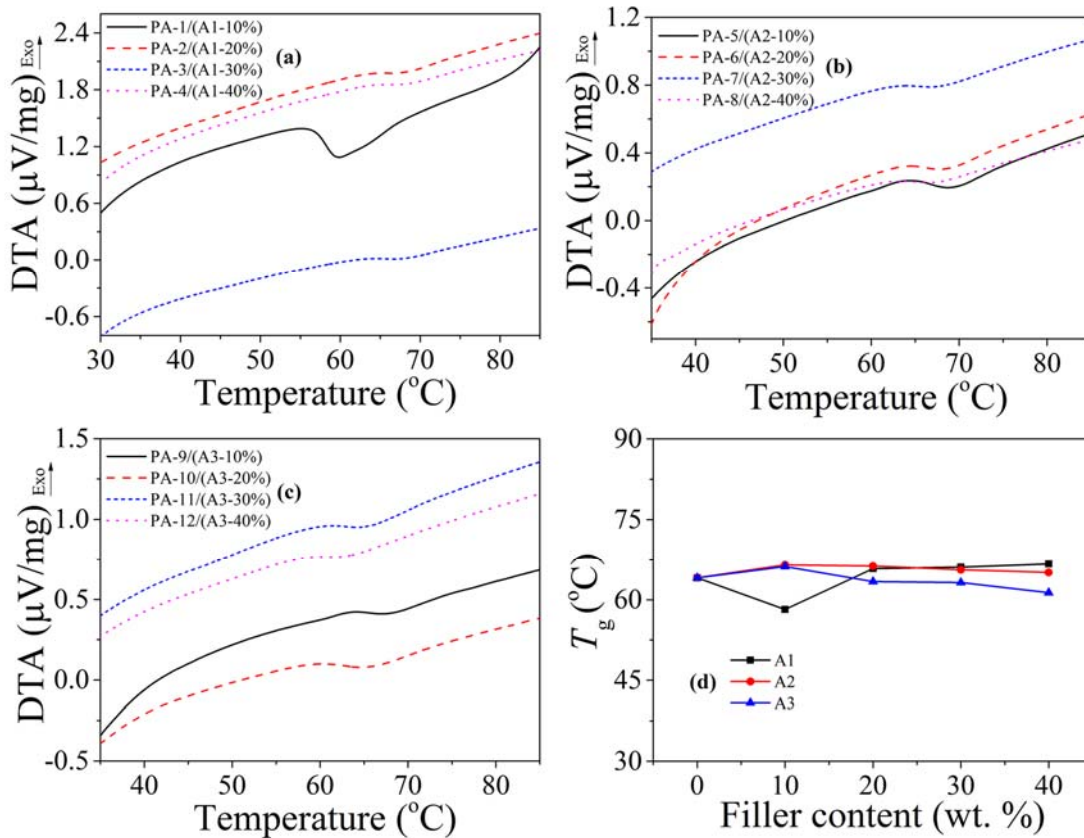


Fig. 5-5 DTA curves of flame retardants-series A ((a) A1; (b) A2; (c) A3) modified PLA composites and (d) T_g of those PLA composites.

(2) The thermal stability of Bx-modified PLA composites

The TGA curves of neat-PLA and flame retardants-series B modified PLA composites under nitrogen are respectively shown in Fig. 5-6, and the analysis results are also summarized in Tab. 4-1. Under nitrogen atmospheres, there is only a one-sharp weight loss stage for all the samples. The decreasing trend of $T_{5\%}$ also can be attributed to the fact that the $\text{O}=\text{P}-\text{O}$ bond in Bx is more active than common $\text{C}-\text{C}$ bond, which is

suggested to form phosphorus-containing radical stabilizers by the quenching mechanism in combustion. Flame retardant Bx-modified PLA composites show slower weight loss rate than that of neat PLA. As charring layer plays a very important role in the performance of flame retardancy, higher char yield obtained accompany with the addition of Bx, indicating high flame retardancy with the addition of flame retardants-series B.

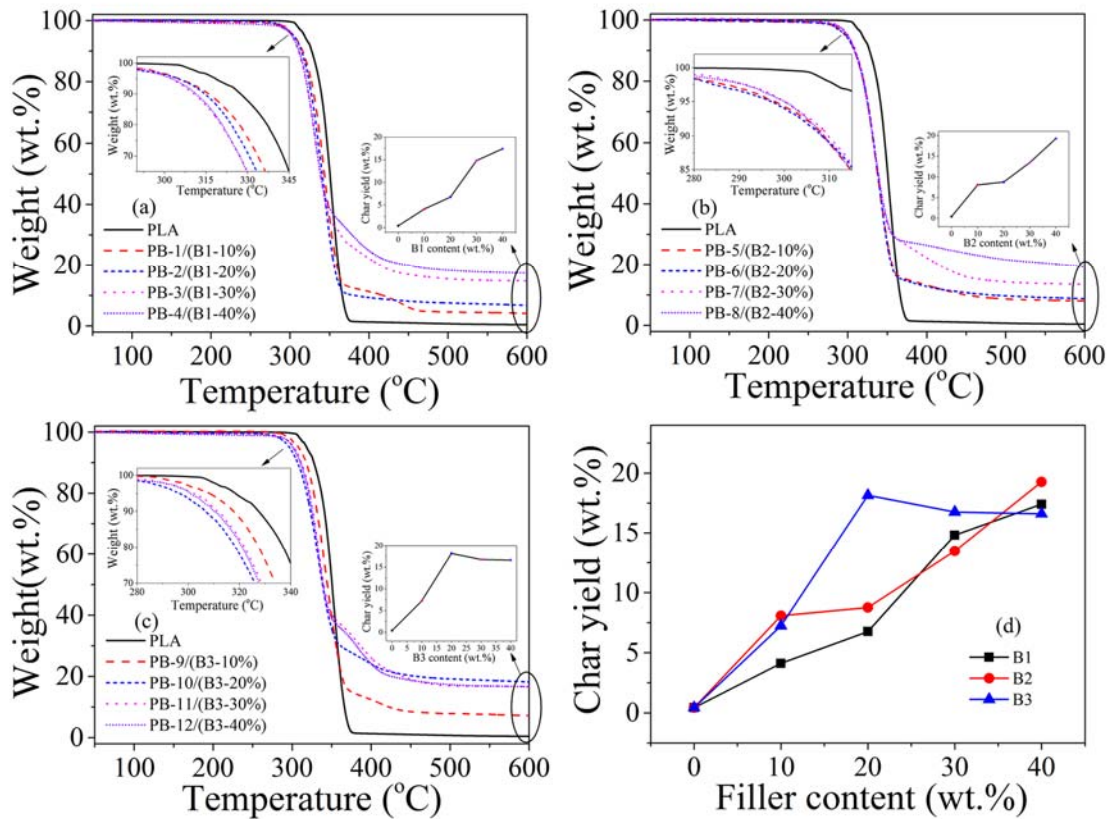


Fig. 5-6 TGA curves of flame retardants-series B ((a) B1; (b) B2; (c) B3) modified PLA composites and (d) char yield of those PLA composites.

Fig. 5-7 shows DTA thermograms of PLA and flame retardants-series B-modified PLA composites. Obtained from that, T_g s of Bx-modified PLA composites are summarized in Fig. 5-7(d) and Tab. 4-1. As expected, all Bx-modified PLA composites show high- T_g , indicating an excellent thermal stability. Moreover, T_g s of all PB-z/(Bx-Y) PLA composites with different flame retardant amount show a slight change to each other. Taking B1-modified PLA composites as instance, T_g s of all the PB-z/(B1-Y) PLA

composites show just a slight change to each other of 63.4 to 64.1 °C.

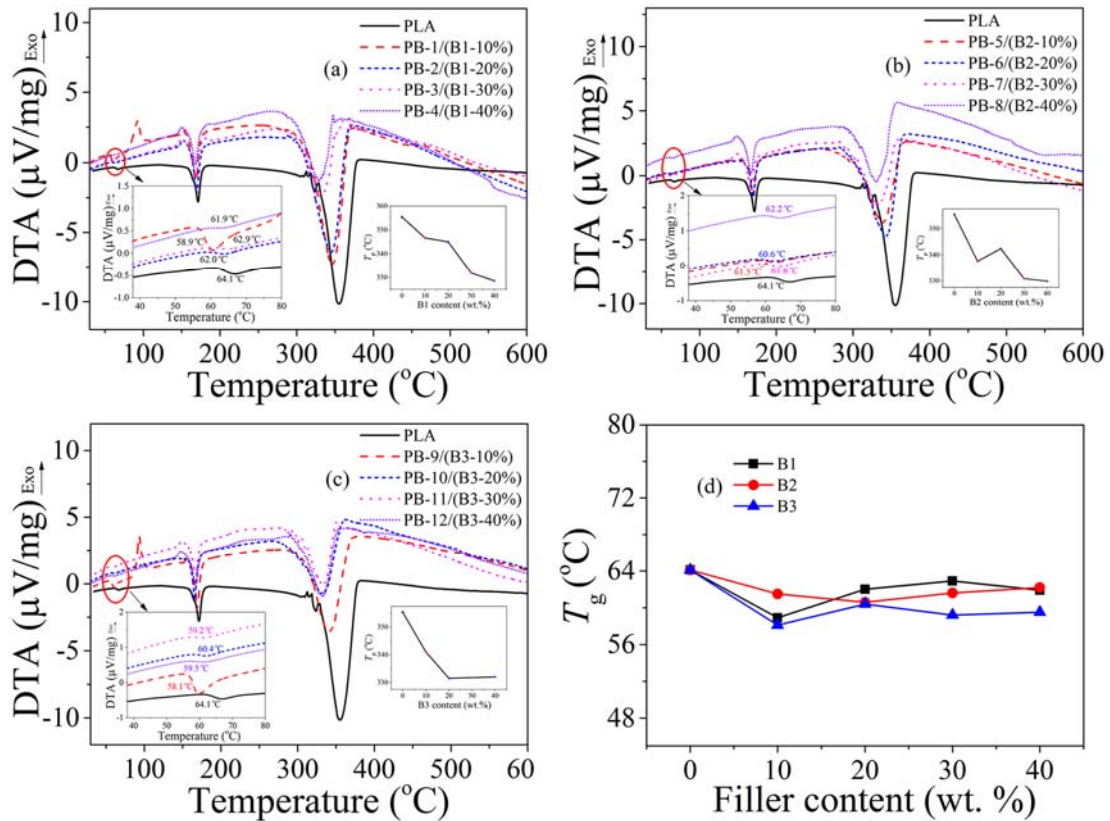


Fig. 5-7 DTA curves of flame retardants-series B ((a) B1; (b) B2; (c) B3) modified PLA composites and (d) T_g of those PLA composites.

(3) The thermal stability of C_x-modified PLA composites

The thermal stability of pure-PLA and flame retardants-series C modified PLA nanocomposites were investigated by TGA under nitrogen atmospheres at a heating rate of 10 °C·min⁻¹. Fig. 5-8 shows the TGA curves of those flame retardant PLA nanocomposites with the thermal decomposition process. For all the samples, there is only a one-sharp weight loss stage. Taking flame retardant C3-modified PLA composites as instance, the onset decomposition temperatures of 5% weight loss ($T_{5\%S}$) are 309.64, 306.8, 304.1 and 304.04 °C for PC-10/(C3/AHP-15%), PC-11/(C3/AHP-20%) and PC-12/(C3/AHP-25%), respectively, which are significantly lower than that of pure PLA (318.4 °C). In previous work, the decreasing trend of $T_{5\%}$ for DOPO-containing flame retardant PLA composites have been explained that the O=P—O bond in is more

active than common C—C bond [38]. In this work, PC-z/(Cx/AHP-Y) PLA nanocomposites with the addition of 1 wt% Cx show lower values of $T_{5\%}$ to that of PC-z/(AHP-Y) composites, probably resulting from aluminum-phosphorus synergistic effect. The anti-fractured O=P—O bond may result in forming phosphorus-containing radical stabilizers by the quenching mechanism in combustion. Additionally, flame retardants-series C modified PLA nanocomposites show slower weight loss rate than that of pure PLA. It is noteworthy that higher char yield can be obtained with simultaneously adding AHP and Cx, as charring layer plays a very important role in the performance of flame retardancy.

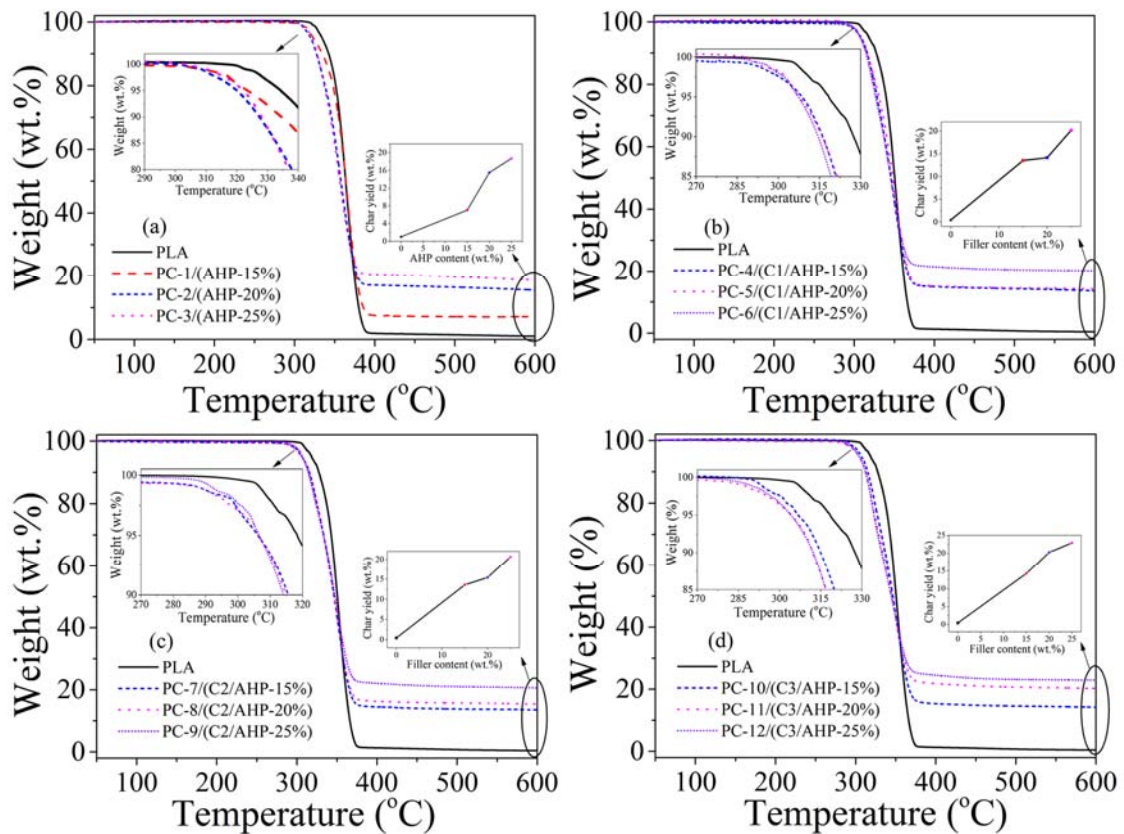


Fig. 5-8 TGA curves of (a) AHP and flame retardants-series C ((b) C1; (c) C2; (d) C3) modified PLA composites measured at a heating rate of 10 °C/min.

Fig. 5-9 shows DTA thermograms of pure-PLA and PC-z/(Cx/AHP-Y) PLA nanocomposites. Obtained from that, values of T_g obtained from Fig. 5-9 are summarized in Tab. 5-2. Taking PC-z/(C3/AHP-Y) PLA nanocomposites as instance,

the value of T_g increase to 60.9 °C with addition of 1 wt.% Cx into PLA matrix. It can be explained by the fact that the addition of functionalized MWCNTs shows influence on PLA molecular chain configuration. Moreover, the values of T_g for PC-z/(C3/AHP-Y) nanocomposites show a slight increase from 57.8 to 58.3 °C with the increasing of phosphorus amount, lower than that of neat PLA (64.1 °C), which can be attributed to the poor chemical compatibility of AHP to PLA.

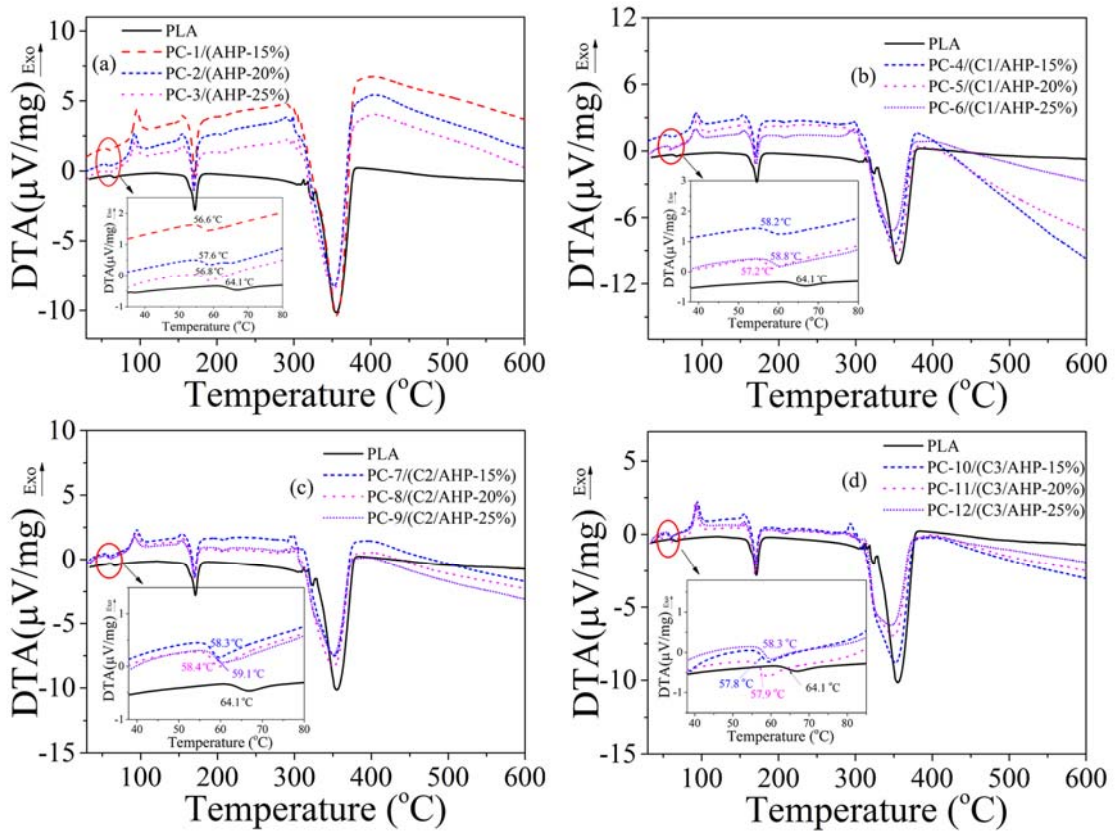


Fig. 5-9 DTA curves of (a) AHP and flame retardants-series C ((b) C1; (c) C2; (d) C3) modified PLA composites measured at a heating rate of 10 °C/min.

5.3.3 Mechanical properties of Cx-modified PLA nanocomposites

The tensile strength, notched impact strength and dynamic mechanical analysis (DMA) were taken to evaluate the mechanical properties of PC-z/(Cx/AHP-Y) (x=1, 2, 3; Y=15%, 20%, 25%; z=1-12) PLA nanocomposites.

(1) Tensile strength of Cx-modified PLA nanocomposites

Fig. 5-10 presents the tensile strength of PC-z/(Cx/AHP-Y) PLA nanocomposites with

the filler ratio changing from 0 to 25 wt. %.

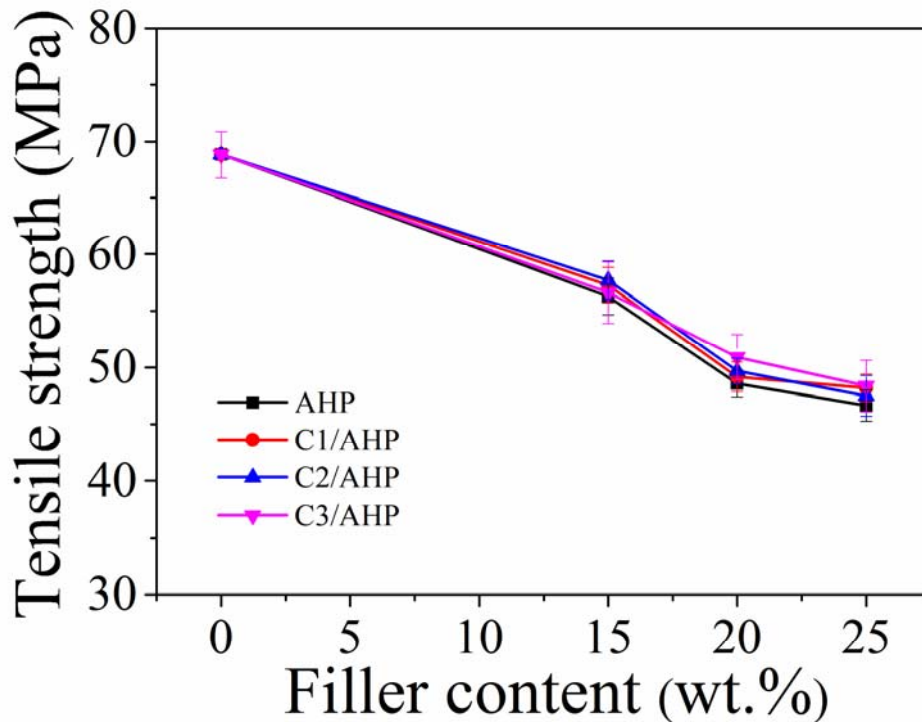


Fig. 5-10 Tensile strength and of AHP- and flame retardants-series C-modified PLA nanocomposites.

For the smaller amounts (15 wt. %) of AHP added into PLA, the tensile strength do not significantly decrease. Fig. 5-10 presents the tensile strength of PC-z/(Cx/AHP-Y) PLA nanocomposites with the filler ratio changing from 0 to 25 wt. %. For the smaller amounts (15 wt. %) of AHP added into PLA, the tensile strength do not significantly decrease. However, with 25 wt.% of AHP adding, tensile strength and fracture strain significantly decrease as shown in the black line of Fig. 5-10. It can be observed that pure-PLA shows high tensile strength of 68.8 ± 2.1 MPa and fracture strain of 5.9%. With 15 wt%, 20 wt% and 25 wt% AHP adding, the tensile strength reduces to 56.3 ± 3.6 MPa, 48.6 ± 3.2 MPa and 46.7 ± 3.4 MPa, respectively. It could be explained that the chemical incompatibility and aggregation of AHP cause stress concentrators, leading to the reduction in mechanical properties of AHP/PLA composites. When 1 wt.% Cx are incorporated, the tensile strengths of the nanocomposite slightly increase comparing

with those PC-z/(AHP-Y) composites. Taking C3 as instance, with the addition of 1 wt% C3, the tensile strengths of the PC-z/(C3/AHP-Y) PLA nanocomposites slightly increase to 69.5, 56.6, 50.9 and 48.4 MPa comparing with those PC-z/(AHP-Y) composites (68.8, 56.3, 48.6 and 46.7 Mpa). The improved tensile strength should be attributed to the better dispersion of AHP which was improved by three-dimensional networked Cx in the nanocomposites. Furthermore, the addition of 1 wt.% Cx gives rise to significant optimization in fracture strain of AHP/PLA composites, presenting better plastic deformation abilities.

(2) Izod notched impact strength of Cx-modified PLA nanocomposites

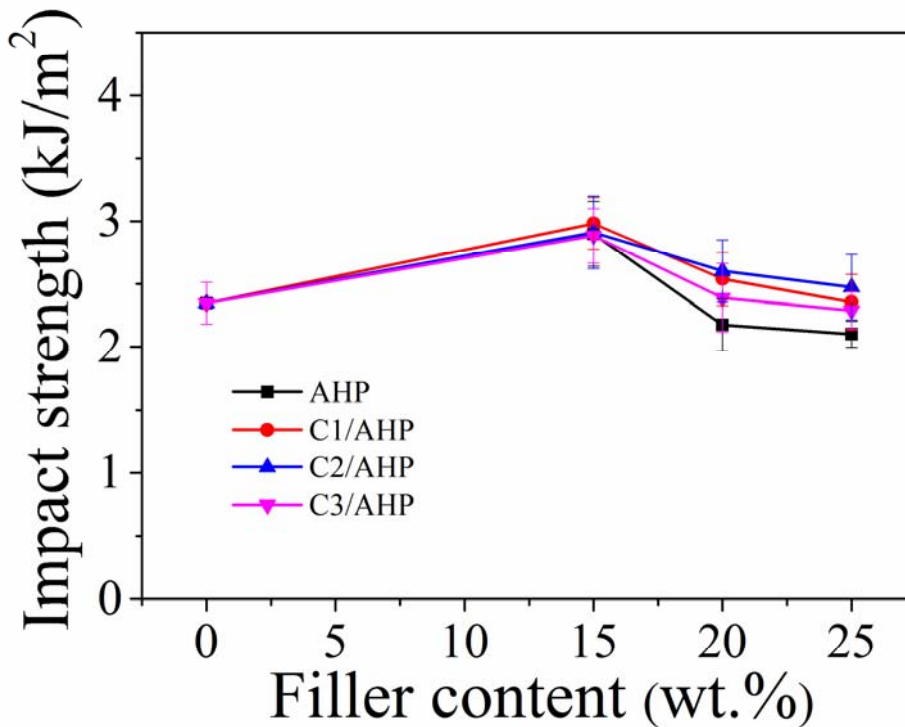


Fig. 5-11 Notched impact strength of AHP- and flame retardants-series C-modified PLA nanocomposites.

Fig. 5-11 presents the changes in notched impact strengths of these nanocomposites with 1 wt% of Cx and filler content varying from 0 wt%, 15wt%, 20wt% to 25 wt%. Pure-PLA showed a high notched impact strength of $2.35 \pm 0.17 \text{ kJ}\cdot\text{m}^{-2}$. It was obvious that notched impact strength increased with filler content of 15 wt%. However, the

notched impact strength slightly decreased when the filler content is over 15 wt%. The increasing trend can be explained by the fact that when AHP filled PLA composites receive impact force, AHP will induce crazes in the matrix because of stress concentration and will increase surface area to absorb the impact fracture energy.

With the addition of Cx into AHP/PLA flame retardant system, the notched impact strength slightly increased. Cx in this system presents a three-dimensional networked-structure and restricts flexible molecular chains of PLA matrix as well as stress concentration of AHP, resulting a decrease of izod impact energy. As AHP-content further increase, the impact energy decreases for these brittle reinforcing AHP/PLA composites. While, functionalized MWCNTs introduced in this condition play a role in hindering the propagation of the crack.

(3) DMA of flame retardants-series C modified PLA nanocomposites

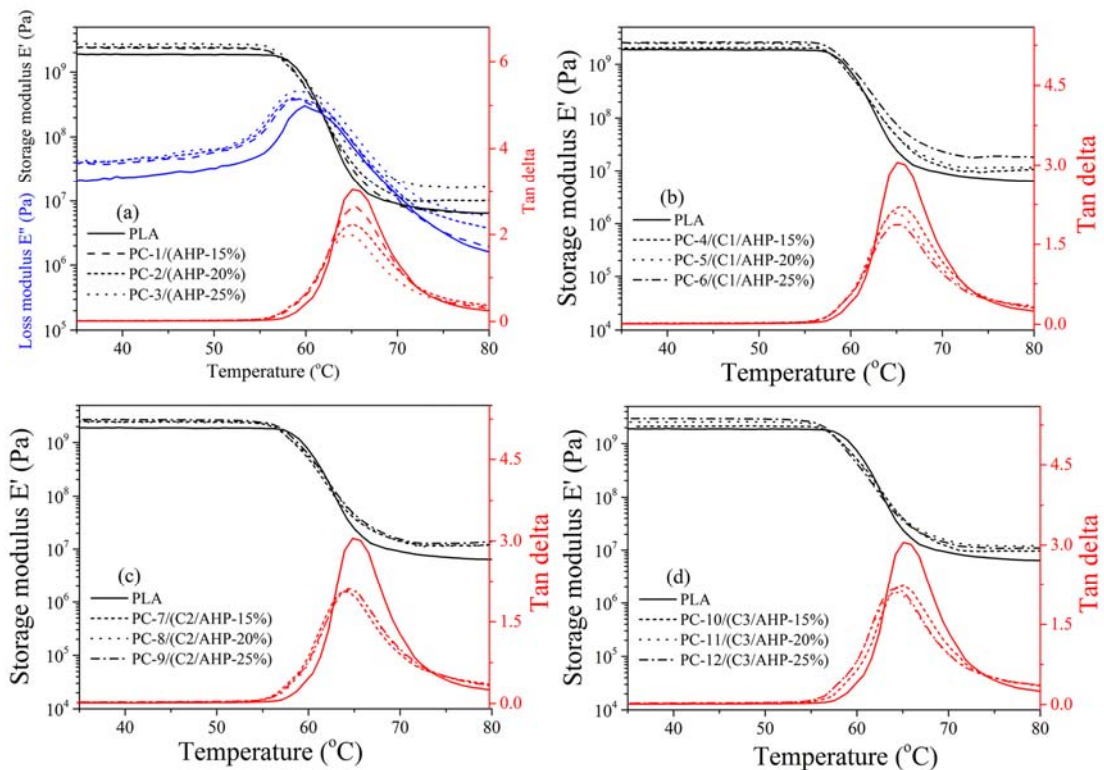


Fig.5-12 DMA thermograms of modified PLA nanocomposites with flame retardant of (a) AHP, (b) C1/AHP, (c) C2/AHP and (d) C3/AHP.

The dynamic mechanical and thermogravimetric properties of flame retardants-series

C modified PLA nanocomposites were also investigated. The storage modulus and loss factors obtained from DMA tests are plotted in Fig. 5-12, and the data is presented in Tab. 4-2. It was evident that the addition of different kinds of flame retardants, C_x, into AHP/PLA flame retardant system impacted the storage modulus. T_{gs} obtained from loss modulus showed good agreement with DTA results. It is noteworthy that T_{gs} of PC-z/(C_x/AHP-Y) PLA nanocomposites obtained from $\tan \delta$ values showed slight variations, following the addition of 1 wt% C_x. This phenomenon for C_x-modified PLA nanocomposites could be attributed to the nano-core-shell structure of C_x, according to the typical mechanical properties and thermal behaviors.

5.4 Conclusions

Three types of DOPO-containing flame retardants, A_x, B_x and C_x, were well dispersed into PLA matrix forming flame-retardant PLA composites. Flame retardancy tests indicated that A_x/B_x-modified PLA composites with A_x or B_x content of 30 wt% could reach UL 94 V-0 flammability rating, with high *LOI* values. Meanwhile, the *LOI* values increase greatly for those PC-z/(C_x/AHP-Y) nanocomposites with only 1 wt. % C_x loading, demonstrating that the flame retardancy improved with the addition of C_x. More importantly, PC-z/(C_x/AHP-15%) nanocomposites with 1 wt.% C_x can achieve UL 94 V-0 rating, which can be attribute to the excellent char formation-promoting properties of nano-structured C_x. Moreover, TGA results showed that all those flame retardant PLA composites produced high char yields. The mechanical properties of C_x-modified PLA nanocomposites deteriorated slightly with addition of C_x, with tensile strengths from 46.7 ± 3.4 to 56.3 ± 3.6 MPa. It is noteworthy that T_{gs} of PC-z/(C_x/AHP-Y) PLA nanocomposites obtained from $\tan \delta$ values showed slight variations, following the addition of 1 wt% C_x. This phenomenon for C_x-modified PLA nanocomposites could be attributed to the nano-core-shell structure of C_x, according to the typical mechanical properties and thermal behaviors.

References

- [1] Armentano, I., Bitinis, N., Fortunati, E. *et al.* Multifunctional nanostructured PLA materials for packaging and tissue engineering. *Progress in Polymer Science*, 2013, 38(10): 1720-1747.
- [2] Jacobsen, S., Degee, P. H., Fritz, H. G. *et al.* Polyactide (PLA)-a new way of production. *Polymer engineering and science*, 1999, 39(7): 1311.
- [3] Nampoothiri, K. M., Nair, N. R., John, R. P. An overview of the recent developments in polylactide (PLA) research. *Bioresource technology*, 2010, 101(22): 8493-8501.
- [4] Graupner, N., Herrmann, A. S., Müssig, J. Natural and man-made cellulose fibre-reinforced poly (lactic acid)(PLA) composites: An overview about mechanical characteristics and application areas. *Composites Part A: Applied Science and Manufacturing*, 2009, 40(6): 810-821.
- [5] Kamm, B., Gruber, P. R., Kamm, M. Biorefineries-industrial processes and products. Wiley-VCH Verlag GmbH & Co. KGaA, 2007.
- [6] Wei, L. L., Wang, D. Y., Chen, H. B., Chen, L., Wang, X. L., Wang, Y. Z. Effect of a phosphorus-containing flame retardant on the thermal properties and ease of ignition of poly (lactic acid). *Polymer Degradation and Stability*, 2011, 96(9), 1557-1561.
- [7] Cheng, K. C., Lin, Y. H., Guo, W. *et al.* Flammability and tensile properties of polylactide nanocomposites with short carbon fibers. *Journal of Materials Science*, 2015, 50(4): 1605-1612.
- [8] Bocz, K., Domonkos, M., Igricz, T. *et al.* Flame retarded self-reinforced poly (lactic acid) composites of outstanding impact resistance. *Composites Part A: Applied Science and Manufacturing*, 2015, 70: 27-34.
- [9] Morgan, A. B., & Wilkie, C. A. (Eds.). Flame retardant polymer nanocomposites. John Wiley & Sons, 2007.
- [10] Laoutid, F., Bonnaud, L., Alexandre, M., Lopez-Cuesta, J. M., & Dubois, P. New prospects in flame retardant polymer materials: from fundamentals to nanocomposites.

Materials Science and Engineering: R: Reports, 2009, 63(3), 100-125.

- [11] Gilman, J. W., Kashiwagi, T., & Lichtenhan, J. D. Nanocomposites: a revolutionary new flame retardant approach. *Sampe Journal*, 1997, 33, 40-46.
- [12] Choi, E. S., Brooks, J. S., Eaton, D. L., Al-Haik, M. S., Hussaini, M. Y., Garmestani, H., ... & Dahmen, K. Enhancement of thermal and electrical properties of carbon nanotube polymer composites by magnetic field processing. *Journal of Applied physics*, 2003, 94(9), 6034-6039.
- [13] Coleman, J. N., Khan, U., Blau, W. J., & Gun'ko, Y. K. Small but strong: a review of the mechanical properties of carbon nanotube–polymer composites. *Carbon*, 2006, 44(9), 1624-1652.
- [14] Baughman, R. H., Zakhidov, A. A., & de Heer, W. A. Carbon nanotubes--the route toward applications. *Science*, 2002, 297(5582), 787-792.
- [15] Pan, H., Wang, W., Pan, Y., Song, L., Hu, Y., & Liew, K. M. Formation of Layer-by-Layer Assembled Titanate Nanotubes Filled Coating on Flexible Polyurethane Foam with Improved Flame Retardant and Smoke Suppression Properties. *ACS applied materials & interfaces*, 2014, 7(1), 101-111.
- [16] Wu, W., Li, M., Zhong, Y., Zong, M., Xiao, S., Li, X., & Xie, F. Thermoxidative stability and char formation mechanism for the introduction of CNTs and MoS₂ into halogen-free flame retarding TPEE. *RSC Advances*, 2016, 6(4), 3267-3275.
- [17] Zhao, Q., Hu, Y., & Wang, X. Mechanical performance and flame retardancy of polypropylene composites containing zeolite and multiwalled carbon nanotubes. *Journal of Applied Polymer Science*, 2016, 133(3).
- [18] Ma, H. Y., Tong, L. F., Xu, Z. B., & Fang, Z. P. Functionalizing carbon nanotubes by grafting on intumescent flame retardant: nanocomposite synthesis, morphology, rheology, and flammability. *Advanced functional materials*, 2008, 18(3), 414-421.
- [19] Kuan, C. F., Chen, W. J., Li, Y. L., Chen, C. H., Kuan, H. C., & Chiang, C. L. Flame retardance and thermal stability of carbon nanotube epoxy composite prepared from sol–gel method. *Journal of Physics and Chemistry of Solids*, 2010, 71(4), 539-543.

-
- [20] Qiao, Z., Gao, C., Sun, B., & Ai, S. Synthesis and Characterization of Functionalized Multi-walled Carbon Nanotubes/Exfoliated Layered Double Hydroxide Nanosheets Hybrids via Electrostatic Force. *Journal of Inorganic and Organometallic Polymers and Materials*, 2013, 23(4), 871-876.
- [21] Mallakpour, S., & Zadehnazari, A. Effect of amino acid-functionalization on the interfacial adhesion and behavior of multi-walled carbon nanotubes/poly (amide-imide) nanocomposites containing thiazole side unit. *Journal of Polymer Research*, 2013, 20(7), 1-12.
- [22] Shi, Y., Long, Z., Yu, B., Zhou, K., Gui, Z., Yuen, R. K., & Hu, Y. Tunable thermal, flame retardant and toxic effluent suppression properties of polystyrene based on alternating graphitic carbon nitride and multi-walled carbon nanotubes. *Journal of Materials Chemistry A*, 2015, 3(33), 17064-17073.
- [23] Yu, W., Fu, J., Chen, L., Zong, P., Yin, J., Shang, D., ... & Shi, L. Enhanced thermal conductive property of epoxy composites by low mass fraction of organic-inorganic multilayer covalently grafted carbon nanotubes. *Composites Science and Technology*. 2016, 125, 90-99.
- [24] Xie, X. L., Mai, Y. W., and Zhou, X. P. Dispersion and alignment of carbon nanotubes in polymer matrix: a review. *Materials Science and Engineering: R: Reports*, 2005, 49(4), 89-112.
- [25] Ma, P. C., Siddiqui, N. A., Marom, G., & Kim, J. K. Dispersion and functionalization of carbon nanotubes for polymer-based nanocomposites: a review. *Composites Part A: Applied Science and Manufacturing*, 2010, 41(10), 1345-1367.
- [26] Zhang, Q., Wu, J., Gao, L., Liu, T., Zhong, W., Sui, G., .& Yang, X. Dispersion stability of functionalized MWCNT in the epoxy–amine system and its effects on mechanical and interfacial properties of carbon fiber composites. *Materials & Design*, 2016, 94, 392-402.
- [27] Wang, X., Hu, Y., Song, L., Xing, W., Lu, H., Lv, P., & Jie, G. Flame retardancy and thermal degradation mechanism of epoxy resin composites based on a DOPO substituted

organophosphorus oligomer. *Polymer*, 2010, 51(11), 2435-2445.

[28] Gu, L., Chen, G., & Yao, Y. Two novel phosphorus–nitrogen-containing halogen-free flame retardants of high performance for epoxy resin. *Polymer Degradation and Stability*, 2014, 108, 68-75.

[29] Xu, M. J., Xu, G. R., Leng, Y., & Li, B. Synthesis of a novel flame retardant based on cyclotriphosphazene and DOPO groups and its application in epoxy resins. *Polymer Degradation and Stability*, 2016, 123, 105-114.

[30] Wang, L., Yu, J., Tang, Z., & Jiang, P. Synthesis, characteristic, and flammability of modified carbon nanotube/poly (ethylene-co-vinyl acetate) nanocomposites containing phosphorus and silicon. *Journal of materials science*, 2010, 45(24), 6668-6676.

[31] Yu, T., Jiang, N., & Li, Y. Functionalized multi-walled carbon nanotube for improving the flame retardancy of ramie/poly (lactic acid) composite. *Composites Science and Technology*, 2014, 104, 26-33.

[32] Zhao, Z., Yang, Z., Hu, Y., Li, J., & Fan, X. Multiple functionalization of multi-walled carbon nanotubes with carboxyl and amino groups. *Applied surface science*, 2013, 276, 476-481.

[33] Dubal, D. P., Gund, G. S., Lokhande, C. D., & Holze, R. Decoration of spongelike Ni(OH)₂ nanoparticles onto MWCNTs using an easily manipulated chemical protocol for supercapacitors. *ACS applied materials & interfaces*, 2013, 5(7), 2446-2454.

[34] Bao, J., Dou, M., Liu, H., Wang, F., Liu, J., Li, Z., & Ji, J. Composition-Dependent Electrocatalytic Activity of Palladium–Iridium Binary Alloy Nanoparticles Supported on the Multiwalled Carbon Nanotubes for the Electro-Oxidation of Formic Acid. *ACS applied materials & interfaces*, 2015, 7(28), 15223-15229.

[35] Song, P., Shen, Y., Du, B., Peng, M., Shen, L., & Fang, Z. Effects of reactive compatibilization on the morphological, thermal, mechanical, and rheological properties of intumescent flame-retardant polypropylene. *ACS applied materials & interfaces*, 2009, 1(2), 452-459.

[36] Carosio, F., & Alongi, J. Ultra-Fast Layer-by-Layer Approach for Depositing Flame

Retardant Coatings on Flexible PU Foams within Seconds. *ACS applied materials & interfaces*, 2016, 8(10), 6315-6319.

[37] Gu, L., Chen, G., and Yao, Y. Two novel phosphorus–nitrogen-containing halogen-free flame retardants of high performance for epoxy resin. *Polymer Degradation and Stability*, 2014, 108, 68-75.

[38] Tang, G., Wang, X., Xing, W., Zhang, P., Wang, B., Hong, N., ... & Song, L. (). Thermal degradation and flame retardance of biobased polylactide composites based on aluminum hypophosphite. *Industrial & Engineering Chemistry Research*, 2012, 51(37), 12009-12016.

Chapter 6 Cold Rolling Process for Flame Retardant PLA Nanocomposites

6.1 Introduction

In chapter 5, the mechanical properties of flame retardant PLA composites are usually deteriorated with addition of flame retardant(s), due to the poor chemical compatibility and dispersibility of flame retardant(s). In order to improve the mechanical properties and ductility of such flame retardant PLA composites, and extend their industrial applications, a cold rolling process was performed in this work.

Commonly, injection molding, extrusion molding, blow molding and rolling molding are available for composite preparation. Besides, it is well known that microstructures including crystalline structure, molecular orientation and crystallinity affect mechanical properties of crystalline polymer. Some researchers have attempted to take advantage of the molecular chain orientation of polymer during extending to improve the mechanical properties of degradable polymer through various molding processes [1-5]. Besides, many researchers have reported that the plastic processing can achieve good mechanical properties, such as die-drawing [6], roller drawing [7], tensile drawing [8], equal channel angular extrusion [9], hydrostatic extrusion [10] and rolling process [11]. In particular, the rolling process can achieve high molecular orientation for polymers while preventing the generation of voids during processing, which has been reported by Nakayama et al. [12]. Therefore, the rolling process has been extensively employed for producing polymers with good properties, such as polyethylene (PE) [13], polyoxymethylene (POM) [14], polypropylene (PP) [15] and others. Both Qiu et al. [16] and Murata et al. [17] investigated the changes of morphologies and mechanical properties in the molded polymers. During the plastic processing, a multilayer structure was formed because of the different cooling process on the surface as well as in the inner part [18]. Moreover, the crystallinity was decreased and the molecular orientation was increased by the rolling

process as observed with micro Fourier transform infrared (FT-IR) spectroscopy [19]. They obtained the internal structure information in the whole cross section of polymer and accurately assessed the change of PP microstructure via the rolling process. However, to the best of our knowledge, there is no research work to study on the effect of crystallinity and orientation on microstructures (i.e. crystal morphology, crystallinity and molecular orientation) and mechanical properties of PLA produced by cold rolling process. Therefore, it is essential to know whether or not the rolling process will change the microstructure of PLA, which is a key for the improvement of the mechanical properties of PLA, especially its ductility.

To improve the ductility of flame retardant PLA and extend its industrial applications, we first introduce rolling process into the flame retardant system to ease the deterioration of mechanical properties by adding flame retardant(s).

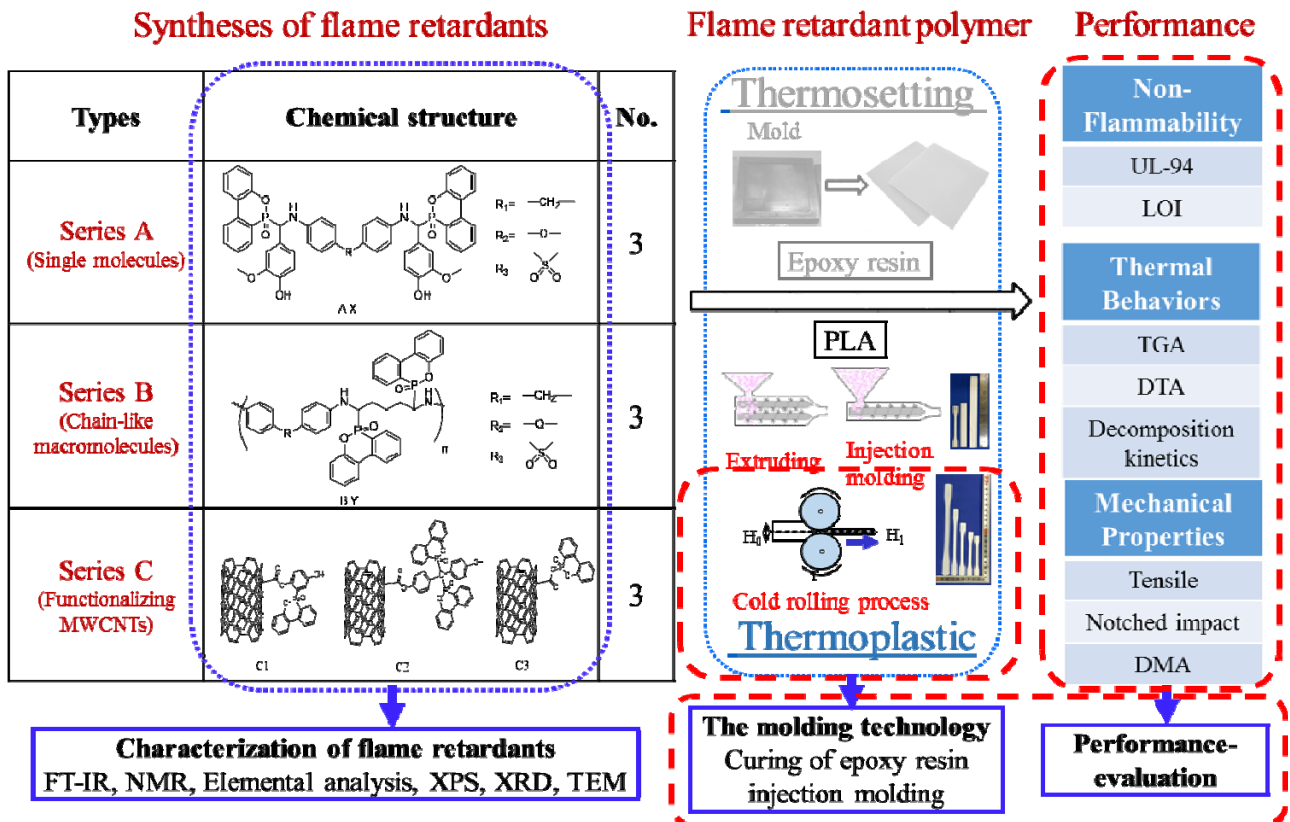


Fig. 6-1 Cold rolling process and performance-evaluation of flame retardant PLA

nanocomposites.

6.2 Experimental

6.2.1 Materials

Flame retardant PC-z/(Cx/AHP-Y) ($x=1, 2, 3$ and denotes the ID of flame retardants-series C; $Y = 10\%, 20\%, 30\%, 40\%$ and denotes the weight percentage content of Cx and AHP; $z=1-12$ and denotes the ID of nanocomposites) PLA nanocomposites were prepared following Chapter 5.

6.2.2 Instruments and Measurements

The rolling process was performed with different rolling ratios (0%, 10%, 30%, 50% and 70%) to evaluate the effect of the rolling ratio on the properties and morphology of PC-z/(Cx/AHP-Y) nanocomposites. The rolling process was carried out by a rolling machine (TKE-0; Imoto Machinery Co., Ltd., Tokyo, Japan) at room temperature (23 ± 2 °C) with a rotation speed of $3 \text{ m} \cdot \text{min}^{-1}$ (Fig. 6-2). The rolling direction was matched to the extrusion direction and the effective width and diameter of each roller were 150 mm and 100 mm, respectively. The rolling ratio ξ was calculated by equation 6-1:

$$\xi = (H_0 - H_1) / H_0 \times 100\% \quad (6-1)$$

Where H_0 is the initial thickness of the specimen, and H_1 is the thickness of the rolled specimen, as shown in Fig 6-2.

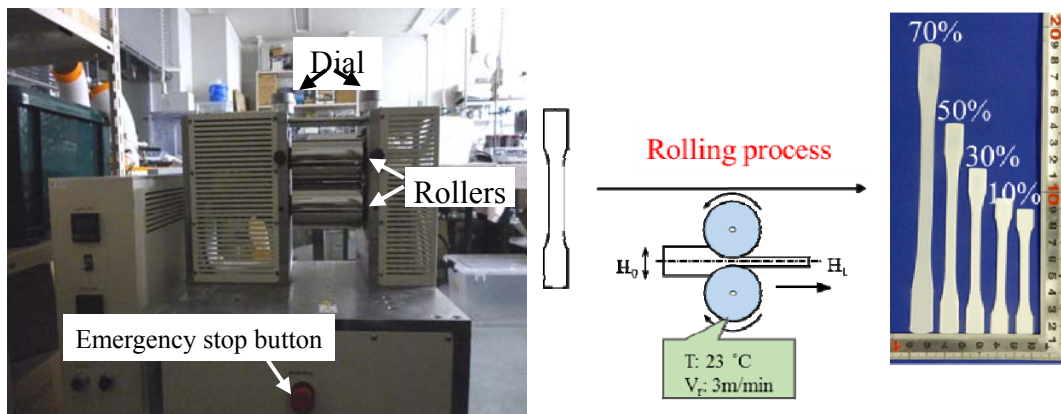


Fig. 6-2 Cold rolling machine and cold rolling process with different rolling ratios (0%, 10%, 30%, 50% and 70%).

6.2.3 Instruments and measurements

Tensile tests of the composites were carried out on a universal testing machine (Instron Ltd Series 3360) according to JIS K7113 with a crosshead displacement rate of $10 \text{ mm}\cdot\text{min}^{-1}$ at $23 \pm 1 \text{ }^\circ\text{C}$. IR thermal imaging (FLIR-SC-620, FLIR Systems, USA) were used for sensing in the tensile test. The scanning electron microscope (SEM) observation was performed on a Hitachi S-4300 scanning electron microscope in high vacuum mode with 5 kV acceleration voltage. Dynamic mechanical analysis (DMA) was performed by using a TA Instrument RSA-G2 by 3-Point Bending mode with an amplitude of $10 \text{ }\mu\text{m}$.

6.3 Results and discussion

6.3.1 Effect of rolling ratio on tensile properties

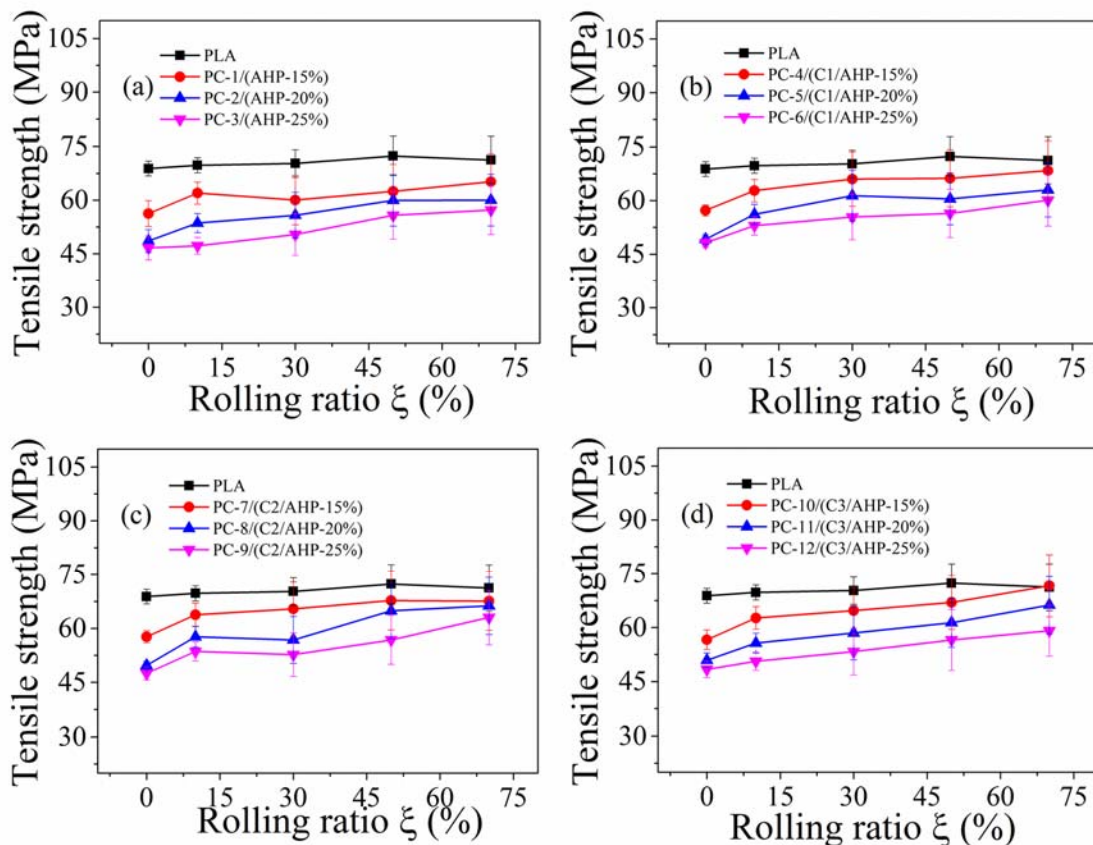


Fig. 6-3 Tensile strength of (a) AHP and flame retardants-series ((b) C1, (c) C2, (d) C3) modified PLA composites with different rolling ratios (0%, 10%, 30%, 50% and 70%).

In order to investigate the effect of rolling ratio on the tensile properties, the tensile properties of (a) AHP- and flame retardants-series ((b) C1, (c) C2, (d) C3)-modified flame retardant PLA nanocomposites with different rolling ratios (0%, 10%, 30%, 50% and 70%) were measured as displayed in Fig. 6-3 and Fig. 6-4. It can be seen from Fig. 6-3 that the tensile strength of flame retardant PLA nanocomposites decrease with the filler ratio increasing from 0 to 25 wt. %. Especially, with 25 wt.% of flame retardant(s) adding, tensile strength and fracture strain significantly decrease as shown in the magenta line of Fig. 6-3 and 6-4. It can be observed that pure-PLA shows high tensile strength of 68.8 ± 2.1 MPa and fracture strain of 5.9%. With 15 wt%, 20 wt% and 25 wt% AHP adding, the tensile strength reduces to 56.3 ± 3.6 MPa, 48.6 ± 3.2 MPa and 46.7 ± 3.4 MPa, respectively. It could be explained that the chemical incompatibility and aggregation of AHP cause stress concentrators, leading to the reduction in mechanical properties of AHP/PLA composites. However, after cold rolling process with rolling ratio of 70%, their tensile strength increased to be 65.2 ± 7.8 MPa, 60.0 ± 7.2 MPa and 57.2 ± 6.9 MPa, respectively. The tensile strength was significantly enhanced by the rolling process. When 1 wt.% Cx are incorporated, the tensile strengths of the nanocomposite slightly increase comparing with those PC-z/(AHP-Y) composites. The improved tensile strength should be attributed to the better dispersion of AHP which was improved by three-dimensional networked Cx in the nanocomposites. Furthermore, the addition of 1 wt.% Cx gives rise to significant optimization in fracture strain of AHP/PLA composites, presenting better plastic deformation abilities. Meanwhile, after rolling-processing, the tensile strength was significantly enhanced after cold rolling process. Moreover, compared the tensile strength of 1 wt% Cx-modified PLA nanocomposite under cold rolling process with that of unrolled one, it shows an increase trend, indicating the mechanical-improvement properties by cold rolling process. It was proven that the cold rolling process could greatly improve the mechanical properties of the low adding Cx modified PLA nanocomposites. Furthermore, the specimens of PC-z/(Cx/AHP-Y) nanocomposites with different fillers amount (0, 15, 20, 25 wt%) at

rolling ratios of 0%, 10%, 30%, 50% and 70% had also been investigated by tensile tests. All the samples show better mechanical properties compared to the unrolled ones, presenting an even plastic deformation.

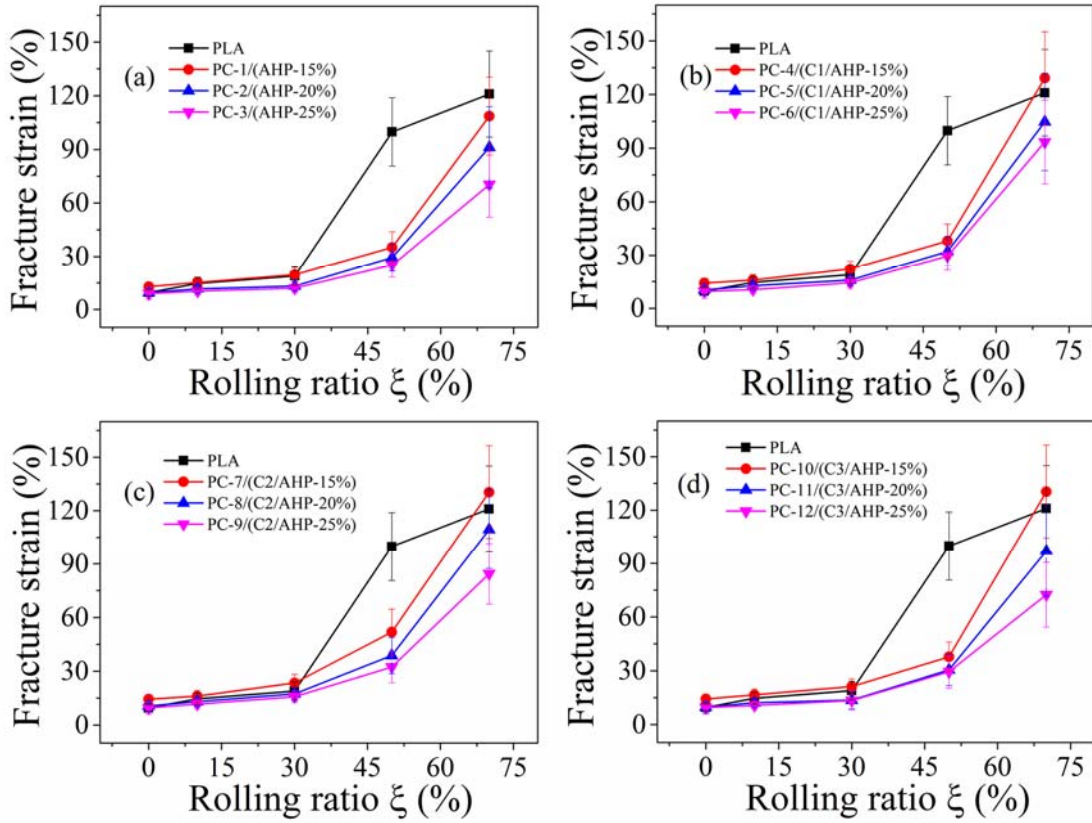


Fig. 6-4 Fracture strain of (a) AHP and flame retardants-series ((b) C1, (c) C2, (d) C3) modified PLA composites with different rolling ratios (0%, 10%, 30%, 50% and 70%).

Furthermore, Fig. 6-4 show fracture strain of the flame retardant PLA nanocomposites with different rolling ratio of 0%, 10%, 30%, 50% and 70%. It can be concluded from Fig. 6-4 that the fracture strain of those flame retardant nanocomposites was increased following with the rolling ratio increasing. With addition of 1 wt.% Cx, when the rolling ratio increased from 0% to 70%, the fracture strain was increased greatly than that of AHP-modified PLA composites. The fracture strain of the PC-z/(Cx/AHP-15%) nanocomposites with 1 wt.% Cx and fillers content of 15 wt% was sharply increased to 120% under the 70% rolling ratio. The fracture strain was increased greatly with the increase of the rolling ratio, which could be considered that the

anisotropy of tensile properties of the flame retardant PLA nanocomposites resulted the obvious difference in the tensile properties.

6.3.2 Mechanism of tensile-reinforcing properties with cold rolling process

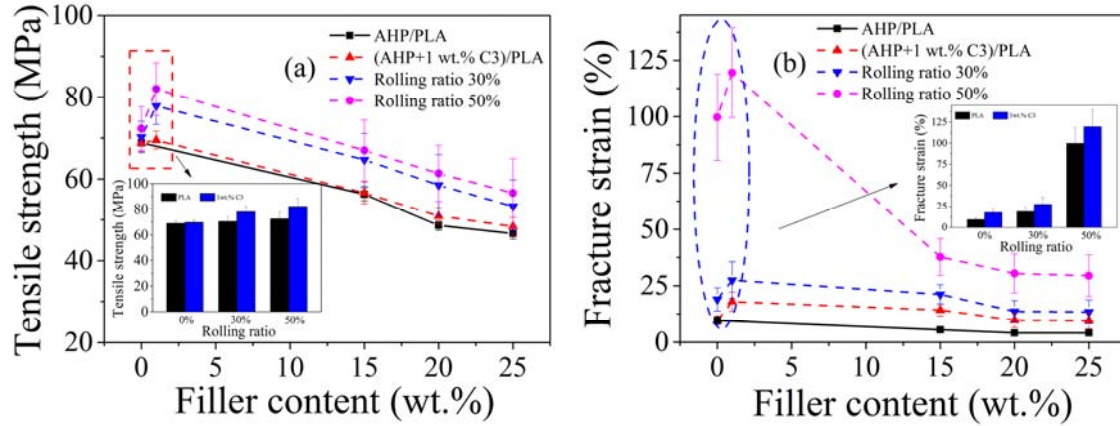


Fig. 6-5 (a) Tensile strength and (b) fracture strain of AHP- and C3-modified PLA at rolling ratio of 0%, 30% and 50%.

In our previous work, an appropriate rolling process was conducive for improving the comprehensive mechanical properties of PLA with the increasing of both tensile strength and fracture strain, indicating that PLA was homogenized during the rolling process [20]. To further improve the mechanical properties for better secondary processing, a cold rolling process was performed on flame retardant PC-z/(C3/AHP-Y) PLA nanocomposites at rolling ratios of 30% and 50%. The obtained results are shown in Fig. 6-5. Inset of Fig. 6-5(a) exhibits the tensile strength bar graph of pure-PLA and 1 wt.% C3 modified PLA nanocomposites with various rolling ratios (i.e., $\xi = 0\%$, 30%, and 50%) parallel to the rolling direction. Obviously, the unrolled 1 wt.% C3 modified PLA was fractured with tensile strength of 69.5 MPa. Meanwhile, after rolling-processing, the tensile strength was significantly enhanced to 77.9 and 82.0 MPa with rolling ratio of 30% and 50% respectively. Moreover, compared the strain of 1 wt.% C3/PLA nanocomposite at the rolling ratio of 50% with that of unrolled one, it shows a suddenly increase to more than 120%, indicating a high ductility (inset of Fig. 6-5(b)). It was proven that the cold rolling process could greatly improve the mechanical property of the

low adding C3 modified PLA. Furthermore, the specimens of PC-z/(C3/AHP-Y) PLA nanocomposites with different fillers amount at rolling ratios of 30% and 50% had also been investigated by tensile tests. All the samples show better mechanical properties compared to the unrolled ones, presenting an even plastic deformation.

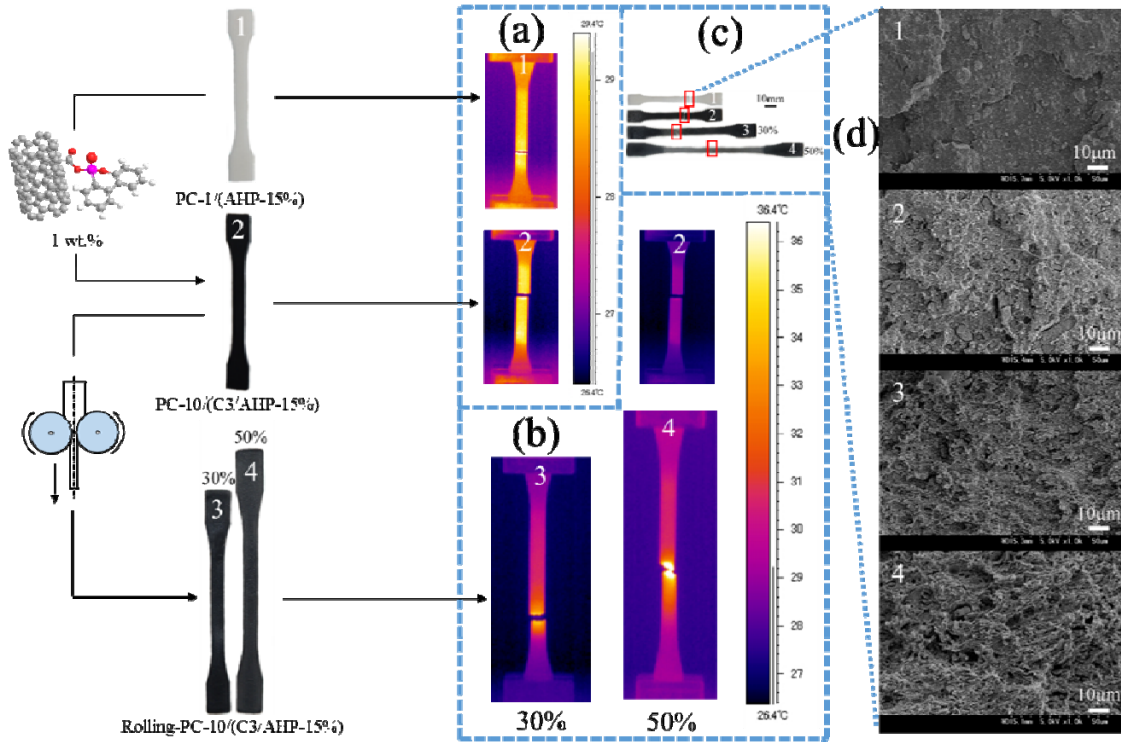


Fig. 6-6 Proposed tensile strength-reinforcing mechanism. (a) Infrared thermography images of PC-1/(AHP-15%) and PC-10/(C3/AHP-15%) at 26.4~29.4 °C; (b) Infrared thermography images of PC-10/(C3/AHP-15%) and associating specimens after rolling process at 26.4~36.4 °C; (c) Photographs and (d) SEM images of PC-1/(AHP-15%), PC-10/(C3/AHP-15%) and their associating specimens after rolling process.

The data in Fig. 6-5 shows that the tensile properties of the rolled PC-z/(C3/AHP-Y) PLA nanocomposites were affected by the rolling process greatly. Thus, a proposed tensile strength-reinforcing mechanism is shown in Fig. 6-6 based on the results of infrared thermography and SEM. With the addition of 1 wt.% C3 (Fig. 6-6(a)), the specimen shows a uniform heat storage property according with higher tensile strength, attributing to the excellent heat transfer performance of functionalized MWCNTs with

three-dimensional networked structure [21-23]. High magnification SEM image for PC-10/(C3/AHP-15%) PLA nanocomposites in Fig. 6-6(d-2) shows such three-dimensional networked-structure and well dispersed AHP. For the specimens after rolling process, it has been reported that the decrease of the crystallinity was due to crystalline deformation and crystals destruction, which led to the increase of plastic deformation during the rolling process [20]. Specimens after rolling process show more excellent heat storage properties during the tensile tests, and present softening effect that due to much higher fracture temperature (Fig. 6-6(b)). Comparing to the typical brittle fracture of unrolled PC-10/(C3/AHP-15%) nanocomposites (Fig. 6-6 (d-2)), the fractured sizes of both rolling-specimens became smaller, indicating the typical characteristics of a ductile fracture (Fig. 6-6(d-3) and (d-4)). Moreover, it was observed that there were many fibrillar-PLA on the fractured surfaces, especially in the case of the 50% rolling ratio (Fig. 6-6(d-4)). Additionally, the Cx-modified PLA specimens were homogenized at a high rolling ratio, thus, the tensile properties with rolling process are reinforced.

6.3.3 Dynamic mechanical analysis (DMA)

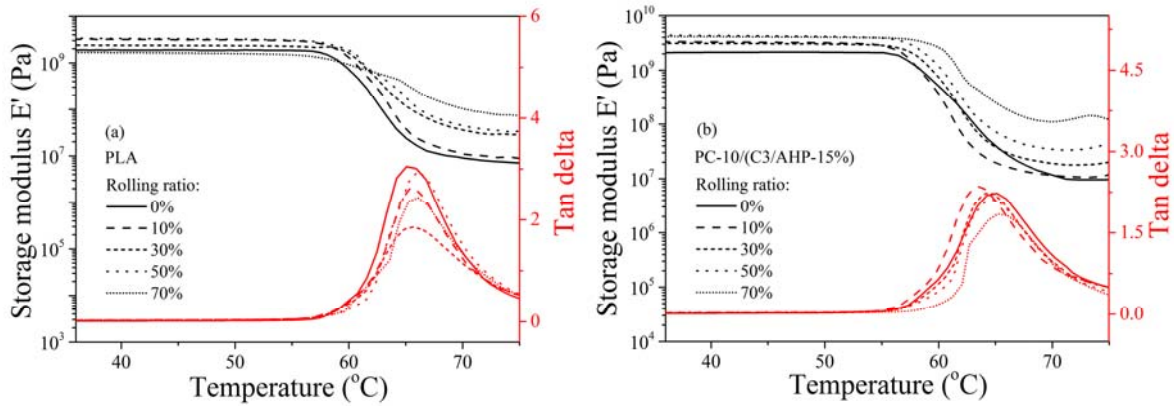


Fig. 6-7 DMA thermograms of PLA and PC-10/(C3/AHP-15%) nanocomposites at rolling ratio of 0%, 10%, 30%, 50% and 70%.

The dynamic mechanical and thermogravimetric properties of flame retardant PC-z/(Cx/AHP-Y) PLA nanocomposites were investigated. And the results are summarized in chapter 5. It can be concluded that the addition of AHP and 1 wt% Cx into

PLA increases the storage modulus of PLA. Values of T_g obtained from $\tan \delta$ show a slightly change following the increasing amount of flame retardant, which can be explained by that three-dimensional networked Cx restrict the movement of PLA chains and AHP, resulting in almost unchanged values of T_g with AHP-content increase.

The storage modulus E' and $\tan \delta$ under different rolling ratios were shown in Fig. 6-7. At the region of below the glass transition temperature, the E' was increased following by the increase of rolling ratio (i.e. $\xi = 10\%, 30, 50\%, 70\%$). For $\tan \delta$, at the region of below the glass transition temperature, the $\tan \delta$ of rolled flame retardant PLA composites change slightly to that of unrolled PLA, but at high temperature region ($60\text{ }^\circ\text{C}$), $\tan \delta$ change greatly. Values of T_g obtained from $\tan \delta$ show a slightly increase following the increase of rolling ratio, which can be explained by the effect of cold crystallization according to the cold rolling process.

6.4 Conclusions

Core-shell nanostructured flame retardant Cx were introduced into aluminum hypophosphite/poly(lactic acid) (AHP/PLA) flame retardant systems to improve both flame retardancy and mechanical properties. In order to improve the mechanical properties and ductility of such flame retardant PLA nanocomposites, as well as extend their industrial applications, a cold rolling process was performed in this work. Such cold rolling process was conducive for improving the comprehensive mechanical properties of flame retardant PLA nanocomposites with the increasing of both tensile strength and fracture strain. With addition of 1 wt% Cx, when the rolling ratio increased from 0% to 70%, the tensile strength and fracture strain was increased greatly than that of AHP-modified PLA composites. Additionally, the Cx-modified PLA nanocomposites were homogenized at a high rolling ratio, resulting reinforced tensile properties according to the cold rolling process.

References

- [1] Oliveira, J., Brichi, G. S., Marconcini, J. M., Mattoso, L. H. C., Glenn, G. M., & Medeiros, E. S. Effect of solvent on the physical and morphological properties of poly (lactic acid) nanofibers obtained by solution blow spinning. *Journal of Engineered Fibers and Fabrics*, 2014, 9(4), 117-125.
- [2] Qiu, J. H. Effects of hot roll process on the morphology and tensile properties of injection-molded polypropylene. *Kobunshi Ronbunshu*, 2006, 63(6), 397-403.
- [3] Qiu, J., Murata, T., Wu, X., Kitagawa, M., & Kudo, M. Plastic deformation mechanism of crystalline polymer materials in the equal channel angular extrusion process. *Journal of Materials Processing Technology*, 2012, 212(7), 1528-1536.
- [4] Qiu, J., Murata, T., Wu, X., Kudo, M., & Sakai, E. Plastic deformation mechanism of crystalline polymer materials during the rolling process. *Journal of Materials Science*, 2013, 48(5), 1920-1931.
- [5] Chapleau, N., Mohanraj, J., Ajji, A., & Ward, I. M. Roll-drawing and die-drawing of toughened poly (ethylene terephthalate). Part 1. Structure and mechanical characterization. *Polymer*, 2005, 46(6), 1956-1966.
- [6] Lee, S. H., Nakayama, K., & Cho, H. H. Fine structure and physical properties of poly (buthylene terephthalate) sheets prepared by roller drawing method. *Fibers and Polymers*, 2008, 9(6), 740-746.
- [7] Bao, R., Ding, Z., Zhong, G., Yang, W., Xie, B., & Yang, M. Deformation-induced morphology evolution during uniaxial stretching of isotactic polypropylene: effect of temperature. *Colloid and Polymer Science*, 2012, 290(3), 261-274.
- [8] Qiu, J., Murata, T., Wu, X., Kitagawa, M., & Kudo, M. Plastic deformation mechanism of crystalline polymer materials in the equal channel angular extrusion process. *Journal of Materials Processing Technology*, 2012, 212(7), 1528-1536.
- [9] Gibson, A. G., Ward, I. M., Cole, B. N., & Parsons, B. Hydrostatic extrusion of linear polyethylene. *Journal of Materials Science*, 1974, 9(7), 1193-1196.

-
- [10] J. Qiu, T. Murata, K. Takahashi and X. Wu. The Plastic Deformation Characteristics of Crystalline Polymer Materials via Rolling Process. *Adv. Mater. Res.* 2012, 391-392, 585-589.
- [11] Wang, L., Qiu, J., & Sakai, E. Microstructures and mechanical properties of polylactic acid prepared by a cold rolling process. *Journal of Materials Processing Technology*, 2016, 232, 184-194.
- [12] Mohanraj, J., Morawiec, J., Pawlak, A., Barton, D. C., Galeski, A., & Ward, I. M. Orientation of polyoxymethylene by rolling with side constraints. *Polymer*, 2008, 49(1), 303-316.
- [13] Qiu, J. Effects of the stress amplitude and the test temperature on the fatigue property of cold rolled PP. *Trans. Jpn. Soc. Mech. Eng. A*, 2002, 68, 65-73.
- [14] Qiu, J. H., Kawagoe, M., Mizuno, W., & Morita, M. Effect on fatigue failure of injection-molded polypropylene sheets by rolling process. *Kobunshi Ronbunshu*, 2000, 57(5), 255-262.
- [15] T. Murata, J. Qiu, E. Sakai, X. Wu and M. Kudo. Morphology Change of Extrusion Molded Crystalline Polymer by Rolling Process. *Adv. Mater. Res.*, 2012, 391-392, 595-599.
- [16] J. Qiu, M. Kawagoe, W. Mizuno and M. Morita. Effect of Morphology and Tensile Properties of Polypropylene by the Rolling Process (in Japanese). *Trans. Jpn. Soc. Mech. Eng. A*, 2000, 66, 867-874.
- [17] Miyata, T., & Masuko, T. Morphology of poly (L-lactide) solution-grown crystals. *Polymer*, 1997, 38(16), 4003-4009.
- [18] Murata, T., Qiu, J., & Wu, X. Effect of rolling temperature on microstructure and tensile properties of polypropylene. *Polymer Engineering & Science*, 2013, 53(12), 2573-2581.
- [19] Puiggali, J., Ikada, Y., Tsuji, H., Cartier, L., Okihara, T., & Lotz, B. The frustrated structure of poly (L-lactide). *Polymer*, 2000, 41(25), 8921-8930.
- [20] Wang, L., Qiu, J., & Sakai, E. Microstructures and mechanical properties of

polylactic acid prepared by a cold rolling process. *Journal of Materials Processing Technology*, 2016, 232, 184-194.

[21] Yu, T., Jiang, N., & Li, Y. Functionalized multi-walled carbon nanotube for improving the flame retardancy of ramie/poly (lactic acid) composite. *Composites Science and Technology*, 2014, 104, 26-33.

[22] Flynn, J. H., & Wall, L. A. A quick, direct method for the determination of activation energy from thermogravimetric data. *Journal of Polymer Science Part B: Polymer Letters*, 1966, 4(5), 323-328.

[23] Garg, P., Alvarado, J. L., Marsh, C., Carlson, T. A., Kessler, D. A., & Annamalai, K. An experimental study on the effect of ultrasonication on viscosity and heat transfer performance of multi-wall carbon nanotube-based aqueous nanofluids. *International Journal of Heat and Mass Transfer*, 2009, 52(21), 5090-5101.

Chapter 7 Conclusions

The advantages of Phosphorus-containing flame retardants (PFRs) include efficacy at low concentration of organics, feasibility of incorporation and processing, relatively low detrimental effects on physical properties, and so on. Today, PFRs are amongst the "workhorse" products in the field of flame-retardant materials, and researches have been focused on finding highly efficient phosphorus sources. Amongst them, research on 9,10-dihydro-9-oxa-10-phosphaphenanthrene 10-oxide (DOPO) group has gained immense interest. Based on the active P—H bond, chemically introducing DOPO into various monomers has become a strategy for preparing novel PFRs. For application, flame-retardant epoxy resins have been widely applied in electrical laminates and encapsulation resins, construction materials, adhesives and protective coatings due to their safeguard against the potential fire hazard. On the other hand, poly(lactic acid) (PLA) has been promoted to be one of the most widely used biodegradable polymers in packaging engineering, biomedical fields, household and automobile engineering, electricity industry and so on, because of their outstanding properties and renewable resources (mainly starch and sugar). However, the PFRs for epoxy resin or PLA has to encounter limitation (or risk): phosphorus resource efficiency, potential eutrophication from phosphorous, as well as the thermal and mechanical properties of flame retardant polymers.

In the present study, three types of DOPO-containing flame retardants (Series A: single molecules; Series B: chain-like macromolecules; Series C: Functionalizing MWCNTs) were synthesized based on the Pudovik reactions. The resultant nine kinds of novel flame retardants were application into epoxy resin and PLA, respectively. Such flame retardant polymer composites showed high performance that: meeting UL 94 V-0 flammability rating; high LOI values; high T_g ; excellent mechanical properties.

In chapter 1, the research backgrounds, research significance, summary of the research and the construction of this thesis are described. The objectives of the research

are to synthesis novel DOPO-containing flame retardants and apply in epoxy resin and PLA.

In chapter 2, the properties of materials used in this thesis, experimental methods and characterizations are presented.

In chapter 3, three types of DOPO-containing flame retardants (Series A: single molecules; Series B: chain-like macromolecules; Series C: Functionalizing MWCNTs) were synthesized based on the Pudovik reactions. Flame retardants series A were characterized by ^1H , ^{13}C and ^{31}P NMR spectroscopy, elemental analysis (EA) and Fourier transform infrared (FT-IR) spectroscopy. For series B, FT-IR and X-ray photoelectron spectroscopy (XPS) were taken to confirm their compositions. The structures and compositions of flame retardants series C were confirmed by FT-IR, Raman, XPS, transmission electron microscope (TEM) and Thermogravimetric analyses (TGA).

In chapter 4, three types of DOPO-containing flame retardants were well dispersed into epoxy resin matrix with DDM as harder forming flame-retardant epoxy resin composites. Flame retardancy tests indicated that Ax/Bx-modified epoxy resin composites with phosphorus content of 0.75 wt% could reach UL 94 V-0 flammability rating with high *LOI* values. Meanwhile, Cx/AlPi/(P%-Y) epoxy resin nanocomposite with 1 wt% Cx and phosphorus content of 1.00 wt% can reach UL 94 V0 rating. Moreover, TGA results showed that all those flame retardant epoxy resin composites produced high char yields. The mechanical properties of Cx-modified epoxy resin nanocomposites deteriorated slightly with addition of Cx, with notched impact strengths from 2.23 ± 0.15 to 2.90 ± 0.22 $\text{kJ}\cdot\text{m}^{-2}$. Despite this, Cx/AlPi/(P%-Y) epoxy resin nanocomposites showed satisfactory mechanical properties for applications with high storage modulus and T_g s.

In chapter 5, three types of DOPO-containing flame retardants were well dispersed into PLA matrix via melt blending forming flame-retardant PLA composites to improve both flame retardancy and mechanical properties. Flame retardancy tests indicated that

Ax/Bx-modified PLA composites with filler content of 30 wt% could reach UL 94 V0 flammability rating, with high *LOI* values. While, Cx-modified PLA nanocomposite with synergistic effect of 1 wt% Cx and AHP content of 15 wt% can reach UL 94 V0 rating. Moreover, TGA results showed that all those flame retardant PLA composites produced high char yields for preventing the anti-dropping. The tensile-enhanced properties of PC-z/(Cx/AHP-Y) PLA nanocomposites can be attributed to that Cx can form three-dimensional network structure and promote the dispersion of AHP in PLA matrix. The notched impact strengths of Cx-modified PLA nanocomposites were slightly increased with introduction of Cx into flame retardant AHP/PLA systems.

In chapter 6, Core-shell nanostructured flame retardant Cx were introduced into aluminum hypophosphite/poly(lactic acid) (AHP/PLA) flame retardant systems to improve both flame retardancy and mechanical properties. In order to improve the mechanical properties and ductility of such flame retardant PLA nanocomposites, as well as extend their industrial applications, a cold rolling process was performed in this work. Such cold rolling process was conducive for improving the comprehensive mechanical properties of flame retardant PLA nanocomposites with the increasing of both tensile strength and fracture strain. With addition of 1 wt% Cx, when the rolling ratio increased from 0% to 70%, the tensile strength and fracture strain was increased greatly than that of AHP-modified PLA composites. Additionally, the Cx-modified PLA nanocomposites were homogenized at a high rolling ratio, resulting reinforced tensile properties according to the cold rolling process.

In chapter 7, general conclusions of the study are made. These high-efficiency flame retardant epoxy resin or PLA composites with good mechanical properties obtained in this study will become a potential candidate for fire- and heat-resistant applications in automotive engineering and building fields with more safety and excellent performance.

Publications

I. 審查付投稿論文

- (1) Liqiang Gu, Jianhui Qiu, Eiichi Sakai
Effect of DOPO-containing Flame Retardants on Poly(lactic acid):
Non-flammability, Mechanical Properties and Thermal Behaviors
Chemical Research in Chinese Universities, Vol.33 (1), (2017), pp.143-149.
- (2) Liqiang Gu, Jianhui Qiu, Eiichi Sakai
A novel DOPO-containing flame retardant for epoxy resin: Synthesis,
nonflammability, and an optimized curing procedure for high performance
High Performance Polymers, 2016, DOI: 10.1177/0954008316664123.
- (3) Liqiang Gu, Jianhui Qiu, Eiichi Sakai
Thermal stability and fire behavior of aluminum diethylphosphinate-epoxy resin
nanocomposites
Journal of Materials Science: Materials in Electronics, Vol.28 (1), (2017),
pp.18-27.
- (4) Chen Qiu, Liqiang Gu, Youwei Yao
Study on Synthesis and Performance of A New Type of Zinc-containing Thermal
Stabilizer for PVC
Plastics Science and technology, Vol.43 (9), (2015), pp.76-82.
- (5) Liqiang Gu, Guoan Chen, Youwei Yao
Two novel phosphorus-nitrogen-containing halogen-free flame retardants of high
performance for epoxy resin
Polymer Degradation and Stability, Vol.108, (2014), pp.68-75.
- (6) Liqiang Gu, Xuejuan Wan, Haiyang Liu, Tianqi Liu, Youwei Yao
A novel ratiometric fluorescence sensor for Zn²⁺ detection
Analytical Methods, Vol.6 (21), (2014), pp.8460-8463.
- (7) Guoan Chen, Liqiang Gu, Youwei Yao
A novel zinc-containing additive for the long-term thermal stabilization of poly
(vinyl chloride)
Polymer Degradation and Stability, Vol.107, (2014), pp.113-119.
- (8) Haiyang Liu, Xuejuan Wan, Liqiang Gu, Tianqi Liu, Youwei Yao
Easily accessible ferric ion chemosensor based on rhodamine derivative and its

reversible OFF-ON fluorescence response

Tetrahedron, Vol.70 (41), (2014), pp.7527-7533.

- (9) Xuejuan Wan, Tianqi Liu, Haiyang Liu, Liqiang Gu, Youwei Yao
Cascade OFF-ON-OFF fluorescent probe: dual detection of trivalent ions and phosphate ions
RSC Advances, Vol.4 (56), (2014), pp.29479-29484.

注：博士論文テーマ関連：4編（(1)～(3)、(5)），その他：5編（(4)、(6)～(9)）

II. 国際会議発表論文

- (1) **Liqiang Gu**, Jianhui Qiu, Eiichi Sakai, Kazushi Itou, Youwei Yao, Min Zhang. A novel phosphorus-containing flame retardant for poly(lactic acid) with high performance, The 12th China-Japan Joint Conference on Composite Materials (CJJCC-12), Kochi, Japan, September 14-18, 2016.
- (2) **Liqiang Gu**, Jianhui Qiu, Eiichi Sakai, Kazushi Itou, Youwei Yao, Min Zhang. An investigation of mechanical properties of the flame retardant poly(lactic acid) by cold rolling process, The 12th China-Japan Joint Conference on Composite Materials (CJJCC-12), Kochi, Japan, September 14-18, 2016.

III. 国内学会発表

- (1) 顧立強、邱建輝、境英一、伊藤一志、姚有為、張敏。
ナノ難燃剤添加によるポリ乳酸の機械特性。2016年10月日本プラスチック成形加工学会成形加工シンポジウム'16、仙台市。
- (2) 顧立強、邱建輝、境英一、工藤素、野辺理恵。
新規リン系難燃剤添加によるポリ乳酸の難燃化および性能評価。2015年9月日本機械学会東北支部第51期秋季講演会、福島県いわき市。
- (3) 顧立強、邱建輝、境英一。
エポキシ樹脂用新規リン系難燃剤の創製および性能評価。2014年9月日本複合材料学会第39回複合材料シンポジウム、秋田市。

Acknowledgements

I would firstly like to acknowledge the guidance and support of my advisor Professor Jianhui Qiu, who works at Department of Machine Intelligence and Systems Engineering, Faculty of Systems Science and Technology of Akita Prefectural University. He imparted the knowledge of material science and technology to me, and his elaborated guidance, considerable encouragement and invaluable discussion make my research of great achievement and my study life unforgettable. Also, thank you for the financial support and the opportunities that were provided to me.

My deepest appreciation goes to the professors in Department of Machine Intelligence and Systems Engineering, Faculty of Systems Science and Technology at Akita Prefectural University, Prof. Mamoru Mizuno, Prof. Nobuhiro Kanazawa and Professor in Department of Mechanical Engineering, Faculty of Engineering and Resource Science at Akita University, Prof. Yotsugi Shibuya for the comments and suggestions, whose advices have inestimable value for my research.

Third, Prof. Eiichi Sakai and Prof. Kazushi Ito (Department of Machine Intelligence and Systems Engineering, Faculty of Systems Science and Technology at Akita Prefectural University), I am grateful for their kind help and assistance in my work.

In addition, I would like to express my sincere thanks to the professors in Advanced Materials Institute, Graduate School at Shenzhen, Tsinghua University, Prof. Youwei Yao, Prof. Guoyi tang and Prof. Guolin Song, for their technical support.

I appreciate the technical support from Prof. Teruo Bitoh, Prof. Yongbo Wu, Prof. Takao Komiyama in Akita Prefectural University; Dr. Makoto Kudo and Ms. Rie Nobe in Akita Industrial Technology Center; Prof. Shaoyun Fu in Chinese Academy of Sciences; Prof. Zuowan Zhou in Southwest Jiaotong University; Prof. Qingqing Ni in Shinshu University, and Prof. Ning Hu in Chongqing University. Thanks for Ms. Qiu, who has taken good care of me in the last three years; And thanks also go to my peer research group members including Xueli Wu, Wenjuan Zhang, Liming Zang, Lijun Wang, Bin

Wang, Baiyi Chen, Longxiang Zhu, Jiao Chen, Haodao Mo, Yanling Yu, Yukiko Takeuchi, Yoshie Sugiura, Suguru Murakami, Yuki Iwase, Yuya Matsumura, Kazuki Nishitoba, Tatsuya Onogaki, Fumiya Saitou, Taiyou Sasaki, Daisuke Shibata, Erika Sato, Keita Gotou, Mizuki Yada, for assisting with my research as well as providing friendship and support.

Gratitude is due to my Japanese teacher, Asuka Toda, Eyiko Kamada, Minako Kudo, Chika Furukawa, Eiko Fujishima and for their support, patience and understanding throughout this endeavor.

A giant thank you also goes to my parents and my wife Ms. Ping Ao, for their moral support, warm encouragement and patience throughout the course of this PhD and indeed for my entire life.

Liqiang Gu

2017.03.22